

Delivery and Scavenging of Nucleic Acids by Polycationic Polymers

by

Jennifer Gamboa Jackman

Department of Biomedical Engineering
Duke University

Date: _____

Approved:

Kam W. Leong, Supervisor

Bruce Sullenger, Co-Chair

Charles Gersbach, Co-Chair

Fan Yuan

William Reichert

Dissertation submitted in partial fulfillment of
the requirements for the degree of Doctor
of Philosophy in the Department of
Biomedical Engineering in the Graduate School
of Duke University

2016

ABSTRACT

Delivery and Scavenging of Nucleic Acids by Polycationic Polymers

by

Jennifer Gamboa Jackman

Department of Biomedical Engineering
Duke University

Date: _____

Approved:

Kam W. Leong, Supervisor

Bruce Sullenger, Co-Chair

Charles Gersbach, Co-Chair

Fan Yuan

William Reichert

An abstract of a dissertation submitted in partial
fulfillment of the requirements for the degree
of Doctor of Philosophy in the Department of
Biomedical Engineering in the Graduate School of
Duke University

2016

Copyright by
Jennifer Gamboa Jackman
2016

Abstract

Electrostatic interaction is a strong force that attracts positively and negatively charged molecules to each other. Such an interaction is formed between positively charged polycationic polymers and negatively charged nucleic acids. In this dissertation, the electrostatic attraction between polycationic polymers and nucleic acids is exploited for applications in oral gene delivery and nucleic acid scavenging. An enhanced nanoparticle for oral gene delivery of a human Factor IX (hFIX) plasmid is developed using the polycationic polysaccharide, chitosan (Ch), in combination with protamine sulfate (PS) to treat hemophilia B. For nucleic acid scavenging purposes, the development of an effective nucleic acid scavenging nanofiber platform is described for dampening hyper-inflammation and reducing the formation of biofilms.

Non-viral gene therapy may be an attractive alternative to chronic protein replacement therapy. Orally administered non-viral gene vectors have been investigated for more than one decade with little progress made beyond the initial studies. Oral administration has many benefits over intravenous injection including patient compliance and overall cost; however, effective oral gene delivery systems remain elusive. To date, only chitosan carriers have demonstrated successful oral gene delivery due to chitosan's stability via the oral route. In this study, we increase the transfection efficiency of the chitosan gene carrier by adding protamine sulfate to the

nanoparticle formulation. The addition of protamine sulfate to the chitosan nanoparticles results in up to 42x higher *in vitro* transfection efficiency than chitosan nanoparticles without protamine sulfate. Therapeutic levels of hFIX protein are detected after oral delivery of Ch/PS/phFIX nanoparticles in 5/12 mice *in vivo*, ranging from 3 -132 ng/mL, as compared to levels below 4 ng/mL in 1/12 mice given Ch/phFIX nanoparticles. These results indicate the protamine sulfate enhances the transfection efficiency of chitosan and should be considered as an effective ternary component for applications in oral gene delivery.

Dying cells release nucleic acids (NA) and NA-complexes that activate the inflammatory pathways of immune cells. Sustained activation of these pathways contributes to chronic inflammation related to autoimmune diseases including systemic lupus erythematosus, rheumatoid arthritis, and inflammatory bowel disease. Studies have shown that certain soluble, cationic polymers can scavenge extracellular nucleic acids and inhibit RNA-and DNA-mediated activation of Toll-like receptors (TLRs) and inflammation. In this study, the cationic polymers are incorporated onto insoluble nanofibers, enabling local scavenging of negatively charged pro-inflammatory species such as damage-associated molecular pattern (DAMP) molecules in the extracellular space, reducing cytotoxicity related to unwanted internalization of soluble cationic polymers. *In vitro* data show that electrospun nanofibers grafted with cationic polymers, termed nucleic acid scavenging nanofibers (NASFs), can scavenge nucleic acid-based

agonists of TLR 3 and TLR 9 directly from serum and prevent the production of NF- κ B, an immune system activating transcription factor while also demonstrating low cytotoxicity. NASFs formed from poly (styrene-*alt*-maleic anhydride) conjugated with 1.8 kDa branched polyethylenimine (bPEI) resulted in randomly aligned fibers with diameters of 486 ± 9 nm. NASFs effectively eliminate the immune stimulating response of NA based agonists CpG (TLR 9) and poly (I:C) (TLR 3) while not affecting the activation caused by the non-nucleic acid TLR agonist pam3CSK4. Results in a more biologically relevant context of doxorubicin-induced cell death in RAW cells demonstrates that NASFs block ~25-40% of NF- κ B response in Ramos-Blue cells treated with RAW extracellular debris, ie DAMPs, following doxorubicin treatment. Together, these data demonstrate that the formation of cationic NASFs by a simple, replicable, modular technique is effective and that such NASFs are capable of modulating localized inflammatory responses.

An understandable way to clinically apply the NASF is as a wound bandage. Chronic wounds are a serious clinical problem that is attributed to an extended period of inflammation as well as the presence of biofilms. An NASF bandage can potentially have two benefits in the treatment of chronic wounds by reducing the inflammation and preventing biofilm formation. NASF can prevent biofilm formation by reducing the NA present in the wound bed, therefore removing large components of what the bacteria use to develop their biofilm matrix, the extracellular polymeric substance, without

which the biofilm cannot develop. The NASF described above is used to show the effect of the nucleic acid scavenging technology on *in vitro* and *in vivo* biofilm formation of *P. aeruginosa*, *S. aureus*, and *S. epidermidis* biofilms. The *in vitro* studies demonstrated that the NASFs were able to significantly reduce the biofilm formation in all three bacterial strains. *In vivo* studies of the NASF on mouse wounds infected with biofilm show that the NASF retain their functionality and are able to scavenge DNA, RNA, and protein from the wound bed. The NASF remove DNA that are maintaining the inflammatory state of the open wound and contributing to the extracellular polymeric substance (EPS), such as mtDNA, and also removing proteins that are required for bacteria/biofilm formation and maintenance such as chaperonin, ribosomal proteins, succinyl CoA-ligase, and polymerases. However, the NASF are not successful at decreasing the wound healing time because their repeated application and removal disrupts the wound bed and removes proteins required for wound healing such as fibronectin, vitronectin, keratin, and plasminogen. Further optimization of NASF treatment duration and potential combination treatments should be tested to reduce the unwanted side effects of increased wound healing time.

Dedication

I dedicate this work to my family.

To my mom and dad for supporting my education all of these years and encouraging me to pursue my PhD. I would not have made it this far had it not been for your love, support, patience, and constant words of encouragement when I needed them the most. Thank you for lifting me out of my lows and for inspiring me in my highs. Your unconditional love is a true blessing and I hope I can continue to make you proud. I love you both so much!

To my husband, Chris, your dedication, commitment, and drive have inspired me from the day that I met you. You have brought me so much happiness and sanity throughout this entire process and I'm so blessed to have you in my life. I love you and I can't wait to move into the next chapter of our life!

Table of Contents

Abstract	iv
List of Tables	xiii
List of Figures	xiv
List of Abbreviations	xxi
Acknowledgements	xxiii
1. Introduction	1
1.1 Gene delivery in hemophilia.....	3
1.1.1 Hemophilia B	3
1.1.2 Viral gene delivery in hemophilia B	5
1.1.3 Non-viral gene delivery and its applications in hemophilia.....	7
1.1.4 Non-viral oral gene delivery and its applications in hemophilia.....	9
1.2 Nucleic acid scavenging	18
1.2.1 The role of nucleic acids in autoimmune diseases.....	19
1.2.2 The role of nucleic acids in biofilm	20
2. Specific Aims	23
2.1 SPECIFIC AIM 1: (A) Development of polycationic gene carriers; (B) Application of polycations for non-viral oral gene delivery to treat hemophilia B.....	23
2.1.1 (A) Development of polycationic gene carriers	23
2.1.2 (B) Applications of polycations for non-viral oral gene delivery to treat hemophilia B	25
2.2 SPECIFIC AIM 2: Development and in vitro testing of nucleic acid scavenging nanofibers.	26

2.3 SPECIFIC AIM 3: Treatment of biofilms using nucleic acid scavenging nanofibers.	27
3. Specific Aim 1: (A) Development of polycationic gene carriers; (B) Non-viral oral gene delivery for the treatment of hemophilia B.....	29
3.1 Introduction and significance.....	29
3.1.1 (A) Development of polycationic gene carriers.....	29
3.1.2 (B) Non-viral oral gene delivery for the treatment of hemophilia B.....	30
3.2 Materials and methods.....	32
3.2.1 Ch/PS/DNA nanoparticle preparation.....	32
3.2.2 Copolymer synthesis.....	33
3.2.3 Copolymer nanoparticle formation.....	36
3.2.4 Particle size and zeta potential.....	36
3.2.5 DNA encapsulation and release.....	36
3.2.6 <i>In vitro</i> cell experiments.....	37
3.2.7 <i>In vivo</i> experiments.....	38
3.3 Results.....	39
3.3.1 (A) Development of polycationic gene carriers.....	39
3.3.2 (B) Non-viral oral gene delivery for the treatment of hemophilia B.....	48
3.4 Discussion.....	59
3.4.1 (A) Development of polycationic gene carriers.....	59
3.4.2 (B) Non-viral oral gene delivery for the treatment of hemophilia B.....	62
3.5 Conclusion.....	67

4. SPECIFIC AIM 2: Development and <i>in vitro</i> testing of nucleic acid scavenging nanofibers.....	69
4.1 Introduction and significance	69
4.2 Materials and methods	72
4.2.1 Poly(styrene-alt-maleic anhydride) electrospun nanofiber formation	72
4.2.2 Scanning electron microscopy (SEM)	73
4.2.3 X-ray photospectroscopy (XPS).....	73
4.2.4 Nucleic acid adsorption.....	74
4.2.5 Cell culture	74
4.2.6 Cell viability	75
4.2.7 Inhibition of Nucleic-acid driven TLR activation using cationic NASFs	76
4.2.8 Doxorubicin cell debris, DAMPs, inhibition of TLR activation by NASFs	76
4.3 Results	77
4.4 Discussion.....	95
4.5 Conclusion.....	100
5. SPECIFIC AIM 3: Treatment of biofilms using nucleic acid scavenging nanofibers. .	103
5.1 Introduction and significance	103
5.2 Materials and methods	106
5.2.1 Preparation of nucleic acid scavenging nanofibers (NASFs)	106
5.2.2 <i>In vitro</i> biofilm studies	108
5.2.3 Formation of staphylococcal biofilms for <i>in vivo</i> experiments.....	109
5.2.4 Fixation of biofilms on NASF for Scanning Electron Microscopy (SEM).....	109

5.2.5 <i>In vivo</i> biofilm infected wound models	110
5.2.6 DNA gels and PCR.....	111
5.2.7 RNA sequencing.....	112
5.2.8 Protein gels and charged protein separation.....	113
5.2.9 Mass spectrometry	114
5.3 Results	115
5.4 Discussion.....	147
5.5 Conclusion.....	159
6. Conclusions.....	162
7. Future studies.....	166
7.1 SPECIFIC AIM 1: (A) Development of polycationic gene carriers; (B) Application of polycations for non-viral oral gene delivery to treat hemophilia B.....	166
7.2 SPECIFIC AIM 2: Development and in vitro testing of nucleic acid scavenging nanofibers.	168
7.3 SPECIFIC AIM 3: Treatment of biofilms using nucleic acid scavenging nanofibers.	170
References	173
Biography.....	186

List of Tables

Table 1: Molar ratios of copolymer components according to copolymer number. Molar ratios are separated by backbone components (CBA/HMBA) and linker components (HIS/DMPA).	46
Table 2: Conditions for electrospinning of fibers incorporating PS with PSMA in 3 mL of solvent, 1:1:1 THF:DMF:Acetone.	91
Table 3: Proteins found exclusively in NASF extracts from db/db mice infected with <i>P. aeruginosa</i> biofilm treated with NASF for 24 hrs from day 1-2 of treatment. Proteins were identified by at least 4 different peptides.	140
Table 4: Common proteins found in NASF extracts from mice infected with bacteria treated with NASF for 0.5 hrs, 3.5 hrs, or 24 hrs. Proteins were identified by at least 4 different peptides.	146

List of Figures

Figure 1: Barriers to non-viral oral gene delivery.	11
Figure 2: Backbone components of copolymers: (A) N,N'-cystaminebisacrylamide (CBA), (B) N,N'-hexamethalyne bisacrylamide (HMBA). Linker components of copolymers: (C) histamine (HIS), (D) 3-(dimethylamino)-1-propylamine (DMPA).	34
Figure 3: Schematic of reactions using CBA, HMBA, DMPA, and HIS. (A) Synthesis of bio-reducible poly (amido amine) random copolymers using CBA as a backbone. (B) Synthesis of bio-reducible poly (amido amine) random copolymers using HMBA as a backbone.	35
Figure 4: Initial screening of LMW chitosan for transfection of HEK293 cells using pGFP as the DNA component. Solid bars represent nanoparticles made with 97% deacetylated LMW chitosan. Striped bars represent nanoparticles made with 77% deacetylated LMW chitosan. (n=3).....	40
Figure 5: Screening of Ch/PS/pGFP nanoparticles in HEK293 (A) and Caco-2 (B) cell lines. Solid lines represent 97% deacetylated LMW chitosan. Striped lines represent 77% deacetylated LMW chitosan. (n=3).....	41
Figure 6: Nanoparticle characterization using pLuc DNA: (A) nanoparticle size distribution of Ch/PS/phFIX, each color distribution represents a separate nanoparticle preparation. The average diameter is 456 ± 49 nm. (B) Average nanoparticle zeta potential, (n=3).....	42
Figure 7: (A) DNA encapsulation of bulk made nanoparticles, (n=3). (B) DNA release from Ch/PS/DNA nanoparticles after incubation in simulated gastric fluid (SGF) at 37°C for 4 hrs, (n=3).....	43
Figure 8: Cell viability of Ch/PS/DNA nanoparticles, where DNA is pLuc, as compared to Lipofectamine/pLuc polyplexes in HEK293 cells (n=3).	44
Figure 9: Transfection efficiency, represented by RLU, using pLuc as DNA in Ch/PS/DNA nanoparticles compared to Ch/DNA nanoparticles in (A) HEK293, (n=5) and (B) Caco-2 cell lines, (n=5).	45
Figure 10: Transfection efficiency in HEK293 of copolymer 3 (backbone molar ratio: 1/9 CBA/HMBA; linker molar ratio: 1/1 HIS/DMPA) and 8 (backbone molar ratio: 3/7	

CBA/HMBA; linker molar ratio: 1/1 HIS/DMPA) compared to Lipofectamine 2000, (n=3).	46
Figure 11: Twinfilin-1 (Twf1) knockdown in primary mouse fibroblasts after miRNA nanoparticle delivery at different miRNA (μg):copolymer (μg). All linker molar ratios DMPA/HIS 1/1, copolymer 3, 8, 13, 16 backbone molar ratios (CBA/HMBA): 1/9, 3/7, 1/1, 7/3, (n=3).	48
Figure 12: Functional hFIX protein levels after <i>in vitro</i> transfection in HEK293 cells, (n=3).	49
Figure 13: Functional hFIX protein levels after <i>in vitro</i> transfection in Caco-2 cells. EZPLEX is a commercially available polymer for gene delivery, (n=3).	50
Figure 14: Schematic of the Transwell system.	52
Figure 15: Functional hFIX protein levels after <i>in vitro</i> transfection in the Transwell model. “Upper chamber” represents functional hFIX detected in media from the upper chamber; “Lower chamber” is from media withdrawn from the lower chamber, (n=3)..	53
Figure 16: hFIX mRNA levels in Caco-2 cells and HEK293 cells following administration of nanoparticles to the upper chamber of the Transwell model, relative to untreated controls.	54
Figure 17: (A) Functional hFIX protein levels after <i>in vitro</i> transfection in the Transwell coculture model. “Upper chamber” represents functional hFIX detected in media from the upper chamber; “Lower chamber” is from media withdrawn from the lower chamber, (n=3). (B) hFIX mRNA levels in Caco-2 cells and HEK293 cells following administration of nanoparticles to the upper chamber of the Transwell coculture model, relative to untreated controls.	55
Figure 18: IVIS images detecting luciferase expression in nude mice following: (A) control 1, control 2, Ch/PS/pLuc treated; intestines from (B) control 2 and (C) treated, from left to right: kidneys and spleen, blank, intestines, liver, blank, stomach.....	56
Figure 19: (A) Representative hFIX immunohistochemistry from a sample of intestine and liver from two different balb/c mice from each group that were orally given a placebo (untreated), Ch/phFIX nanoparticles, or Ch/PS/phFIX nanoparticles. (B) hFIX concentration as determined by ELISA from untreated or nanoparticle treated balb/c mice blood samples, diamonds indicate untreated, squares indicates Ch/PS/phFIX,	

circles indicate Ch/phFIX. (C) hFIX concentration as determined by ELISA from Hemophilic B mice that were untreated or orally fed Ch/PS/pLuc (sham nanoparticle), Ch/PS/phFIX, or Ch/phFIX nanoparticles.	58
Figure 20: Schematic of nucleic acid scavenging by (A) free polycationic polymers versus (B) nanofiber bound polycationic polymers.....	71
Figure 21: (A) SEM image of neutral PSMA nanofibers; (B) SEM image of 1.8 kDa modified PSMA nanofibers; (C) (i) Survey scan of neutral PSMA fibers, (ii) High-resolution XPS scan for C 1s of neutral PSMA fibers, (1) is C=O, (2) is C-O, (3) is C-C, (iii) Survey scan of bPEI conjugated NASF, (iv) High-resolution XPS scan for C 1s of bPEI conjugated NASF showing the presence of (1) C=O, (2) C-O, (3) C-N, (4) C-C.	79
Figure 22: (Ai-Aiv) Fluorescent microscope images of polycationic nanofibers after 4hrs interaction with AlexaFlour488-CpG (Left); (B) quantification of average fluorescence after interaction with AlexaFlour488-CpG normalized to polycationic nanofiber alone and compared to the initial amount of CpG added.	81
Figure 23: Salmon sperm DNA maximum adsorption curve for a 3 mm diameter disc of NASF (n=3).....	81
Figure 24: (A) Cell viability of STO and Ramos-Blue cells after 4 hrs of interaction with polycationic nanofibers; (B) Live/Dead assay performed on NHDF cells where Live cell % was determined at 24 and 48 hrs.	83
Figure 25: Secreted alkaline phosphate levels from Ramos-Blue cells. SEAP levels after pre-incubation of neutral fibers (60/100% PSMA Fiber) or NASFs with CpG as compared to CpG alone and baseline levels of SEAP (Untreated); * denotes $p \leq 0.001$, (n=3).	84
Figure 26: SEAP levels after pre-incubation of NASFs with agonists as compared to agonists alone and untreated SEAP levels of Ramos-Blue cells); (n=3) * denotes $p \leq 0.001$ as compared to agonists alone.....	86
Figure 27: Co-incubation of NASFs with Ramos-Blue cells and agonists. 60% NASF and PAMAM-NASF significantly block TLR activation by CpG and Poly(I:C) and maintain SEAP levels comparable to baseline, Untreated; (n=3), * denotes $p < 0.0001$, # denotes $p < 0.05$ as compared to agonists alone.	88
Figure 28: Blocked SEAP production from Ramos-blue cells by NASF. Initial DOX dose to Raw cells describes the amount of DOX used to treat Raw cells 48 hrs prior to using	

the Raw cell debris for activation of Ramos-blue cells. Polycationic nanofiber blocking demonstrates the polycationic nanofiber's ability to prevent NF- κ β production by scavenging immune-stimulating cell debris from the media; * denotes $p < 0.0001$ as compared to cells without DOX cell debris and without NASF, ϵ denotes $p < 0.03$ as compared to DOX dose at 9 $\mu\text{g/mL}$ with no NASF. 90

Figure 29: SEM images of the fibers spun according to the conditions listed in Table 2. (A) R4 with an average fiber diameter of $1.82 \pm 0.06 \mu\text{m}$, (B) R6 with an average fiber diameter of $1.20 \pm 0.06 \mu\text{m}$, (C) R7 with an average fiber diameter of $1.98 \pm 0.08 \mu\text{m}$, (D) R8 with an average diameter of $2.51 \pm 0.06 \mu\text{m}$ 92

Figure 30: Cell viability after treatment with two 3x3 cm pieces of R8 + bPEI in 400 μL of media. 94

Figure 31: NF- κ β activation in HEK-TLR cells following administration of the agonist alone (white bars), agonist + [R8 + bPEI fiber] (black bars), agonist + free bPEI (grey bars), agonist + PAMAM-G3 (dotted bars); (n=3) * indicates $p < 0.05$ as compared to agonist alone. 95

Figure 32: Reduction of *P. aeruginosa* biofilm mass by NASF. NASF is added to *P. aeruginosa* in solution in a 4 mm diameter disc; 1x indicates 1 disc, 2x indicates 2 discs, 3x indicates 3 discs, (n=3). * Indicates $p < 0.001$ as compared to biofilm group, # indicates $p < 0.05$ as compared to 1xNASF group. 116

Figure 33: Reduction of *S. aureus* and *S. epidermidis* biofilm mass by NASF. NASF is added to the bacterial suspension as a 4 mm diameter disc, (n=3). The Kimwipe group represents an uncharged, absorbable material control; * indicates $p < 0.001$ compared to Biofilm. 117

Figure 34: The reduction of planktonic bacterial growth by NASF in *S. aureus* and *S. epidermidis* over 24 hrs as indicated by colony forming unit (CFUs). 3mm and 4mm represent the diameter of the NASF discs that were added to the bacterial solution. Each well received one NASF disc (n=3); * indicates $p < 0.001$, % indicates $p \leq 0.002$ as compared to untreated. 118

Figure 35: Scanning electron images from *in vitro* studies; (A) *P. aeruginosa* biofilm infiltrating NASFs after 24 hr incubation; (B) *P. aeruginosa* biofilm on the surface of the NASFs after 48 hr incubation; (C) *S. aureus* interaction with NASFs after 24 hr incubation; (D) *S. epidermidis* interaction with NASFs after 48 hrs. 119

Figure 36: Results from pilot *P. aeruginosa* biofilm study in db/db mice. (A) Photo of untreated mouse wound. (B) Image of *P. aeruginosa* infected biofilm wound. (C) Wound closure of untreated versus *P. aeruginosa* biofilm infected open wounds over 18 days. 121

Figure 37: Wound closure of db/db mice given wounds that were left alone (Untreated) (n=5), infected with *P. aeruginosa* biofilm (Biofilm) (n=8), or infected with *P. aeruginosa* biofilm and treated with NASF (NASF treated) (n=8) – NASF were changed daily..... 122

Figure 38: Wound closure of db/db mice given wounds that were left alone (Untreated) (n=5), left alone and treated with NASF (Untreated, NASF) (n=5), infected with *P. aeruginosa* biofilm (Biofilm) (n=8), or infected with *P. aeruginosa* biofilm and treated with NASF (NASF treated) (n=8) – NASF were changed daily for 7 days. 124

Figure 39: Representative images at 20x magnification of ZO1 tight junction fluorescent staining and DAPI staining of wounds extracted from db/db mice: (A) *P. aeruginosa* biofilm wounds and (B) untreated wounds with no biofilm..... 125

Figure 40: Representative images at 20x magnification of ZO2 tight junction fluorescent staining and DAPI staining of wounds extracted from db/db mice: (A) *P. aeruginosa* biofilm wounds, (B) *P. aeruginosa* biofilm wounds treated with NASF for 7 days, (C) untreated wounds with no biofilm, (D) wounds with no biofilm treated with NASF for 7 days. 126

Figure 41: Representative images of H&E staining from db/db extracted wounds: (A) untreated wound with no biofilm, (B) *P. aeruginosa* biofilm wound treated with NASF for 7 days, (C) *P. aeruginosa* biofilm infected wound (yellow box highlights the inflammatory cells), (D) magnification of inflammatory cells in the *P. aeruginosa* biofilm infected wound..... 127

Figure 42: DNA gel from crude NASF extracts from db/db mice wounds on day 2 (lanes 1-5) or day 3 (lanes 6-14) of NASF treatment: NASF treated *P. aeruginosa* biofilm wounds (lanes 1-2, 6-13), NASF treated wounds with no biofilm (lanes 3-5, 14). 128

Figure 43: DNA gel from DNA separated out by TRIzol extraction of crude NASF extracts from db/db mice wounds, 1 kb DNA ladder is in lane 1 of both the top and bottom gels. Red arrows indicate prominent DNA bands found in all samples. Top gel shows NASF treated *P. aeruginosa* biofilm wounds from day 1 (lanes 2-9) and day 2 (10-15). Bottom gel shows DNA from day 2 (lanes 1-5) or day 3 (lanes 6-14) of NASF treatment: NASF treated *P. aeruginosa* biofilm wounds (lanes 1-2, 6-13), NASF treated wounds with no biofilm (lanes 3-5, 14)..... 130

Figure 44: DNA gels of PCR products of DNA extracts from (A) db/db mice treated with NASF and infected with *P. aeruginosa*, lanes 4 and 6, or treated with NASF without biofilm present, lanes 3 and 5; (B) NASF extracts from *in vitro* *P. aeruginosa* biofilms, lanes 2 and 4, or neutral PSMA nanofibers, lanes 3 and 5, as compared to *in vivo* NASF extracts from *P. aeruginosa* infected db/db mouse wounds, lane 6, using primer set 2; (C) NASF extracts from *in vitro* *P. aeruginosa* biofilms, lanes 3 and 5, or neutral PSMA nanofibers, lanes 4 and 6, as compared to *in vivo* NASF extracts from *P. aeruginosa* infected db/db mouse wounds, lane 7, using primer set 1. Lane 1 is GeneRuler Low Range DNA Ladder. 131

Figure 45: Venn diagram of the number of RNAs that were extracted from NASF on *P. aeruginosa* biofilm treated db/db wounds (Biofilm, NASF - purple) versus NASF on db/db wounds with no bacterial biofilm (Untreated, NASF-yellow)..... 133

Figure 46: RNAseq heat map from RNA extracts of db/db wounds from four different mice including two that were without biofilm (Untreated, NASF) and 2 that were with *P. aeruginosa* biofilm (Biofilm, NASF). 134

Figure 47: Average total protein extracted from NASF used on wounds in db/db mice infected with *P. aeruginosa* (Biofilm, NASF) or uninfected (Untreated, NASF). Each bar indicates an individual mouse. 136

Figure 48: Total protein extracted from NASF used to treat db/db mice that were infected with *P. aeruginosa* (lanes 2-9) or not infected (lane 10). Ladder in lane 1 is Spectra HR protein ladder. Each lane indicates an extract from a different mouse..... 137

Figure 49: Protein gels after separation of positively charged and negatively charged proteins from db/db mice that were infected with *P. aeruginosa* (lanes 2-9) or not infected (lane 10) with Spectra HR protein ladder in lane 1; (A) positively charged proteins, (B) negatively charged proteins. 138

Figure 50: Venn diagram displaying the number of proteins extracted from wounds treated with NASF in db/db mice for 24 hrs that were biofilm free (Untreated, NASF) or infected with *P. aeruginosa* biofilm (Biofilm, NASF) from day 1-2 of NASF treatment. . 139

Figure 51: Venn diagram displaying the number of proteins extracted from wounds treated with NASF in db/db mice for 24 hrs that were biofilm free (Untreated, NASF) or infected with *P. aeruginosa* biofilm (Biofilm, NASF) from day 6-7 of NASF treatment. . 140

Figure 52: DNA gel of crude extracts from NASF used on C57 mice infected with *S. epidermidis* preformed biofilms (lanes 3 and 4) or uninfected (lanes 5 and 6). Lanes 3 and 5 had 0.5 hrs NASF exposure, lanes 4 and 6 had 3.5 hrs, and lane 1 is a 1 kb DNA ladder. 142

Figure 53: Average total protein extracted from NASF used on wounds in C57 mice infected with *S. epidermidis* (Biofilm) or uninfected (Untreated). 0.5 hrs and 3.5 hrs indicate how long the NASF was exposed to the wound bed..... 144

Figure 54: (A) Protein gel of NASF extracts from: lane 2- 0.5 hrs with *S. epidermidis* biofilm, lane 3-3.5 hrs with *S. epidermidis* biofilm, lane 4-0.5 hrs uninfected, and lane 5-3.5 hrs uninfected. Venn diagrams displaying the number of proteins extracted from wounds treated with NASF in C57 mice for (B) 0.5 hrs with *S. epidermidis* infection (Biofilm) or without infection (Untreated), (C) 3.5 hrs with *S. epidermidis* infection or without infection..... 145

Figure 55: Venn diagram of proteins detected from NASF extracts of infected wounds treated with NASF for different time durations..... 146

Figure 56: Schematic of how NASF acts on *P. aeruginosa* biofilms-NASF attracts the biofilm to itself thereby allowing easy removal of biofilm from the adjacent surface.... 149

List of Abbreviations

FIX	Factor IX
AAV	Adeno-associated virus
FVIII	Factor VIII
GI	Gastro intestinal tract
Ch	Chitosan
PS	Protamine sulfate
PSMA	Poly(styrene-co-maleic anhydride)
PAMAM	Poly(amido) amine
bPEI	Branched poly-ethylenimine
NA	Nucleic acid
NASF	Nucleic acid scavenging fiber
Ch/PS/DNA	Nanoparticles consisting of chitosan, protamine sulfate, and plasmid DNA
LMW	Low molecular weight
pGFP	GFP plasmid
pLuc	Luciferase plasmid
phFIX	Human FIX plasmid
SGF	Simulated gastric fluid

CBA	N-N'-cystaminebisacrylamide
HMBA	N,N'-hexamethylene bis(acetamide)
HIS	Histamine
DMPA	3-(dimethylamino)-1-propylamine
SLE	Systemic Lupus Erythematosus
RA	Rheumatoid arthritis
MS	Multiple sclerosis
PRR	Pattern recognition receptor
TLR	Toll-like receptor
EPS	Extra Polymeric Substance
DAMP	Damage-associated molecular pattern

Acknowledgements

I would like to acknowledge funding sources, labs, and personnel that have helped me throughout my PhD studies.

Funding sources include the Society of Duke Fellows, the Center for Biotechnology and Tissue Engineering, and the National Science Foundation Graduate Research Fellowship Program.

I would like to acknowledge Bruce Sullenger and his lab in the Department of Surgery for adopting me as a graduate student when my PI moved to Columbia. I would like to thank Latif Bashirov and Luke Poveromo from Howard Levinson's lab at Duke University for helping with the wound healing animal experiments. I acknowledge the Herzog lab at University of Florida for their help in the oral delivery of Ch/PS/DNA nanoparticles to hemophilic B mice. Finally, thanks to the Soman Abraham lab at Duke University for the donation of the Staphylococcal bacteria strains.

1. Introduction

DNA is composed of monomeric units called nucleotides that are composed of three different components: a nitrogen containing base, a pentose, and a phosphate group. The nucleotides are covalently bonded together through the phosphate groups by a phosphodiester linkage. The phosphate groups make up the backbone of the DNA and characteristically have a pKa close to 1, causing them to be completely ionized and negatively charged at a neutral pH of 7¹. This negative charge can be exploited for interaction with positively charged moieties due to an electrostatic interaction. These electrostatic interactions are present in exchanges between DNA with cationic polymers. The positively charged loci of cationic polymers interact with the negatively charged phosphate backbone of DNA and self-assemble into particles². These particles are commonly used for applications in gene delivery, but have more recently been used for applications in a new concept termed nucleic acid scavenging, where positively charged polymers are used to remove nucleic acids from solution in order to dampen the inflammatory response caused by toll-like receptor (TLR) activation.

Polycations are used for many biomedical applications including gene delivery, miRNA delivery, and more recently, nucleic acid scavenging. The first two applications are typically performed using virus, however, viral vectors run the risk of being immunogenic and the possibility of random genomic integration results in the danger of

oncogenic affects ^{3,4}. An alternative to viral gene delivery is using polycations for non-viral gene delivery. The electrostatic interaction between polycations and anionic nucleic acids results in encapsulation of the nucleic acid in a protective nanoparticle. The nanoparticle is a carrier that shuttles the nucleic acid into the cell for gene production (DNA delivery) or knockdown (miRNA/siRNA delivery). Gene delivery has been tested for treatment of many diseases including hemophilia A, hemophilia B, and cancer. Non-viral miRNA delivery is not as common as gene delivery, but miRNAs have many important roles in cellular processes and have been associated with various diseases including hypertrophy, obesity, diabetes, hearing loss, and liver disease as well as cardiovascular, muscular, and neurodegenerative diseases ⁵. Although it is possible to inject naked genes and miRNA directly into the site of interest, this achieves only minimal effect due to nucleic acid degradation. Nanoparticles provide protection for the genes and miRNAs so that they can be delivered systemically or even orally, a more user-friendly approach to therapeutics. Many nucleic acid delivery carriers have been developed with limited translation into the clinic, efficiency of non-viral delivery remains low and viral carriers remain risky, therefore leaving room for improvement in non-viral carrier development.

Polycations can also be used with an alternative endpoint aiming to eliminate cellular uptake of nucleic acids instead of encouraging cellular uptake, this process is

termed nucleic acid scavenging. Nucleic acid scavenging works by neutralizing extracellular nucleic acids before they can interact with TLRs that stimulate an inflammatory immune response that is associated with various autoimmune diseases including systemic lupus erythematosus, bacterial sepsis, irritable bowel disease, multiple sclerosis, and rheumatoid arthritis. Current therapies addressing excessive TLR activation aim at blocking the receptors themselves, however, redundancy in TLRs makes it difficult to completely reduce TLR activation by solely blocking receptors. By using polycations as nucleic acid scavengers, studies have shown the ability to reduce the inflammation caused by TLR activation. The general electrostatic interaction between the polycation and the nucleic acid neutralizes a broad range of nucleic acids therefore preventing TLR activation on a broader scale than TLR receptor inhibition.

This work describes the use of the electrostatic interactions of negatively charged DNA and/or RNA and positively charged polymers for applications in gene delivery and nucleic acid scavenging.

1.1 Gene delivery in hemophilia

1.1.1 Hemophilia B

Hemophilia B, also known as Christmas disease, is an X-linked disease that affects approximately 1 in 30,000 males. Hemophilia B causes a factor IX (FIX) deficiency that results in a bleeding disorder that is classified as severe, moderately

severe, or mild depending on the FIX activity (<1%, 2-5%, 6-30%, respectively, as compared to normal levels) ⁶⁻⁸. FIX is a 55 kDa polypeptide found at an average concentration of 3-5 µg/mL in the blood ⁹. FIX is an important coagulation factor in the intrinsic blood clotting pathway, it is activated by factor XI and then forms a complex with factor VIII to activate factor X. Factor X then begins the cascade of the common blood clotting pathway which eventually leads to the formation of a clot ¹⁰.

Patients suffering from hemophilia B experience abnormal bleeding, especially in the joints and soft tissues ¹¹. Initial therapies for hemophilia B included purified FIX concentrate extracted from pooled human plasma or prothrombin-complex concentrates ⁷. Although effective, these treatments demonstrated a high risk of transmission of pathogenic viruses including hepatitis, human immunodeficiency virus, and parvovirus. In order to reduce these risks, a prophylactic therapy of recombinant FIX was developed. These recombinant proteins were made by modifying cells to express the gene for human FIX without using any plasma-derived proteins, therefore eliminating the risk of viral infection ¹¹. Although recombinant proteins improved hemophilia B treatment, the treatment remains burdensome, expensive, and only available to ~20% of the hemophilic population who live in more economically resourced countries ¹². Treating a patient prophylactically with hFIX concentrate costs ~\$300,000 a year with a potential lifetime cost of ~\$20 million ¹³; with more drugs coming on the market, there

may be more competitive pricing to lower the cost to patients, however, there is potential for new therapies that are less expensive with less frequent administrations and with more permanent outcomes.

1.1.2 Viral gene delivery in hemophilia B

One alternative to recombinant protein therapy for hemophilia is gene therapy, a process by which an exogenous gene is delivered to a cell, specifically to the nucleus, to be transcribed and translated into a biologically active protein ^{4,14}. The most effective method of gene therapy is using a modified virus as the gene carrier; these are viruses that no longer contain the pathogenic components. Viruses used for gene delivery include lentiviruses, adenoviruses, and adeno-associated viruses (AAV), among others, each having their own set of pros and cons. Lentiviruses have the ability to integrate into the chromosome of non-dividing cells; however, they are highly pathogenic viruses that have the potential to revert back into the wild-type virus. Adenoviruses can deliver genes up to 35 kb, they transduce both dividing and non-dividing cells at high efficiency, however, they do not integrate into the chromosome therefore making the gene expression transient and they often elicit a strong immune response due to immune recognition of the viral proteins. Advantages of AAV include it's nonpathogenic nature, the ability to infect both dividing and non-dividing cells, and the

ability to integrate into the host genome; disadvantages include labor intensive processing techniques and limited gene insertion size ^{4,14}.

After decades of success of preclinical studies of viral gene delivery, there have been some recent advances in the first clinical studies. Most of the clinical trials done in humans using hFIX genes use AAVs as the gene carriers ⁸. Initial gene delivery studies had trouble overcoming the antibody response to both the AAV virus and the hFIX protein in some patients therefore resulting in clinically irrelevant circulating levels of hFIX protein in the blood ⁸. However, several more recent studies have been able to overcome these issues by using different AAV serotypes, changing the mode of administration, and optimizing the FIX gene for this application. One such clinical trial is one that was published in 2000 by Kay et. al. where they injected an AAV expressing hFIX into skeletal muscle. Observation of the first three patients in this trial showed no evidence of germline vector transmission and no inhibitory antibodies. Two out of the three patients showed increased levels of hFIX in circulation, however, only one patient had levels above 1% of normal, enough to match the success of FIX protein administration ¹⁵. A phase1/2 study by Manno et. al. used a recombinant AAV serotype 2 vector expressing hFIX that was infused through the hepatic artery into seven patients. The results showed acute toxicity with therapeutic levels of 3% and 11% in two patients given the highest dose. Yet, the hFIX expression only lasted up to 8 weeks and was

accompanied by elevation in liver transaminases, leading to further studies that suggested that the transduced hepatocytes were being destroyed by cell-mediated immunity targeting antigen of the AAV capsid causing the decline in hFIX expression ¹⁶.

These previous studies demonstrated a need for an AAV delivery system with a reduced risk of formation of inhibitory antibodies to both the vector and the expressed protein. Inhibitory antibodies to the expressed protein was the most detrimental outcome as it results in an immune reaction to all delivered protein therefore making subsequent recombinant protein administration useless. Prevention of inhibitory antibodies had to be achieved while maintaining a low risk of unintentional germline transmission of vector sequences ¹⁵. To address these issues, Monahon et. al. developed a GMP-grade, liver targeted AAV, scAAV8, a rhesus macaque serotype that is unknown to most human hosts and therefore reduces the antibody response to the vector. Additionally, they used a gain-of-function FIX variant, FIXR338L, with <10% empty capsid, resulting in overall higher expression of the gene ¹². This scAAV8-FIXR338L gene delivery system is currently in clinical trials with hopes of becoming a FDA approved viral gene delivery system.

1.1.3 Non-viral gene delivery and its applications in hemophilia

Viral vectors risk random integration and limit the size of the delivered gene; non-viral gene delivery, although achieving only transient and low gene expression

levels, overcomes these drawbacks. Non-viral gene delivery is achieved by interacting positively charged polymers with negatively charged DNA in order to form nanoparticles. Nanoparticles are particles of varying shape ranging in size from 10 to 1000 nm. Their small size allows for a higher surface area to volume ratio and therefore provides greater loading capacity for targeting molecules or any other surface modification¹⁷. Nanoparticles are advantageous because they protect the DNA from degradative components in circulation, allowing them to reach their cellular target intact. Nanoparticles also provide the flexibility to engineer the particles to target specific tissues, organs, or cell types by binding of ligands to the surface of the particles^{18,19}. Unlike viral vectors, nanoparticles do not contain cell penetrating mechanisms; instead, most nanoparticles enter the cell through active transport which includes endocytosis, pinocytosis, or micropinocytosis. Endocytosis involves uptake by a phagocytic cell, which could be ligand dependent whereas micropinocytosis and pinocytosis do not require ligand recognition for nanoparticle uptake. After uptake, the nanoparticle goes into the endosome which normally leads to transport to the degradative lysosome compartment unless escape from the endosome is achieved²⁰. The lysosome has a highly acidic environment, pH 4.5-5.5²¹ and numerous enzymes that can be detrimental to the integrity of the nanoparticle assemblies if they reach this compartment and therefore it is desirable to achieve endosomal escape into the

cytoplasm of the cell. Once the nanoparticles and/or their DNA contents reach the cytoplasm, they can then access the nucleus where the cellular machinery can transcribe the delivered gene to eventually be expressed as a protein.

Most non-viral gene delivery applications in hemophilia involve *ex vivo* modification of cells, followed by re-implantation of the cells that express the hFIX or hFVIII protein. For example, Lopez et. al. transfected human mesenchymal stem cells with a naked hFIX plasmid tagged with GFP using nucleofection, and these genetically modified cells were injected into the caudal vein of mice. From the injection of transfected cells they were able to detect hFIX in the blood and in the tissue of the mice²². Another study done in humans with severe hemophilia A used electroporation to transfect dermal fibroblasts with a hFVIII plasmid and the modified dermal fibroblasts were re-administered to the patients. The results showed a clinically relevant increase in FVIII levels in 4 out of 6 patients, showing potential for this therapy²³. Even though these therapies are classified as non-viral therapies, they do not use nanoparticles as described above. Nanoparticles can make it possible to deliver the plasmids directly into the patient instead of using *ex vivo* methods.

1.1.4 Non-viral oral gene delivery and its applications in hemophilia

Methods of nanoparticle delivery include injection (ie. particle bombardment using a gene gun²⁴), implantation (ie. protein depots), inhalation, transdermal, and oral

delivery²⁵. Among all of these methods, oral delivery emerges as the most desirable due to the convenience of route of administration and patient compliance, especially when long term or daily use is required²⁶⁻²⁸. The oral delivery route also provides the benefit of ease of packaging and transport by requiring a lyophilized and encapsulated form of the product, making it possible to provide these therapeutics for use in third-world countries²⁹, whom do not have access to advanced medical technology or therapeutics.

Although there are many benefits to oral delivery, the design of an orally delivered system is difficult due to the external barriers in the gastro-intestinal (GI) tract that are designed to breakdown and destroy intruders. However there is a solution, the use of nanoparticles provides protection from the acidic and enzymatic environment of the GI tract. Common contents for nanoparticles in oral delivery include proteins, nucleic acids, and drugs.

The barriers to oral delivery include the acidity of the gastro-intestinal environment, enzymes, the mucus layer that lines a majority of the GI tract, and the tight junctions of the epithelium (Figure 1). One of the major barriers is the varying and harsh acidic environment of the GI tract, which includes the stomach and the intestines. The stomach has an acidic pH that ranges from 1.0-2.5^{30,31}, the small intestine has a pH that ranges from 6.6 at the proximal end to 7.5 at the ileum, the caecum has a slight pH drop to 6.4, and the pH from the right to the left colon rises progressively to 7.0³⁰. This pH

variation in the GI tract makes it difficult to maintain nanoparticle integrity throughout the entirety of the system. In addition, the contents of gastric fluids present an additional obstacle to nanoparticle oral delivery due to a plethora of enzymes³². The enzymes present in the gastric and intestinal fluids have the potential to degrade nanoparticle materials, DNA, RNA, and proteins. Specifically, the duodenum of the small intestine contains bile salts and degradative enzymes including amylase, trypsin, and lipase³¹, which degrade starch, proteins, and fats respectively. The stomach contains gastric juices which include hydrochloric acid, which makes the stomach acidic, pepsin, which degrades proteins, and mucus, which has a high cell turnover rate³³. The small intestine contains pancreatic juices consisting of pancreatin, trypsin, lipase, peptidases (breaks peptide bonds), and maltase (degrades maltose)³⁴. All of these degradative enzymes make it difficult to deliver proteins, nucleic acids, or drugs orally.

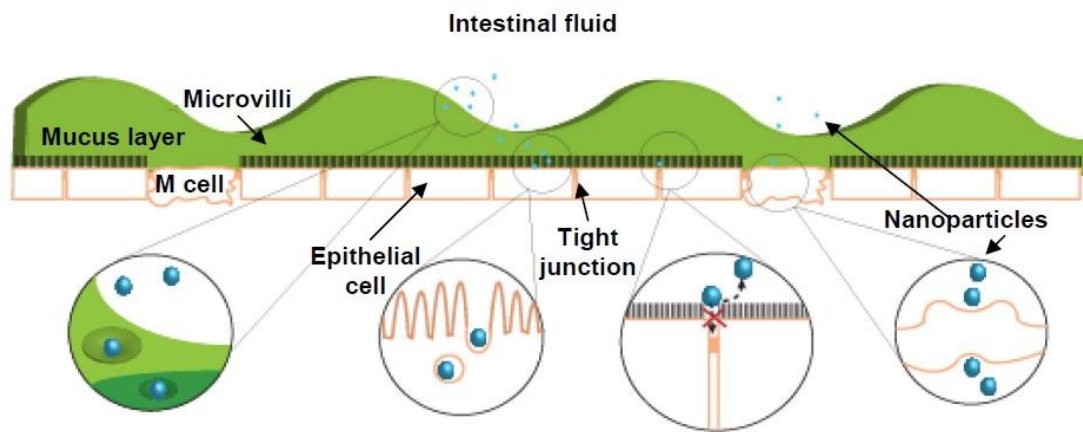


Figure 1: Barriers to non-viral oral gene delivery.

The mucus layer that lines the surface of the GI tract can present another barrier for the nanoparticles to cross and can result in rapid nanoparticle clearance due to quick cell turnover. The average thickness of the mucus layer varies from 170 μm in the gut to 10 μm in the ileum to 100 μm in the colon, making the mucus layer difficult to model *in vitro*^{35,36}. The loosely adherent outer mucus layer presents a barrier to oral delivery because any nanoparticles attached to this layer are quickly lost due to rapid mucus cell turnover, approximately 2-5 days in the small intestine of humans³⁷, which results in quicker nanoparticle clearance rather than sustained presence³⁸. The mucosal intestinal lining is one of the largest immunological compartments in the body³² and therefore can also lead to the loss of nanoparticles through immune attack and subsequent removal by the immune system.

The passage of highly charged and large molecules through the cell membrane of cells in the epithelial layer is prevented³⁹, which emphasizes the importance of using nano-sized particles. However, the transport of nanoparticles is also dependent on size, chemical makeup of the particle, and properties of the intestinal epithelium⁴⁰. Paracellular transport occurs by passive diffusion that is limited by the presence of tight junctions^{39,40}, however, some nanoparticles are known to be able to open the tight junctions and enhance peptide delivery⁴¹⁻⁴³, which is beneficial in maintaining construct viability due to the lack of proteolytic encounters when transport occurs through the

tight junctions³⁹. However, tight junctions present a major barrier to delivery in that they do not allow particles greater than 2 nm to pass²⁰ and therefore greatly limit the potential amount of transport through the paracellular route. One study shows that in lightly fixed epithelial strands, open tight junctions appear to have approximately 18 nm spacing from center to center, confirming the size limitation of passage through the opened tight junction⁴⁴. Even if the particles are able to make it past the tight junction barrier, the underlying layer limits passage of nanoparticles to 13-15 nm²⁰.

Although there are many barriers to oral delivery, there are also benefits to this method, which make it a viable delivery route for nanoparticles containing nucleic acids, proteins, and drugs. Some of the advantages of oral delivery include a large surface area for nanoparticle uptake in the intestine, a sticky mucus lining, and the microfold cells (M cells) in the Peyer's Patch. The large surface area for nanoparticle uptake is a highly beneficial trait of the GI tract⁴⁵, with the small intestine having a surface area of 250 m². Typically, hydrophilic, polar solutes are able to diffuse through the paracellular route instead of the transcellular route. However, the transcellular route is a more likely route for nanoparticle delivery. With its large surface area, there is increased chance for uptake and transport can occur through passive, active, or facilitated means⁴⁰. Nanoparticles tend to be transported by the transcellular route due to their size and surface functional groups⁴⁶.

The benefit of the mucus lining is that it consists of a viscous hydrated gel that reduces the shear affect from the movement of gastric juices ³², thus if a nanoparticle can stick to the firmly adherent mucus layer, located beneath the loosely adherent mucus layer, it has an increased chance of transcellular migration into the lower layers of the epidermal wall, the epithelial layer, and the lamina propia ³⁸. Also located among the epithelium in the small intestine is the large immunological organ, the Peyer's Patch, which contains a specialized cell type, M cells, that increase the transcytotic ability of the nanoparticles. M cells are characterized as atypical epithelial cells that actively phagocytose macromolecules and microbes and deliver them to underlying organized lymphoid particles ⁴⁷. M cells are highly efficient antigen deliverers and have been credited with aiding in the transport of nanoparticles from the small intestine through the Peyer's Patch and into circulation in the body after they have been orally delivered to the gut.

The advantages of using nanoparticles for oral delivery include protection of the nucleotide contents from degradative enzymes, increased mucoadhesion, and increased retention in the GI tract. Increased mucoadhesion through the use of nanoparticles has the benefit of improving the oral delivery of poorly adsorbed drugs, proteins, and nucleotides by increasing the time and amount of interaction with the mucus layer of the intestine ^{38,48,49}. It is hypothesized that this increased mucosal interaction is through

electrostatic interactions between the positively charged nanoparticle and the negatively charged mucus and endothelial layer ^{48,49} or through a physical capture of the nanoparticle by the mucus layer ⁴⁸. However, mucoadhesion can also be achieved through hydrophobic interaction, van der Waals interactions, and polymer chain penetration ³⁸. Nanoparticles can have greater mucoadhesive properties with the use of mucoadhesive polymers, which include Eudragit, poly(acrylic acid), sodium alginate, and chitosan ^{48,49}. Although the mucoadhesive properties can be beneficial, they can also provide a means of quick exit if the nanoparticles become associated with the loosely attached mucus layer which is rapidly shed by the stomach ³⁸, therefore it is preferred to achieve attachment in the deeper mucus layer, which is shed less often and provides a longer interaction between the nanoparticle and the GI tract.

The protection of the gene from proteolytic enzymes ³⁸ and acidic environments provides another benefit for the use of nanoparticles for oral gene delivery. Not only can the nanoparticle protect its contents from degradation by enzymes, but it can also provide controlled release through nanoparticle enzyme degradation which varies according to the enzymes present at different parts in the GI tract ⁵⁰. Along the same lines, pH-sensitive polymers such as acrylates or anionic polymers can result in controlled release of the drug, protein, or nucleic acid contents ¹⁷. By selecting the appropriate pH-sensitive materials, the drug release can be controlled and therefore can

increase absorption of the released contents at a targeted location over a controlled amount of time. Commonly used pH-sensitive materials include Eudragit (L100-55, L100, and S100), hydroxypropyl methylcellulose phthalate, and hydroxypropylmethyl cellulose acetate succinate which dissolve at pH 5.5, 6.0, 7.0, 5.5, and 5.5 respectively. When tested *in vivo* these pH-sensitive materials had varying release profiles dependent on the pH at which they dissolve [31].

A couple of studies have successfully applied oral gene delivery to treat hemophilia A while one more recent study looked into the treatment of hemophilia B. All three of these oral gene delivery systems used chitosan as the cationic polymer. Chitosan is a biodegradable, cationic polysaccharide that has been studied extensively for gene delivery^{51,52}. Chitosan nanoparticles have been applied to oral gene delivery studies due to their stability at low pH, therefore protecting the entrapped DNA from digestion in the gut, and their increased transcellular and paracellular transport across gut epithelium due to their affinity for mucosal surfaces and their ability to mediate the opening of tight junctions^{51,53}. Chitosan is a natural product that is formed by alkaline deacetylation of chitin, an abundant component in crustacean shells. The greater the deacetylation of chitosan, the greater the positive charge density. The amino groups on the chitosan have a pKa of 6.5, making them cationic at slightly acidic pH, a pH that is found widely in the gut and therefore can inherently maintain nanoparticle integrity

throughout the acidic GI tract. The biodegradability and biocompatibility of chitosan is understood because it is catabolized into N-acetyl glucosamine that is then processed via the synthetic pathway of glycoproteins and excreted as carbon dioxide ⁵⁴. These characteristics of chitosan make it an ideal polycation for the formation of DNA nanoparticles meant for oral delivery.

In the study by Bowman et. al., chitosan and FVIII DNA, a B-domain deleted human FVIII plasmid, polyplexes were administered to hemophilia A mice at a dose ranging from 250-600 µg of FVIII DNA. They were able to detect transgene DNA in both the local and systemic tissues following oral administration of nanoparticles; circulating, functional FVIII protein levels reached peak levels of 2-4% at day 22 after delivery ⁵². In the study done by Dhadwar et. al. chitosan and cFVIII DNA, a canine FVIII cDNA plasmid, polyplexes were fed to hemophilia A mice at 450 µg of cFVIII DNA. Mice fed with these nanoparticles experienced increased FVIII activity on day 1 of 130 mU while regressing back to baseline by day 4 post treatment. A phenotypic change in treated mice resulted in cessation of bleeding and stable clot formation within 15 min of trauma, however, by day 4 and 7 post-treatment, this phenotypic correction was lost. Additionally, FVIII plasmid DNA was detected in the intestine and in small amounts in the liver, and no antibodies to FVIII were detected ⁵¹. Both of these studies used high molecular weight chitosan of ~213-390 kDa with deacetylation levels >62%. These

studies were the first to show the ability to achieve FVIII gene expression following oral gene delivery using chitosan/DNA nanoparticles.

In the most recent study performed by Quade-Lyssy et. al., they worked on optimizing the FIX plasmid for applications in oral gene delivery. The most successful FIX mutant led to almost 2000% FIX activity *in vitro* and had several mutations including a mutation to the collagen IV binding site. These mutations resulted in FIX mutants with enhanced binding affinity to the substrate FX and cofactor FVIII while the mutation in collagen IV increased collagen IV binding potentially leading to FIX storage depots that continuously released small amounts of protein to maintain FIX activity. High molecular weight chitosan of >75% deacetylation was used to test oral delivery of the FIX gene mutants in hemophilia B mice and resulted in high levels of FIX in the gut and >14% of normal FIX activity leading to partial phenotypic correction⁵⁵. This study showed the feasibility of delivering the FIX gene orally using a chitosan nanoparticle while noting that they did not pay any attention to the chitosan delivery system, therefore, this system could be improved even more by appropriate engineering of the nanoparticle.

1.2 Nucleic acid scavenging

Nucleic acid scavenging shares the same general concept of gene delivery in that a polycationic polymer interacts with the negatively charged backbone of a NA. Instead

of delivering the NA to the cell, the goal is to prevent the interaction between cellular receptors and the NA. Essentially, nucleic acid scavenging is a technique whereby polycationic polymers bind extracellular NA and prevent them from causing adverse effects. These effects can include hyper inflammation in patients with autoimmune disease or the composition of biofilm extracellular polymeric substance and sustained inflammation in chronic wounds.

1.2.1 The role of nucleic acids in autoimmune diseases

Extracellular nucleic acids can elicit pro-inflammatory responses by activating both the innate and adaptive immune systems. Plasmacytoid dendritic cells (PDC) are responsible for a majority of this immune activation as they express high levels of Toll-like receptors (TLRs) that are activated by pathogenic nucleic acids (e.g. viral RNAs, bacterial DNAs) as well as nucleic acids released by necrotic cells⁵⁶⁻⁵⁹. In healthy individuals, pathogenic nucleic acids and high levels of necrotic cells only present upon infection (viral, bacterial, etc.). Chronic high levels of circulating extracellular nucleic acids in the blood has been linked to chronic activation of TLRs by endogenous nucleic acids which can lead to various pro-inflammatory autoimmune diseases including systemic lupus erythematosus (SLE), rheumatoid arthritis (RA), and multiple sclerosis (MS). In the case of autoimmune diseases, antibodies to eDNA lead to the formation of immune complexes where the antibodies aid in cellular uptake allowing for TLR

activation to occur leading to cytokine production and prolonged immune activation. Additionally, the antibody and eNA immune complexes deposit in tissues leading to inflammation and more cell damage ⁶⁰, causing a vicious cycle of pro-inflammatory symptoms. Although chronic TLR activation is hypothesized to be the root cause of various inflammatory diseases, a majority of the focus has been on SLE and studies in lupus-prone MRL/lpr mice have confirmed that activation of TLR7 and TLR9, nucleic acid receptors, are directly linked to the chronic inflammation associated with SLE ⁶¹⁻⁶³. This leads researchers to believe that numerous autoimmune diseases are a direct result of over activation of TLR7 and TLR9 receptors.

1.2.2 The role of nucleic acids in biofilm

A biofilm is a structured community of microbial cells that are connected by a self-produced extracellular polymeric substance (EPS) ⁶⁴. Biofilms are commonly found on the surface of implanted objects in humans as well as in chronic wounds. A shared characteristic of all biofilms is their resistance to antibiotics due to their reduced growth rates. Studies have also shown that biofilm bacteria are also highly resistant to ultraviolet light, dehydration, and phagocytosis ^{65,66} making them hard to nutrient starve and impossible to defeat by the innate immune response. Because biofilms are so resistant to the treatments commonly used to eliminate planktonic bacterial infections,

alternate ways to tackle biofilm burden are currently being studied. Some suggest that targeting the EPS may aid in preventing/removing biofilm ⁶⁵.

The EPS is composed of a complex mixture of molecules including exopolysaccharides, proteins, lipids, RNA, and eDNA ⁶⁶⁻⁶⁹. In most biofilms, the bacteria account for less than 10% of the total mass whereas the EPS makes up the remaining 90%. The eDNA in the EPS of biofilms is involved in cohesion of biofilms, exchange of genetic information, adhesion, and aggregation of bacterial cells ^{66,69}. Not only is eDNA found in the EPS, but it is also known to favor bacterial aggregation via attractive acid-base interactions and cationic bridging ⁶⁹ during the initial stages of biofilm formation. Some studies have shown that reducing the presence of DNA can prevent biofilm formation and/or disrupt already formed biofilms. One study showed that adding DNase I to a forming biofilm prevented biofilm formation and was able to dissolve biofilms that were 12, 36, and 60 hrs old ⁶⁸. Another study by Tetz et. al. looked at the effect that DNase had on biofilm formation and found that reducing eDNA led to altered biofilm formation that allowed for increased penetration of antibiotics. This study confirmed the presence of DNA fragments of ~30 kb in both gram-positive and gram-negative bacteria, including *Pseudomonas aeruginosa* and *Staphylococcus aureus*, by direct analysis of purified extracellular polymeric molecules ⁶⁷. In general, eDNA has a very important role in the establishment and maintenance of biofilms. This makes

removal of eDNA a valuable technique for preventing and/or reducing the formation of biofilms.

2. Specific Aims

The objective of this dissertation work is to engineer polycations for use in electrostatic interactions with anionic molecules. The polycation formulations are applied to multiple disease states including hemophilia B, chronic inflammatory disease states, and biofilms. Two different approaches are being tested using engineered polycations and their interaction with nucleic acids: (1) nucleic acid delivery and (2) nucleic acid scavenging. We aim to develop polycations that are easy to synthesize and useful as broad technologies that can be applied to various biomedical applications. This research demonstrates a new nanoparticle formulation that results in therapeutic levels of hFIX after oral delivery of a hFIX plasmid for the treatment of hemophilia B and the development of a polycationic nanofiber that is capable of local removal of extracellular nucleic acids for reduction of inflammatory responses and the prevention of biofilm formation.

2.1 SPECIFIC AIM 1: (A) Development of polycationic gene carriers; (B) Application of polycations for non-viral oral gene delivery to treat hemophilia B.

2.1.1 (A) Development of polycationic gene carriers

In this section, we aimed to develop superior gene carriers by the synthesis of new copolymers for systemic delivery and a tertiary component nanoparticle using chitosan and protamine sulfate for oral gene delivery. We hypothesized that

copolymers made with specific amounts of biodegradability, endosomal escape properties, and DNA condensation capacities would increase transfection efficiency when made into a nanoparticle. We also hypothesized that adding the tertiary component, protamine sulfate, to the low molecular weight chitosan nanoparticle would aid in condensing DNA to protect the DNA extracellularly while low molecular chitosan would increase intracellular DNA release, leading to overall higher transfection efficiencies than chitosan/DNA nanoparticles alone. The copolymers combined components that have specific characteristics that are advantageous for gene delivery including N-N'-cystaminebisacrylamide for biodegradability, N-N'-hexamethylene bis(acetamide) for stability, histamine for the proton sponge effect/endosomal escape, and 3-(dimethylamino)-1-propylamine for nucleic acid condensation. These copolymers were synthesized by random polymerization and tested for gene delivery capacity using a luciferase plasmid for luciferase protein production and for miRNA delivery using a combination of 4 different miRNAs: 1, 133, 208, and 499 for twinfillin-1 knockdown. From this data, the two most effective copolymers for gene delivery were determined from the original six that were synthesized.

The tertiary component nanoparticle containing low molecular weight chitosan, protamine sulfate, and DNA was optimized as well. All optimization steps were done in both HEK293 and Caco-2 cells. The first optimization was done to determine which

chitosan/DNA nanoparticle was the most effective, then the tertiary component, protamine sulfate, was added in various amounts to the best chitosan/DNA nanoparticle to determine which protamine sulfate dose improved protein expression after nanoparticle administration. The best chitosan/protamine sulfate/DNA nanoparticle from these optimization steps was characterized for overall charge and size and validated with a second plasmid. The overall goal of this section was to optimize a nanoparticle to be used for oral gene delivery.

2.1.2 (B) Applications of polycations for non-viral oral gene delivery to treat hemophilia B

In the previous section of aim 1, chitosan (Ch), a commonly used cationic polysaccharide for gene delivery, was used in combination with the highly polycationic peptide, protamine sulfate (PS) to engineer a gene delivery nanoparticle that improved transfection efficiency as compared to chitosan gene delivery particles. In this section of aim 1 the Ch/PS/DNA nanoparticles were used for oral delivery of a hFIX plasmid for treatment of hemophilia B, a severe bleeding disorder that prevents blood clotting. Oral gene delivery has advantage over the current hemophilia B treatment of direct injection of recombinant hFIX protein by providing a method where direct production, translation, and protein modifications of the protein occur in the individual's cells therefore providing functional, "self" proteins. Additionally, there is an estimated decrease in cost and ease of administration. To test the optimized Ch/PS/DNA

nanoparticles, the efficacy of hFIX production was validated *in vitro* in HEK293 and Caco-2 cells as well as in the Transwell model to represent intestinal delivery. In the final experiments, the nanoparticles were administered to mice and the therapeutic output was determined by hFIX levels in the blood and hFIX protein expression in the small intestine and liver. We hypothesized that addition of protamine sulfate to low molecular weight chitosan nanoparticles would increase transfection efficiency following oral gene delivery.

2.2 SPECIFIC AIM 2: Development and *in vitro* testing of nucleic acid scavenging nanofibers.

In this aim, poly(styrene-co-maleic anhydride) (PSMA) was electrospun into a fibrous sheet, that was then modified with cationic amine containing polymers to make a positively charged nucleic acid scavenging fiber (NASF) for nucleic acid binding. The DNA binding capacity of the NASF was validated using CpG and salmon sperm DNA binding quantification and *in vitro* cell assays showed the efficacy of the NASFs in a cell based system. A consistent, replicable way for NASF formation was developed and multiple polycations were tested in the process to determine the optimal polycation to achieve consistent nucleic acid scavenging. Branched poly-ethyleneimine (bPEI 1.8 kDa, 25 kDa) and poly(amido)amine (PAMAM) dendrimers, among others were tested with 1.8 kDa bPEI resulting in the best properties. Initial functionality of the polycationic nanofibers was determined using fluorescently labeled CpG DNA binding and salmon

sperm DNA binding. Following validation of DNA binding capacity, the nanofibers were tested in *in vitro* cell systems.

Extracellular NAs have been shown to be potent activators of the innate immune system and result in TLR (3,7,9) activation, the removal of NAs from solution reduces the Nf- κ B response, and can be used to indicate successful NA scavenging. Briefly, we employed Ramos-Blue cells that stably express an NF- κ B/AP-1-inducible SEAP (secreted embryonic alkaline phosphatase) reporter construct and several TLRs (e.g. TLR2, 3, 7 and 9). NF- κ B activation was assessed by quantifying SEAP level in cell culture supernatant. To show that the NASFs selectively interact with NAs and do not merely act as a sponge for all Nf- κ B stimulators, various uncharged or positively charged activators were incubated with the mesh and subsequent Nf- κ B activation was determined. We hypothesized that we could develop a PSMA nanofiber that could be modified with polycations and effectively act as a nucleic acid scavenging mesh in *in vitro* systems.

2.3 SPECIFIC AIM 3: Treatment of biofilms using nucleic acid scavenging nanofibers.

In this aim the NASF was tested for its ability to scavenge NA *in vivo* in an open wound, biofilm infected mouse model. Initially, *in vitro* biofilm reversal was studied using various biofilm forming bacteria including *Pseudomonas aeruginosa*, *Staphylococcus aureus*, and *Staphylococcus epidermidis*. Two mouse models were used in this aim: a

diabetic mouse chronic wound model infected with *Pseudomonas aeruginosa* and a C57 mouse infected with Staphylococcus preformed biofilm. These mouse systems were used to model how the NASFs affect the formation of biofilms and how they act on already formed biofilms, respectively, *in vivo*. The clinical endpoints of NASF were measured by determining wound healing time and performing histology on the wound bed. Functional endpoints were extracted by analyzing the types of compounds that the NASF pulled from the wound bed including DNA, RNA, and protein and determined whether these components were primarily of bacterial or mouse origin. We hypothesized that the NASFs would be able to prevent biofilm formation, increase wound healing time, and that they would remove primarily DNAs and RNAs from the biofilm infected wounds.

3. Specific Aim 1: (A) Development of polycationic gene carriers; (B) Non-viral oral gene delivery for the treatment of hemophilia B

3.1 Introduction and significance

3.1.1 (A) Development of polycationic gene carriers

Aim 1A focuses on the development of different nucleic acid nano-carriers that are applied to both DNA and miRNA delivery. Because Ch/DNA nanoparticles have been previously used in oral gene delivery, we aimed to enhance the Ch/DNA polyplexes by adding a tertiary component. In this development section, the optimization of the ternary Ch/PS/DNA nanoparticle is discussed, while applications of the particle for treatment of hemophilia B are discussed in Aim 1B. Additionally, a series of copolymers were synthesized to improve systemic gene delivery, and preliminary studies of their effectiveness were demonstrated using miRNAs in a disease state that is not extensively studied but used as an initial platform for efficacy; this system is described below.

Recovery from cardiac injury results in inadequate cardiomyocyte regeneration consequentially leading to increased fibrosis which causes loss of function and deterioration of tissue structure. Recent studies have shown transplantation of partially reprogrammed fibroblasts to ischemic hearts, however, there are concerns about the maturity and functionality of *ex vivo* cell-derived cardiomyocytes, the low survival and

retention, and the potential tumor risk ⁷⁰. These concerns can be overcome by direct reprogramming of somatic cells into cardiomyocytes using miRNAs. miRNAs are single stranded non-coding RNA sequences of 18-25 nucleotides that regulate gene expression by direct mRNA cleavage or translation repression. miRNAs are involved in multiple aspects of cardiac hypertrophy including cardiac growth and fibrosis, problems that are also present after cardiac injury. Hypertrophy in the heart is present after cardiac injury, endocrine disorders, or other physiological disorders and leads to heart failure and sudden death if prolonged ⁷¹. Work from the Dzau lab showed that a combination of miRNA 1, 133, 208, and 499 were capable of inducing direct cellular reprogramming of fibroblasts to cardiomyocyte-like cells. In this aim, we screened a copolymer library for use in gene delivery and we collaborated with the Dzau lab to test the same copolymers as miRNA carriers for reprogramming of fibroblasts. We also developed the Ch/PS/DNA nanoparticle platform for further exploration as an oral gene delivery agent to treat hemophilia B, which is further described in Aim 1B.

3.1.2 (B) Non-viral oral gene delivery for the treatment of hemophilia B

Current protein replacement therapies require multiple IV injections that are expensive, painful, and inconvenient. Oral gene therapy - where exogenous genes are administered orally for therapeutic effects - can overcome these problems. Viral vectors risk random integration and limit the size of the delivered gene; non-viral gene delivery,

although achieving only transient and low gene expression levels, overcomes these drawbacks. To date, oral gene delivery using chitosan (Ch), a cationic, mucoadhesive, polysaccharide and DNA nanoparticles for treatment of hemophilia A has shown disease improvement from a severe to a mild state ^{51,52}, which is effective but leaves much room for improvement. A more recent study showed effective oral gene delivery by creating a human factor IX (hFIX) plasmid with higher activity and improved tissue permeability, however, no modifications were made to the chitosan gene carrier ⁵⁵. We hypothesize that we can improve the efficiency of chitosan gene delivery by adding a small amount of protamine sulfate (PS), a highly cationic protein, to the Ch/DNA nanoparticles to ultimately improve *in vivo* transfection efficiency. Protamine sulfate has previously been used in gene delivery as a way to condense DNA ⁷²⁻⁷⁴, making a smaller, protected nanoparticle with increased DNA resistance to degradation by nucleases ⁷⁵. In addition to acting as a condenser, protamine is a desirable component based on its function in nature as a nucleus localizing peptide, helping the sperm of mature fish deliver genomic material into the nucleus during fertilization ^{76,77}, therefore indicating that it may have the potential to aid in guiding the plasmid DNA to the nucleus following cellular uptake. Protamine sulfate has also been used specifically as a tertiary component to enhance gene delivery by various non-viral gene carriers including lipid based vectors ^{72,74,78} as well as in quaternary complexes including fish sperm DNA and

stearic acid grafted chitosan oligosaccharides⁷⁶. An additional change that we have made to the standard composition of Ch/DNA nanoparticles used in other oral delivery studies was using low molecular weight (LMW) chitosan as opposed to high molecular weight (HMW) chitosan. LMW chitosan was chosen for its shorter length which is expected to decrease DNA entanglement and allow for more efficient release of DNA following cellular uptake. Stabilizing the nanocomplexes extracellularly through the use of protamine sulfate and increasing DNA release intracellularly with the use of shorter, low molecular weight chitosan will result in increased hFIX levels following transfection, which we show in both *in vitro* and *in vivo* studies.

3.2 Materials and methods

3.2.1 Ch/PS/DNA nanoparticle preparation

Ternary nanoparticles were formed by bulk mixing with a ratio of 5:1:5 (w:w:w) of plasmid DNA to protamine sulfate to low molecular weight chitosan (~30kDa, ~97% deacetylated) (Sigma-Aldrich, St. Louis, MO); chitosan was further deacetylated using a protocol similar to the described by No and Meyers⁷⁹. Briefly, 50% NaOH (w/w) was added at 100°C for 30 min using a solid to solvent ratio of 1:10 (w/v), the mixture was cooled over ice water, and vacuum filtered. Deacetylation amount was calculated using a pH titration method described by Zhang et. al.⁸⁰ where chitosan (~0.25g) was dissolved in hydrochloric acid (0.1 M, 20 mL), sodium hydroxide (0.1 M) was added to titrate the

solution, at least 4 values of pH were recorded to determine the degree of deacetylation. To form the Ch/PS/DNA polyplexes, plasmid DNA was mixed with protamine sulfate, chitosan was added while vortexing, and the dispersion was vortexed for 20 seconds and left at room temperature for 30 minutes. Chitosan and plasmid nanoparticles were formed by bulk mixing 1:1 (w:w) of chitosan to plasmid DNA; chitosan was added to the plasmid DNA while vortexing, vortexed for 20 seconds, and left at room temperature for 30 minutes. Chitosan was dissolved in 0.2 M sodium acetate buffer (pH 5.2) (Sigma-Aldrich) at a concentration of 1 mg/mL. Plasmid DNA and protamine sulfate were dissolved in water at 0.2 $\mu\text{g}/\mu\text{L}$ and 1 mg/mL, respectively. Particles were used immediately for *in vitro* experiments and lyophilized for *in vivo* use. Fresh nanoparticles were lyophilized after adding a 15% (w/w) solution of trehalose, dihydrate (Calbiochem, Billerica, MA) in water such that the v/v ratio of nanoparticles to 15% trehalose was 1:4. Nanoparticles plus trehalose were frozen immediately after preparation at -80°C and then lyophilized.

3.2.2 Copolymer synthesis

Random copolymers were synthesized from the purified monomers by mixing the appropriate amounts of each monomer in a brown reaction vial with 3 mL of 1:4 methanol:water at 45°C for 5 days under argon. 3 mL of pH 4 water was added to the reaction at room temperature and 6M HCl was added to the resulting solution until it

reached pH 4. The copolymer was collected by centrifugation using Ultra Centrifugal Filter Unit with a 3 kDa cutoff (EMD Millipore, Billerica, MA) and lyophilized for solvent removal. This lyophilized copolymer product was used for further copolymer analysis and for applications with nucleic acids.

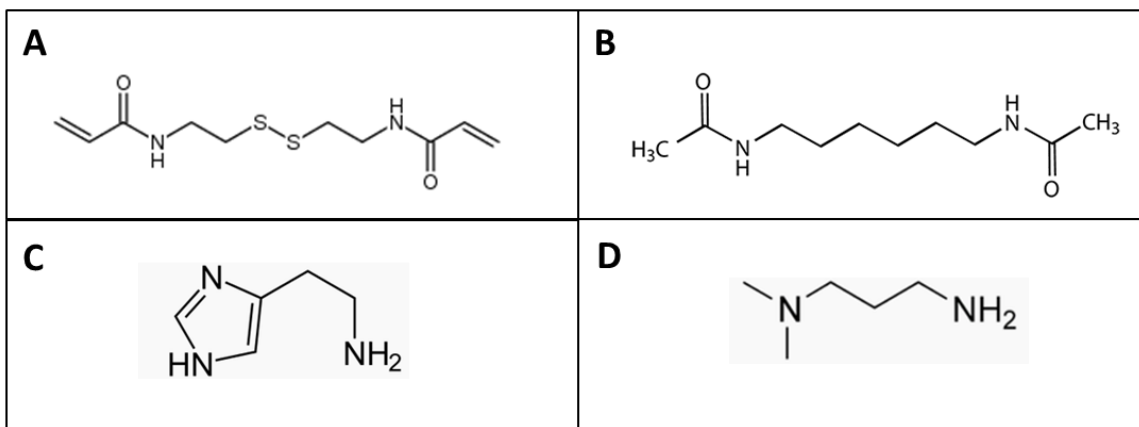


Figure 2: Backbone components of copolymers: (A) N,N'-cystaminebisacrylamide (CBA), (B) N,N'-hexamethalyne bisacrylamide (HMBA). Linker components of copolymers: (C) histamine (HIS), (D) 3-(dimethylamino)-1-propylamine (DMPA).

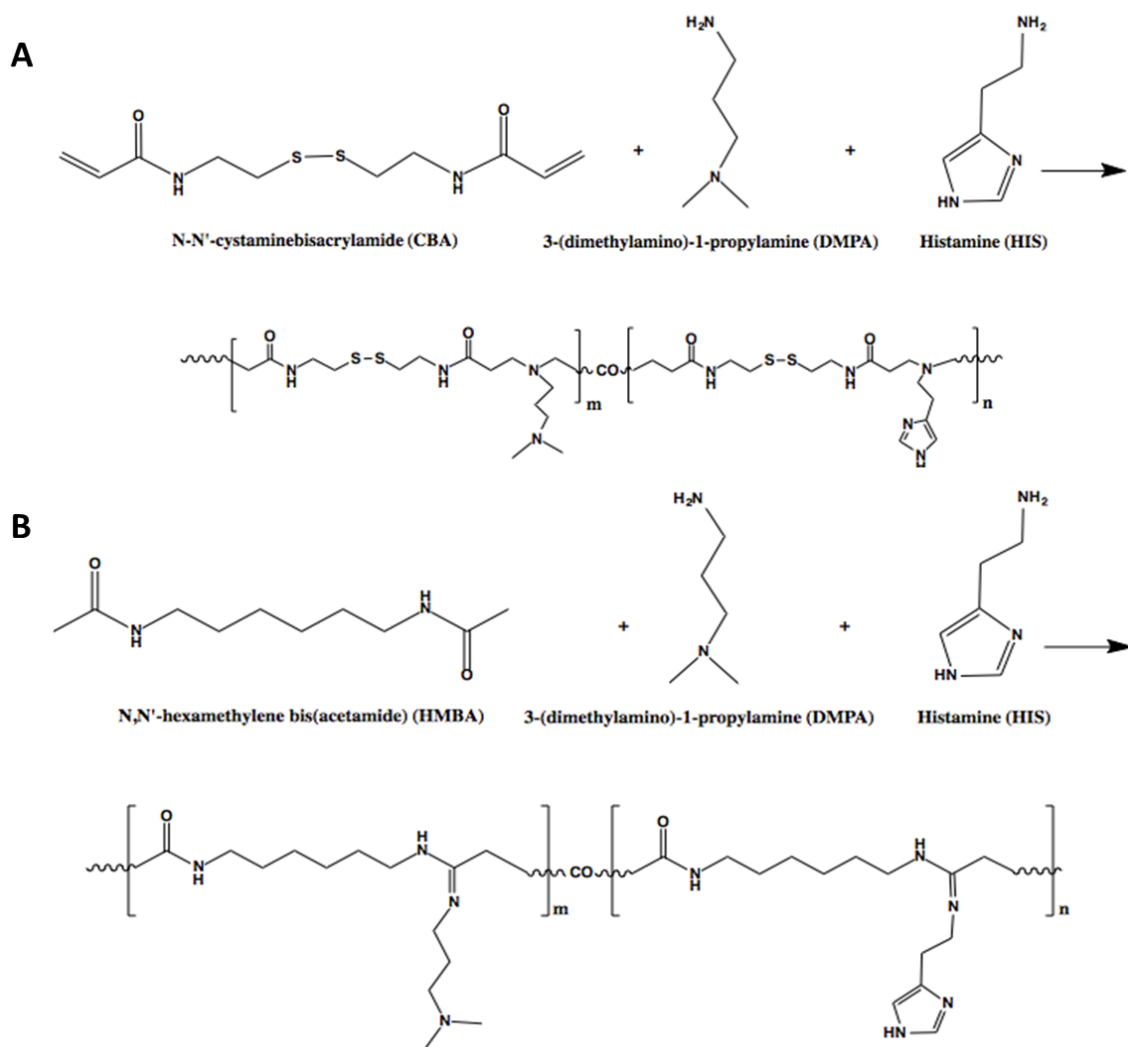


Figure 3: Schematic of reactions using CBA, HMBA, DMPA, and HIS. (A) Synthesis of bioreducible poly (amido amine) random copolymers using CBA as a backbone. (B) Synthesis of bioreducible poly (amido amine) random copolymers using HMBA as a backbone.

3.2.3 Copolymer nanoparticle formation

For copolymer/DNA nanoparticle formation, copolymer was added to the DNA and vortexed for approximately 20 sec. at DNA:copolymer weight ratios of 1:30 to 1:60. The DNA used was a pLuc plasmid and the output measured was luminescence quantified at 48 hrs after nanoparticle delivery by a Steady-Glo Luciferase Assay (Promega, Madison, WI). For copolymer/miRNA nanoparticle formation, copolymer was added to a miRNA mixture and vortexed for approximately 20 sec. at miRNA:copolymer weight ratios of 1:30 to 1:60. The miRNA was a mixture of 4 different miRNAs: 1, 133, 208, and 499 provided by the Dzau lab at Duke University. The effectiveness of the miRNA delivery system was determined by gene knockdown of twinfilin-1 measured 48 hrs after nanoparticle delivery.

3.2.4 Particle size and zeta potential

Particle size and zeta potential were determined immediately after nanoparticle formation using a Zetasizer Nano ZS90 (Malvern, Malvern, United Kingdom). All measurements were taken with the samples diluted in 1 mL of DI water.

3.2.5 DNA encapsulation and release

For DNA encapsulation, Ch/PS/DNA or Ch/DNA nanoparticles were prepared as described above using either pLuc or phFIX. A sample of the solution was taken from the fresh nanoparticles and a PicoGreen Assay (Thermo Fisher Scientific, Waltham, MA)

was used to determine the amount of free plasmid DNA in the solution. For DNA release, 2 µg of pLuc or phFIX in the form of Ch/PS/DNA were added to 200 µL of simulated gastric fluid (SGF). SGF at a pH of 1.2 was prepared by dissolving 2 g of sodium chloride and 3.2 g of purified pepsin (derived from porcine stomach mucosa) in 7 mL of hydrochloric acid, and then water was added to reach 1000 mL. The nanoparticles were incubated in SGF at 37°C for 0.25, 0.5, 1, 2, and 4 hrs. A PicoGreen Assay was used according to the manufacturer's protocol to determine the amount of DNA in solution after each time point.

3.2.6 *In vitro* cell experiments

All *in vitro* cell culture experiments were performed in serum containing media, HEK293 (ATCC) or Caco-2 (ATCC) cells were plated and nanoparticles were added 18-24 hrs later so that the final DNA concentration was 0.002 µg/µL. The nanoparticles were incubated with the cells at 37°C for 4 hrs, the nanoparticles were removed, fresh media was added to the cells, and the transfection efficiency was measured 48 hrs later using the Steady-Glo Luciferase Assay System (Promega). The initial *in vitro* screening process comparing 77% deacetylated chitosan and 97% deacetylated chitosan at various Ch/DNA ratios and Ch/PS/DNA ratios was done using a GFP plasmid in both HEK293 and Caco-2 cells. Transwell experiments were performed by plating 200 µL of 3x10⁵ Caco-2 cells/mL on the Transwell membrane (Corning, Corning, NY); the cells were

incubated for ~21 days until the TEER reached 260-450 Ωcm^2 . For the Transwell coculture model 90 μL of Caco-2 cells at 3×10^6 cells/mL and 100 μL of HT29MTX cells at 3×10^5 cells/mL were added to the upper chamber of the Transwell insert. Media was changed daily in the upper chamber (300 μL) and the lower chamber (600 μL) until the TEER reached 260-450 Ωcm^2 . In both Transwell models, after validating monolayer formation, HEK 293 cells were plated in the bottom chamber, and ~18-24 hrs later, nanoparticles were added for 4 hrs to the upper chamber of the Transwell. Factor IX activity was determined using a Biophen FIXa assay (Aniara, West Chester, OH) and FIX mRNA was quantified with qPCR using the following primers:

CAGTTCCAGAAGGGCAATGT and CGCAGGTTGTTTTGAATGGT.

3.2.7 *In vivo* experiments

For *in vivo* experiments, mice were administered a total of 200 μg (for luciferase studies) or 600 μg (for all hFIX studies) of lyophilized nanoparticles re-suspended in water via oral gavage. Delivery of luciferase plasmid (pLuc) was conducted with 6 nude mice where 2 mice were administered water alone and 4 mice were administered the Ch/PS/pLuc nanoparticle solution in a single dose. Luciferase levels were measured 48 hrs after nanoparticle administration using IVIS imaging (Caliper/Xenogen, Hopkinton, MA). Delivery of human factor IX plasmid (phFIX) was conducted with both BALB/c mice and hemophilic B knock-out mice (C3H background). In BALB/c mice experiments

8 mice were given Ch/phFIX, 8 mice received Ch/PS/phFIX, and 4 mice remained untreated by receiving an equal volume of water via oral gavage. In hemophilic B mice experiments, 4 mice were given Ch/phFIX, 4 mice received Ch/PS/phFIX, 2 mice were administered Ch/PS/pLuc as a sham plasmid control, and 1 mouse was left completely untreated. These mice were given a 600 µg DNA dose of nanoparticles over a 5 day period, therefore receiving 120 µg of plasmid DNA per day in the form of a nanoparticle, and the final blood draws and organ removal were done 72 hrs after the final nanoparticle dose was administered. Human factor IX levels in mice plasma were determined using a hFIX ELISA with a Monoclonal Anti Human Factor IX Clone HIX-1 capture antibody (Sigma-Aldrich) and goat anti-human FIX Affinity Purified HRP (Affinity Biologicals, Ancaster, ON Canada) as the detection antibody. Organs were collected, fixed in 10% formalin for 48 hrs at 4°C, embedded in paraffin, followed by immunohistochemistry analysis using Anti-Factor IX antibody (Abcam, Cambridge, United Kingdom).

3.3 Results

3.3.1 (A) Development of polycationic gene carriers

Various combinations of PS and LMW chitosan were screened in HEK293 cells using either an eGFP plasmid (pGFP) or a luciferase plasmid (pLuc) for transfection efficiency. The first round of screening was done with two different degrees of

deacetylation of LMW Ch, 77% and 97%, with different Ch/DNA weight ratios, Figure 4.

This screening was done to determine which Ch/DNA ratio to move on to the next experiment where we added protamine sulfate.

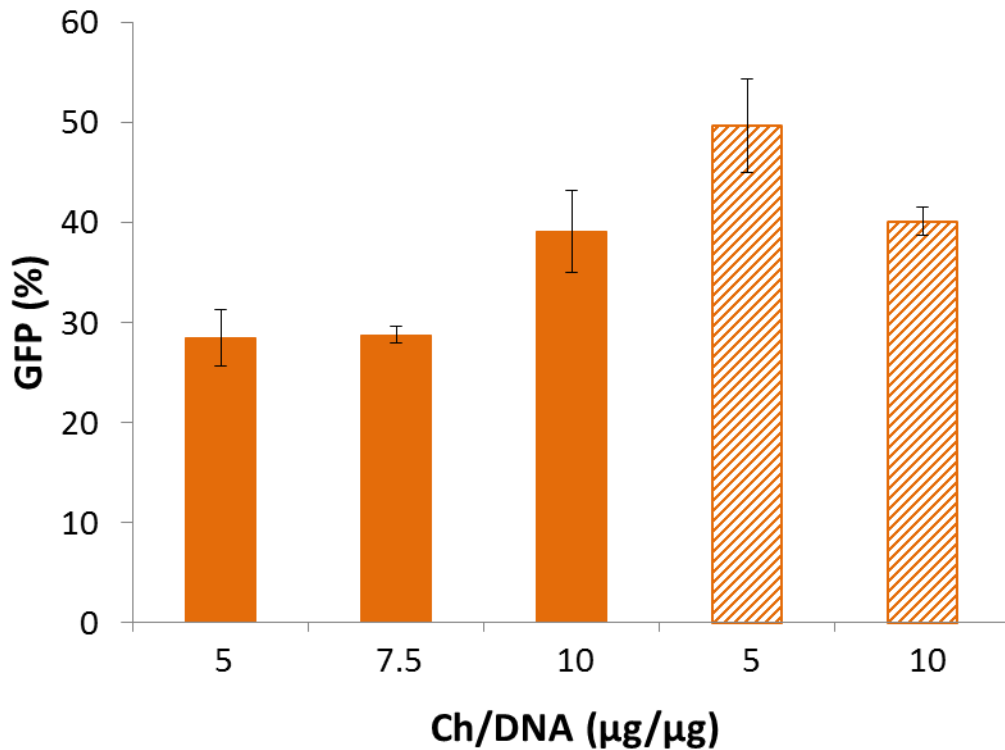


Figure 4: Initial screening of LMW chitosan for transfection of HEK293 cells using pGFP as the DNA component. Solid bars represent nanoparticles made with 97% deacetylated LMW chitosan. Striped bars represent nanoparticles made with 77% deacetylated LMW chitosan. (n=3)

Although not significant, the weight ratio of 10/1 in the 97% DA chitosan and the 5/1 weight ratio in the 77% DA chitosan trended towards best transfection efficiency and both of these ratios of Ch (77% and 97% DA) to DNA were taken forward to the next

screening. In the next screening, various amounts of PS were integrated into the particles and they were tested for transfection efficiency in two different cell lines, Hek293 and Caco-2, a human colon carcinoma cell line that is commonly used as a model for intestinal cells⁸¹. The results from this screening (Figure 5) determined that the best combination of Ch/PS/DNA was 10 μ g/2 μ g/2 μ g using the 77% deacetylated chitosan.

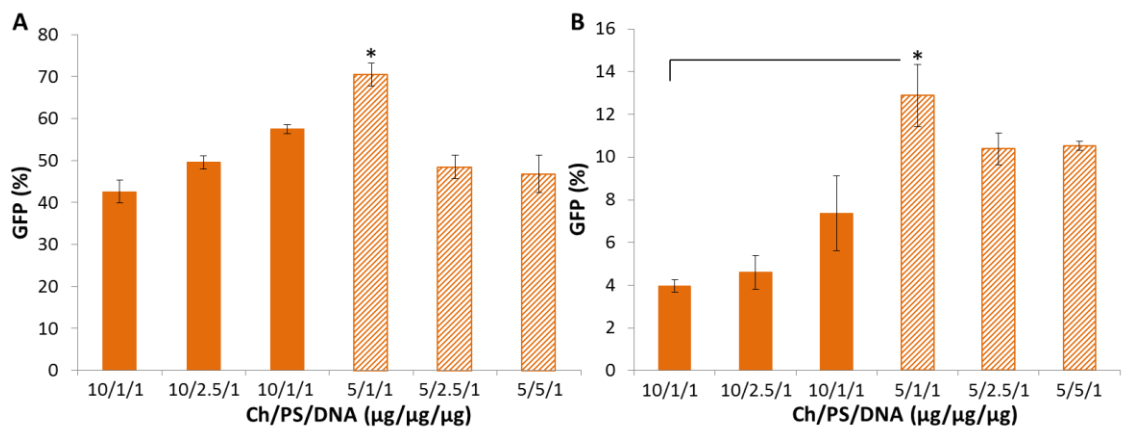


Figure 5: Screening of Ch/PS/pGFP nanoparticles in HEK293 (A) and Caco-2 (B) cell lines. Solid lines represent 97% deacetylated LMW chitosan. Striped lines represent 77% deacetylated LMW chitosan. (n=3)

The nanoparticles were sized and the overall charge was measured. The size of Ch/PS/DNA ranged from ~200-500 nm (Figure 6A), a size that is consistent with the nanoparticles used for other oral gene delivery applications, which show an average particle size of ~300 nm⁵² and 200-400 nm⁵¹. The Ch/DNA nanoparticles had a slightly larger size ranging between ~500-600 nm. The smaller diameter of the Ch/PS/DNA

indicates that the PS is aiding in tighter DNA condensation. The zeta potential shown in Figure 6B demonstrates the overall charge of the nanoparticles; both are positively charged around 30 mV. The overall positive charge of both formulations indicates that the polycations are covering the exterior of the nanoparticle, therefore protecting the inner DNA contents.

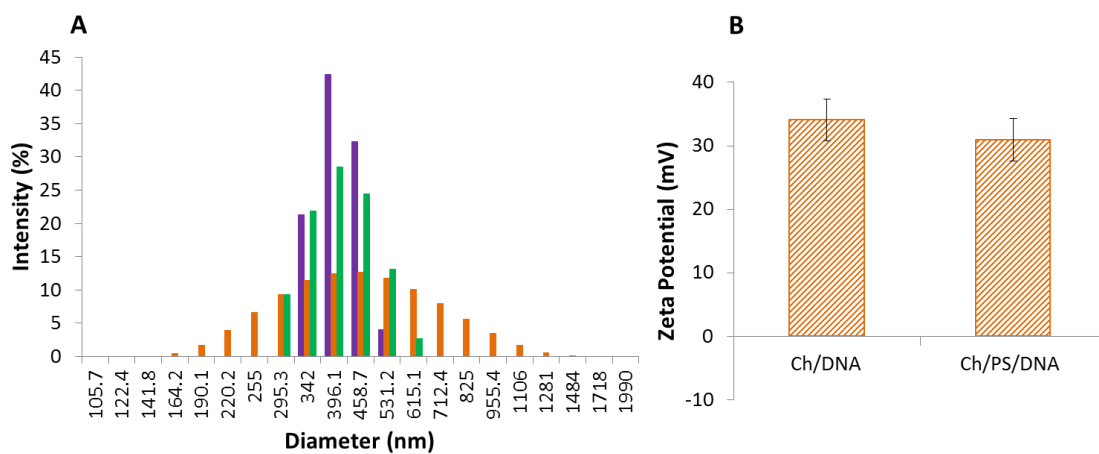


Figure 6: Nanoparticle characterization using pLuc DNA: (A) nanoparticle size distribution of Ch/PS/phFIX, each color distribution represents a separate nanoparticle preparation. The average diameter is 456 ± 49 nm. (B) Average nanoparticle zeta potential, (n=3).

The nanoparticles were further characterized by DNA encapsulation efficiency and DNA release. The encapsulation efficiency of Ch/PS/DNA nanoparticles was significantly higher than that of Ch/DNA nanoparticles, almost 100% versus ~94% (Figure 7A). For efficient oral gene delivery, the nanoparticles must be stable in the stomach and retain their contents so that they can be intact when uptaken by cells in the

intestine. This makes the stability of the nanoparticles in gastric fluid important for successful delivery. DNA release was measured in simulated gastric fluid (SGF) by incubating Ch/PS/DNA nanoparticles at 37°C in SGF for a total of 4 hrs, the maximum time that the nanoparticles are expected to remain in the stomach. Less than 10% of the original amount of DNA added to the nanoparticles was lost over 4 hrs in the SGF, Figure 7B. This indicates that the Ch/PS/DNA nanoparticles are stable in SGF at 37°C over 4 hrs.

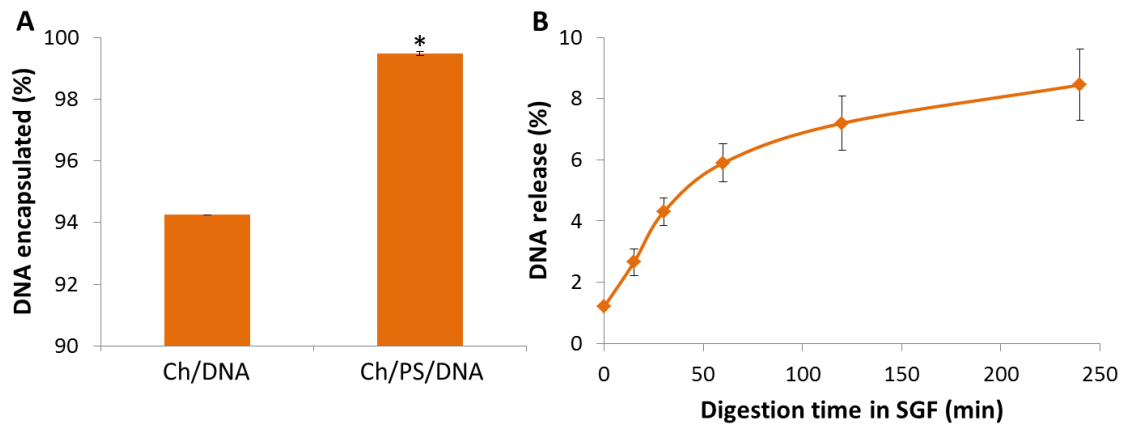


Figure 7: (A) DNA encapsulation of bulk made nanoparticles, (n=3). (B) DNA release from Ch/PS/DNA nanoparticles after incubation in simulated gastric fluid (SGF) at 37°C for 4 hrs, (n=3).

The cell viability in HEK293 cells after treatment with Ch/PS/DNA nanoparticles was compared to the cell viability after treatment with Lipofectamine 2000, a commercially available lipid gene carrier that is too toxic for *in vivo* applications but has consistently high levels of transfection. The results illustrate that Ch/PS/DNA

nanoparticles are less toxic than Lipofectamine nanoparticles in HEK293 cells, Figure 8.

Overall the HEK293 cells retain ~85-90% cell viability after 4 hrs of exposure to the nanoparticles, indicating relatively low nanoparticle toxicity.

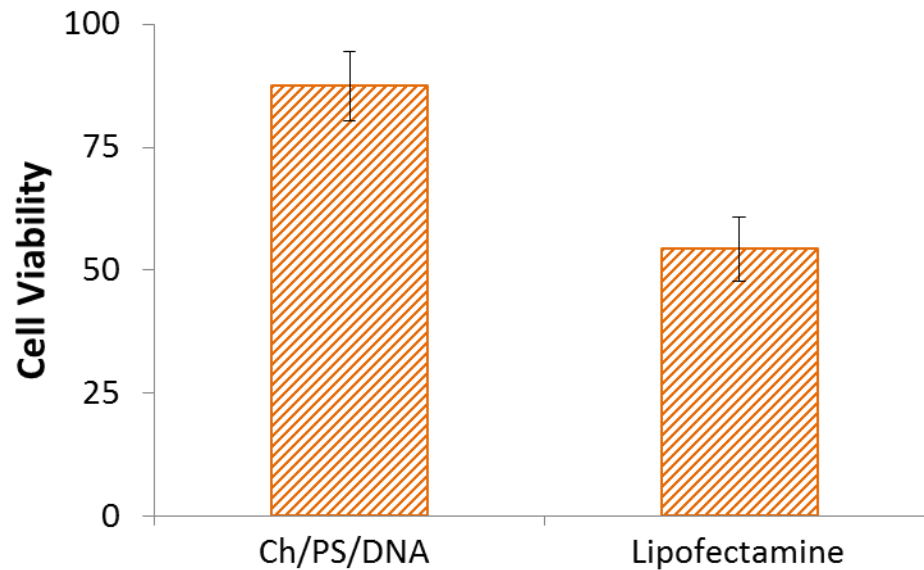


Figure 8: Cell viability of Ch/PS/DNA nanoparticles, where DNA is pLuc, as compared to Lipofectamine/pLuc polyplexes in HEK293 cells (n=3).

After confirming minimal toxicity of the nanoparticles, the Ch/PS/DNA polyplexes were tested using a plasmid other than pGFP in order to validate their utility to express different genes. The optimal Ch/PS/DNA nanoparticle formulation of 10 μ g/2 μ g/2 μ g was compared to Ch/DNA at its optimal formulation of 10 μ g/2 μ g using a luciferase plasmid, pLuc, to express the luciferase protein which is subsequently detected by luminescence. Figure 9A shows luciferase expression in HEK293 cells following nanoparticle delivery and Figure 9B shows luciferase expression in Caco-2

cells after the same treatment. The results show Ch/PS/DNA being ~800,000 times better than Ch/DNA in HEK293 cells and ~600 times better in Caco-2 cells.

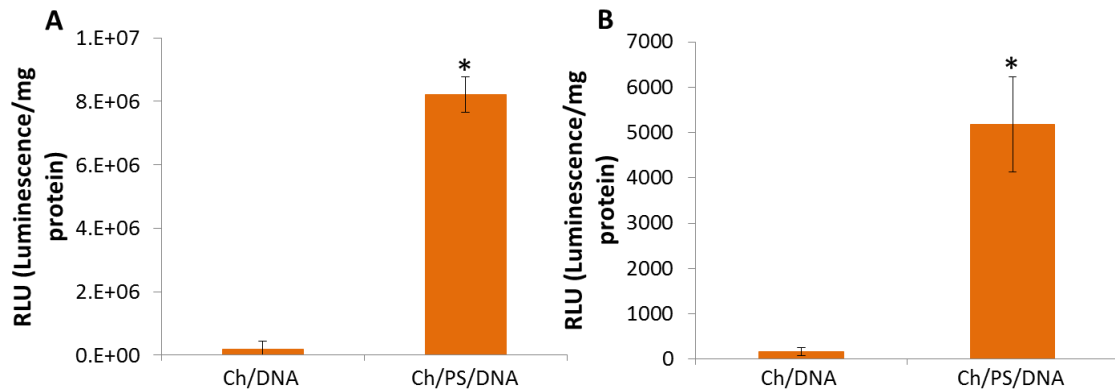


Figure 9: Transfection efficiency, represented by RLU, using pLuc as DNA in Ch/PS/DNA nanoparticles compared to Ch/DNA nanoparticles in (A) HEK293, (n=5) and (B) Caco-2 cell lines, (n=5).

Copolymers were screened for gene delivery in HEK293 and Caco-2 cells by forming nanoparticles at different DNA:copolymer ratios ranging from 1:30-1:60. HEK293 cells were chosen because they are a cell line that is easy to transfect and would demonstrate initial efficacy of the nanoparticles made with the newly synthesized copolymers. The DNA used for screening was the luciferase plasmid (pLuc) and transfection efficiency was quantified by luciferase expression. The following copolymers were screened in HEK293 cells: 3, 8, 13, 18, 23, and 28, their compositions are described in Table 1. The most successful copolymers for gene delivery were found to be 3 and 8 (Figure 10) and these copolymers were moved forward into miRNA delivery.

Table 1: Molar ratios of copolymer components according to copolymer number. Molar ratios are separated by backbone components (CBA/HMBA) and linker components (HIS/DMPA).

Copolymer #	CBA	HMBA	HIS	DMPA
3	10	90	50	50
8	30	70	50	50
13	50	50	50	50
16	70	30	50	50
23	100	0	50	50
28	0	100	50	50

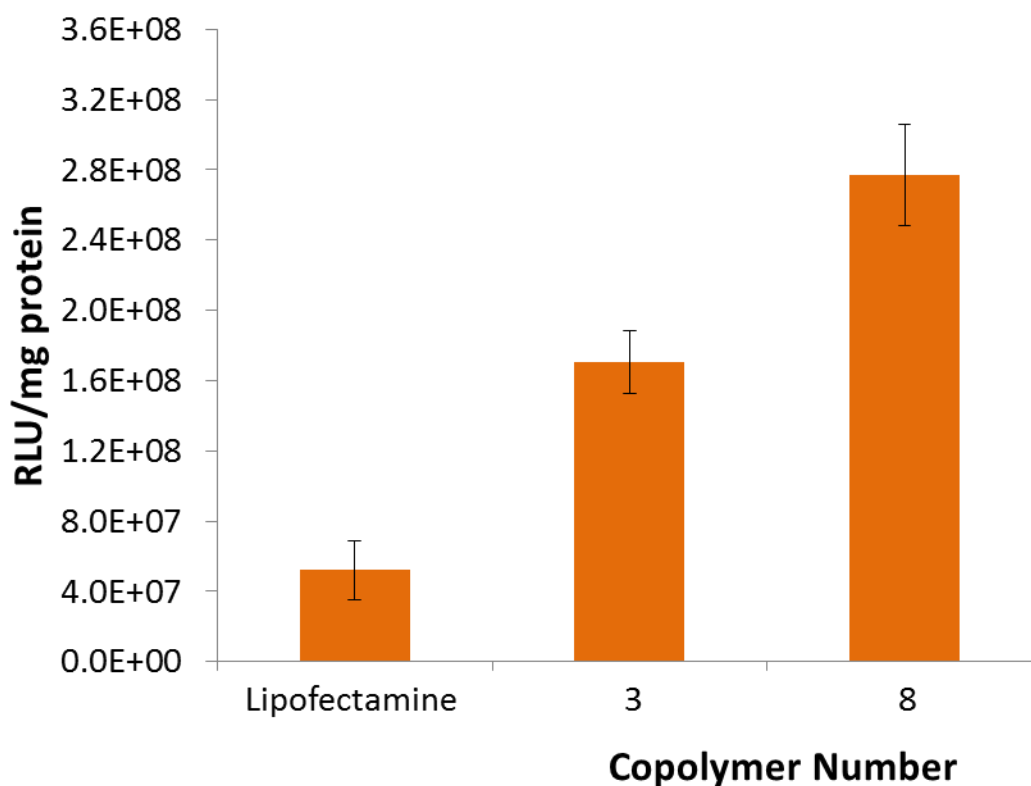


Figure 10: Transfection efficiency in HEK293 of copolymer 3 (backbone molar ratio: 1/9 CBA/HMBA; linker molar ratio: 1/1 HIS/DMPA) and 8 (backbone molar ratio: 3/7 CBA/HMBA; linker molar ratio: 1/1 HIS/DMPA) compared to Lipofectamine 2000, (n=3).

Testing of the copolymers for miRNA delivery was done in collaboration with the Dzau lab to determine if direct reprogramming of fibroblasts could be done with a non-viral delivery platform. Copolymers were screened for miRNA delivery by forming nanoparticles at different miRNA:copolymer ratios ranging from 1:30-1:60. Transfection was tested in mouse primary fibroblasts using a single dose of nanoparticles. Gene knockdown of twinfilin-1 was measured 48 hrs after nanoparticle administration. Twinfilin-1 is an actin-binding protein that regulates cytoskeleton structure and dynamics. Overexpression of twinfilin-1 is associated with low levels of miRNA-1 therefore successful miRNA delivery can be determined directly by measuring the decrease in twinfilin-1. The results in Figure 11 show the effective nanoparticle delivery as demonstrated by twinfilin-1 knockdown.

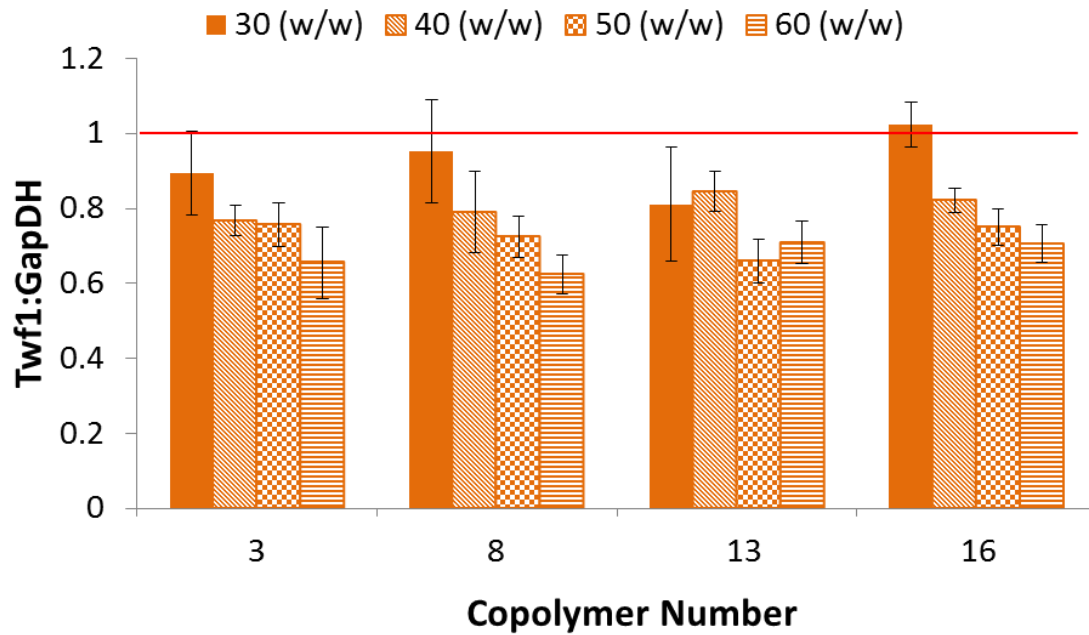


Figure 11: Twinfilin-1 (Twf1) knockdown in primary mouse fibroblasts after miRNA nanoparticle delivery at different miRNA (μg):copolymer (μg). All linker molar ratios DMPA/HIS 1/1, copolymer 3, 8, 13, 16 backbone molar ratios (CBA/HMBA): 1/9, 3/7, 1/1, 7/3, (n=3).

3.3.2 (B) Non-viral oral gene delivery for the treatment of hemophilia B

After demonstrating higher transfection efficiency with the Ch/PS/DNA nanoparticles using model genes, pGFP and pLuc, nanoparticles made with phFIX were tested to show that the hFIX plasmid could be encapsulated, protected, and delivered by the Ch/PS/DNA carrier and to determine if functional protein could be produced following delivery with these particles. We obtained an hFIX plasmid with a CMV

promoter from the Herzog lab at the University of Florida. Transfection with Ch/PS/phFIX resulted in detectable levels of functional hFIX protein and these levels were significantly higher than the hFIX protein levels achieved after Ch/phFIX transfection in HEK293 cells, Figure 12. To translate this to a more relevant cell type, the hFIX protein levels were measured following transfection in Caco-2 cells as well, Figure 13. To provide a comparison for protein production in Caco-2 cells, a commercially available polymer based nanoparticle formulation of EZPLEX and the phFIX was added to the experiment. All three particle types: Ch/PS/phFIX, Ch/phFIX, and EZPLEX had detectable levels of functional hFIX, indicating that the hFIX plasmid could be delivered and expressed by this cell type.

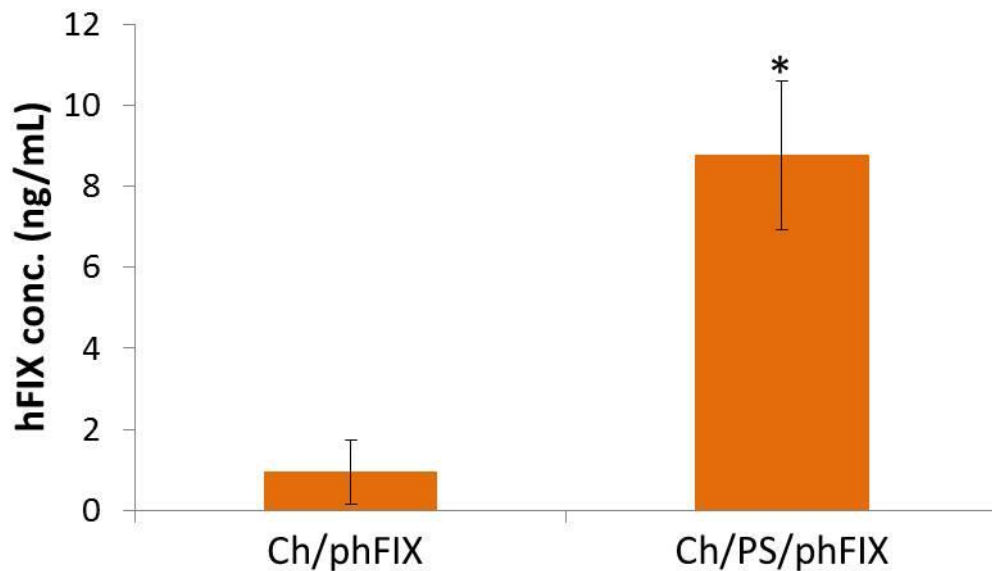


Figure 12: Functional hFIX protein levels after *in vitro* transfection in HEK293 cells, (n=3).

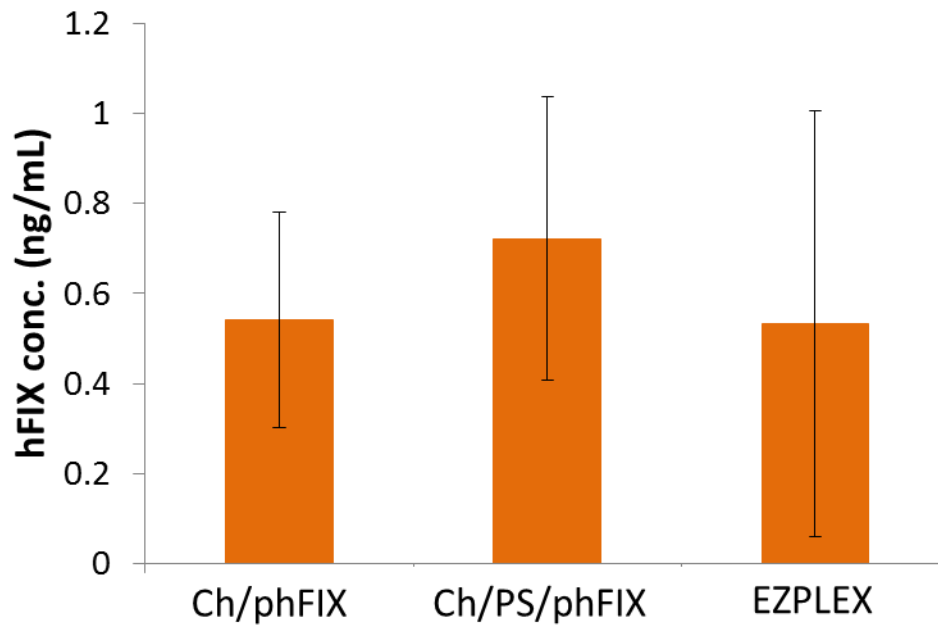


Figure 13: Functional hFIX protein levels after *in vitro* transfection in Caco-2 cells. EZPLEX is a commercially available polymer for gene delivery, (n=3).

To model the transfection efficiency in the polarized small intestine cell lining, the Transwell setup shown in Figure 14 was used. This model is a great *in vitro* method to show potential intestinal delivery as the upper chamber represents the intestinal lumen, the Caco-2 monolayer models the intestine itself, and the lower chamber represents systemic blood circulation. The nanoparticles, either Ch/PS/phFIX or Ch/phFIX, were administered to the apical side of the Caco-2 monolayer, into the well of the Transwell insert. Functional hFIX was detected in both the upper and lower chambers of the Transwell following nanoparticle administration, Figure 15. The hFIX in the upper chamber was due to transfection of the Caco-2 cell in the monolayer of the

Transwell insert; however, it was not clear if the Caco-2 cells or the HEK293 cells were responsible for the hFIX detected in the lower chamber. To determine which cells were expressing the protein, qPCR was performed on both the Caco-2 cells in the monolayer and the HEK293 cells on the basolateral side of the monolayer following transfection. The qPCR results showed that the highest hFIX mRNA levels were found in the Caco-2 cells (Figure 16) therefore indicating that the Caco-2 cells were the cells that were being transfected and most of the protein being detected in the lower chamber was due to transfection of the Caco-2 monolayer and release of the protein onto the basolateral side of the Transwell insert. These same results were confirmed in a coculture Transwell model (Figure 17). This confirms the potential of the desired *in vivo* outcome which involves transfection of the intestinal cells and the release of functional hFIX protein on the basolateral side of the intestine, increasing bioavailability.

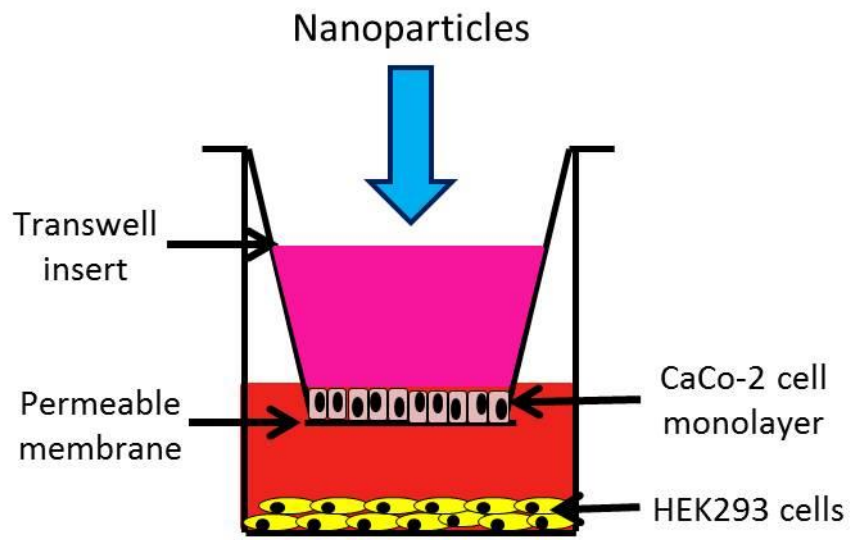


Figure 14: Schematic of the Transwell system.

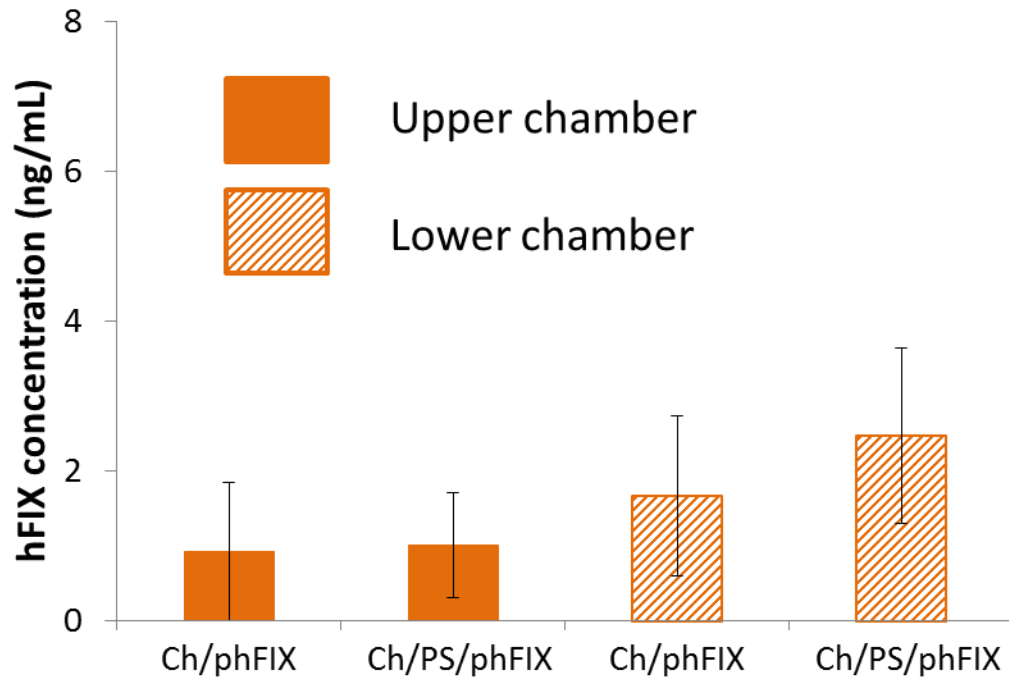


Figure 15: Functional hFIX protein levels after *in vitro* transfection in the Transwell model. “Upper chamber” represents functional hFIX detected in media from the upper chamber; “Lower chamber” is from media withdrawn from the lower chamber, (n=3).

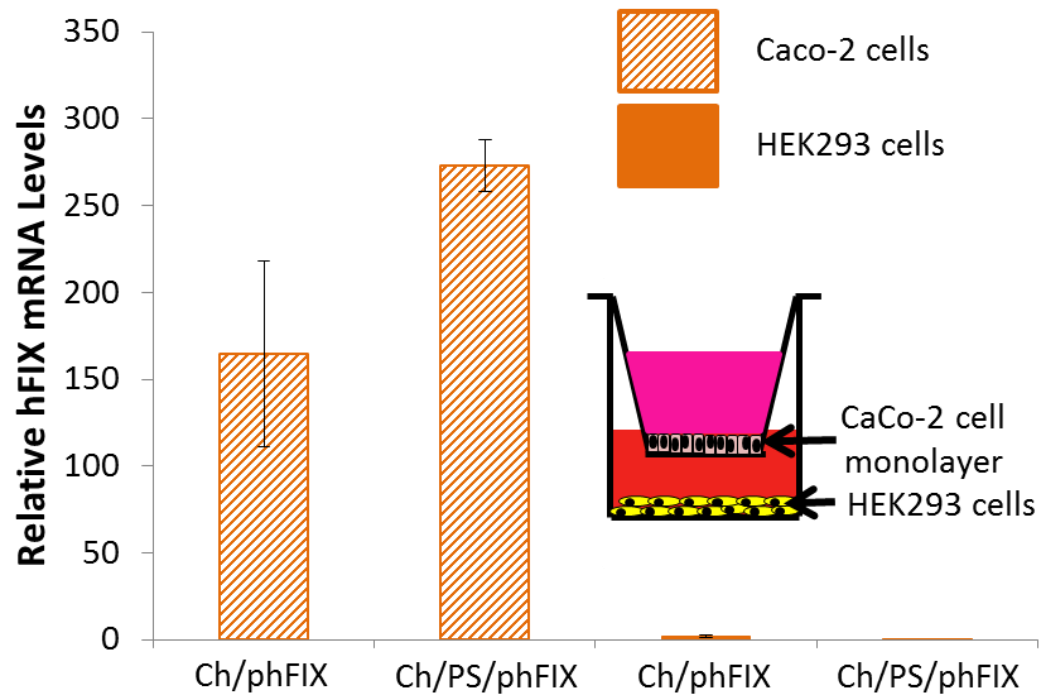


Figure 16: hFIX mRNA levels in Caco-2 cells and HEK293 cells following administration of nanoparticles to the upper chamber of the Transwell model, relative to untreated controls.

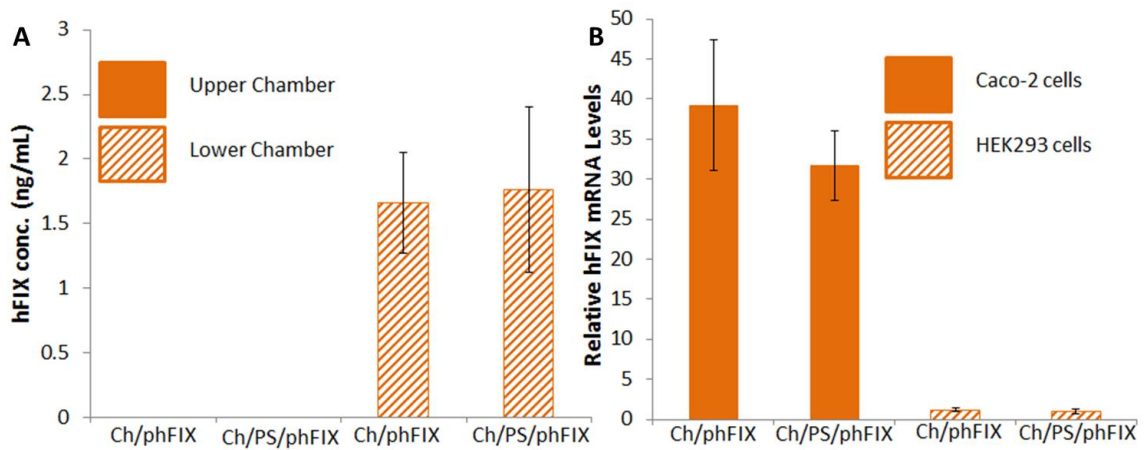


Figure 17: (A) Functional hFIX protein levels after *in vitro* transfection in the Transwell coculture model. “Upper chamber” represents functional hFIX detected in media from the upper chamber; “Lower chamber” is from media withdrawn from the lower chamber, (n=3). (B) hFIX mRNA levels in Caco-2 cells and HEK293 cells following administration of nanoparticles to the upper chamber of the Transwell coculture model, relative to untreated controls.

After *in vitro* validation, we moved on into preliminary studies in mice. A preliminary study using Ch/PS/pLuc nanoparticles was performed by delivering a single 200 μ g dose via oral gavage to nude mice. IVIS imaging was used to detect luciferase transfection 48 hrs after the nanoparticle feeding. Results showed that 1 out of 4 mice had luciferase expression (Figure 18), specifically in the intestine and the stomach, indicating the potential for functional protein production following oral delivery of Ch/PS/DNA nanoparticles. Additionally, because we used a single dose, there was potential for increased protein production by adding additional doses.

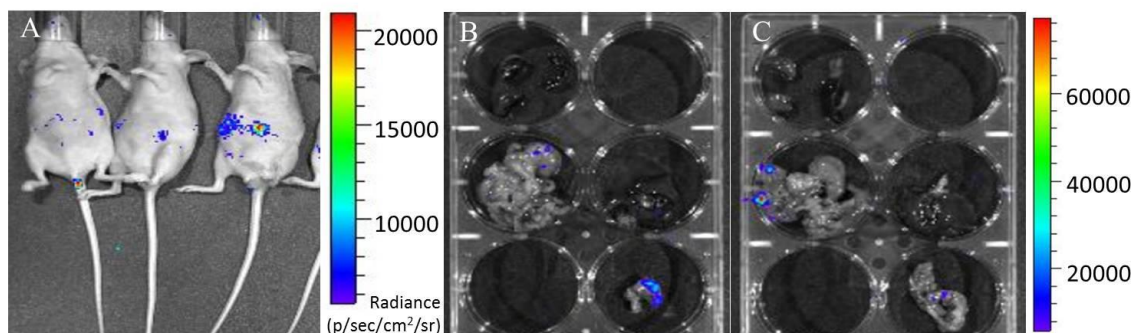


Figure 18: IVIS images detecting luciferase expression in nude mice following: (A) control 1, control 2, Ch/PS/pLuc treated; intestines from (B) control 2 and (C) treated, from left to right: kidneys and spleen, blank, intestines, liver, blank, stomach.

Further animal studies addressed hFIX protein production deficiencies by testing the oral administration of Ch/PS/phFIX and Ch/phFIX nanoparticles in BALB/c and hemophilic B mice. Results from BALB/c mice demonstrated that Ch/PS/phFIX nanoparticles achieved detectable hFIX protein levels in the blood of 3 out of 8 mice, ranging from 3.3 ng/mL to 34.3 ng/mL, whereas untreated mice showed no detectable hFIX protein and Ch/phFIX treated mice showed marginal detection of hFIX protein, 2.2 ng/mL, in 1 out of 8 mice (Figure 19B). Immunohistochemistry (Figure 18A) of segments of the small intestine and the liver 72 hrs after the last oral administration of nanoparticles showed the presence of hFIX in both organs of mice treated with Ch/PS/phFIX and Ch/phFIX, with Ch/PS/phFIX treated mice appearing to have higher FIX protein levels, whereas no detectable hFIX levels were seen in the untreated mice. In

addition to testing in BALB/c mice, a smaller population of hemophilic B mice was used to test the nanoparticles in a more clinically relevant model. This study showed that 2 out of the 4 mice treated with Ch/PS/phFIX nanoparticles had detectable hFIX protein in their blood as compared to Ch/phFIX, untreated, and Ch/PS/pLuc (used as a sham nanoparticle) which had no detectable hFIX protein levels in their blood (Figure 19C).

3.4 Discussion

3.4.1 (A) Development of polycationic gene carriers

There are two important characteristics of chitosan that influence its effectiveness as a nucleic acid carrier: molecular weight and deacetylation. The molecular weight is dependent on the number of repeated glucosamine units per molecule⁸². High molecular weight chitosan has been widely used as a gene carrier^{29,51,52,54} due to its potential for higher positive charge and stability, however, higher nanoparticle stability leads to problems of DNA unpacking which can reduce final DNA expression levels⁸³. Additionally, higher molecular weight chitosan may also lead to increased toxicity in humans due to liver accumulation and higher charge density^{83,84}; although this problem may be circumvented when delivering nanoparticles orally instead of intravenously. For these reasons and based on gene delivery testing, studies have shown that low molecular weight (LMW) chitosan is superior to high molecular weight chitosan for gene delivery^{83,85,86}. Based on this logic, we attempted to increase final protein production after oral gene delivery using a nanoparticle made with LMW chitosan. The nanoparticles were optimized for chitosan to DNA ratio to determine the best conditions for a LMW chitosan nanoparticle. Because the ternary component is meant to enhance the gene delivery, the best Ch/DNA combination was used to test the effect that protamine sulfate optimization had on transfection efficiency. The ratio of 5/1/1

Ch/PS/DNA with 77% DA chitosan was significantly better in both HEK293 and Caco-2 cell lines and therefore it was the nanoparticle chosen for all subsequent experiments.

Further characterization of the nanoparticles showed that the Ch/PS/DNA nanoparticles only released ~8% of the DNA contents over a 4 hr period in simulated gastric fluid. This is important because upon ingestion, contents remain in the stomach for approximately 4 hrs⁸⁷ before traveling to the small intestine where the nanoparticle uptake/transfection should occur. Because of the well-known biocompatibility of chitosan^{84,88,89}, the toxicity of our Ch/PS/DNA nanoparticles was only screened in HEK293 cells at the *in vitro* testing dose and this showed minimal toxicity.

Although chitosan is a successful carrier for oral gene delivery, it has limited transfection efficiency when applied systemically. In order to investigate nanoparticles for transfection following systemic delivery, polycationic copolymers were synthesized to emphasize specific characteristics that are important in gene delivery. One of the most crucial elements in nucleic acid delivery is the balance between stability of nanoparticles extracellularly and the ability to release nanoparticle contents once uptaken by cells. To address this issue, we synthesized a copolymer library that varied the biodegradability of the backbone components by using CBA, which contains a disulfide bond that is degradable in the lysosome, and HMBA, which is not biodegradable⁹⁰. The copolymers also integrated two different backbone linking

monomers, HIS and DMPA. HIS provided an imidazole component which is associated with the proton sponge effect causing endosomal rupture and nanoparticle release into the cytoplasm, while DMPA provided primary and tertiary amines to aid in DNA condensation ⁹¹. Varying the molar ratio of each of these components allowed us to create a small copolymer library that was screened for plasmid DNA and miRNA delivery. miRNA delivery differs from gene delivery in that miRNA do not need to reach the nucleus, but can have the desired effect in the cytoplasm.

Although we suspected that the optimal carrier for plasmid DNA and miRNA would be different, it appeared that carriers that worked best for plasmid DNA delivery also successfully delivered miRNA. For gene delivery, copolymers 3 and 8 had the best transfection efficiency (the data from the other copolymers tested was not shown), even surpassing that of the commercially available, gold standard Lipofectamine 2000. Both successful gene carriers, copolymers 3 and 8, have backbones with more HMBA, giving the copolymer (and subsequent nanoparticle) more stability with only low levels of biodegradability resulting from the presence of CBA. For the linker components, they both have equal amounts of DMPA and HIS, giving the formulated nanoparticles equal amounts of condensing and buffering capabilities, therefore protecting the DNA cargo while allowing for endosomal escape. Although there was some Twf1 knockdown with nanoparticles made from copolymers 3, 8, 13, and 16 with the miRNA combination, the

knockdown was not impressive and high amounts of polymer:miRNA weight ratios, 60:1 at the maximum, were required to reach minimal knockdown levels, which were determined to be too low for downstream effects *in vivo*⁷⁰. Therefore, these copolymers were determined not ideal for miRNA delivery. Further studies with these copolymers were not pursued because the copolymers had high batch to batch variation and were highly unstable, making long term storage impossible.

3.4.2 (B) Non-viral oral gene delivery for the treatment of hemophilia B

The size of Ch/PS/DNA ranged from ~200-500 nm, which is consistent with other oral gene delivery applications using chitosan that have average particle sizes of ~300nm⁵² and 200-400nm⁵¹. The Ch/DNA nanoparticles that we used as comparison in all of the studies have a slightly larger size range ~500-600 nm, demonstrating that they might not be condensing the DNA as well as the Ch/PS/DNA nanoparticles that have the addition of protamine sulfate aiding in condensation. The size of the Ch/PS/DNA nanoparticles is notably ideal for phagocytosis, which has been shown to increase as nanoparticles increase in size from ~100-1000 nm⁹². Phagocytosis is highly relevant in oral gene delivery because of the presence of M cells in the Peyer's Patch of the intestine that increase the transcytotic transport of nanoparticles through the endothelial layer⁹³. For these reasons, it is evident that the size of the Ch/PS/DNA nanoparticles is viable for effective oral gene delivery.

To make the first steps towards treating hemophilia B, an hFIX plasmid was tested in our nanoparticle platform to validate the functionality of the plasmid when delivered by Ch/PS/phFIX. Both HEK293 and Caco-2 cells could stably express functional hFIX protein following nanoparticle delivery, however, only in the HEK293 cells was there significantly higher functional hFIX levels from Ch/PS/phFIX delivery as opposed to Ch/phFIX. This is most likely due to the ease of transfection in the HEK293 cells allowing the difference in transfection efficiency between Ch/PS/DNA and Ch/DNA nanoparticles to be easily observed. In the Caco-2 comparison, the transfection efficiency of particles made with EZPLEX was shown alongside Ch/PS/DNA and Ch/DNA. With a pLuc plasmid in HEK293 cells, the EZPLEX nanoparticles performed significantly better than both the Ch/DNA and Ch/PS/DNA nanoparticles (data not shown). When comparing the functional hFIX levels following transfection with the aforementioned nanoparticles, there was no significant difference, indicating the difficulty in transfecting Caco-2 cells as compared to HEK293 cells. This points at the difficulty in transfecting the cell types in the GI tract and highlights the challenge of developing oral gene delivery carriers. The Ch/PS/DNA nanoparticles are able to compete with the transfection levels achieved by one of the most effective commercially available gene carriers in Caco-2 cells, therefore showing its potential as a gene carrier in the oral setting.

CaCo-2 monolayers can be grown in a monolayer in a Transwell setup to model the passage of the nanoparticles through the epithelial layer. The Transwell model provides a system that allows insight into the transport of the nanoparticles through the model epithelial layer. In the Transwell experiments, the CaCo-2 monolayer was grown on the upper membrane and HEK293 cells were seeded on the bottom well to measure transfection in both the cells on the upper membrane and those plated on the bottom of the well. A different variation of the Transwell model involves the coculture of CaCo-2 cells and a human adenocarcinoma cell line, HT29-MTX. This coculture system is used to model the mucus-secreting goblet cells, the second most prevalent cell type in the gut epithelium, providing a layer of mucus to represent the mucus layer that lines the intestine and to better model the nanoparticle transport in the system^{81,94}.

The Transwell model is effective because there is no crossover between the media in the upper chamber and the lower chamber; therefore all material exchange must occur through the Caco-2 monolayer. The formation of the Caco-2 monolayer was validated by measuring the trans epithelial electrical resistance (TEER) across the cell coated membrane⁹⁵. Typically, a higher TEER value is representative of a more compact cell layer while a decrease in TEER causes greater cell layer permeability⁹⁶. To confirm that the nanoparticles were not just passing through a damaged Caco-2 monolayer, the TEER was measured at 4 hrs and 24 hrs and confirmed to be above $260 \Omega\text{cm}^2$ ⁹⁵, the

minimal acceptable TEER value to model the Caco-2 monolayer. The Transwell experiments demonstrated that the Ch/PS/DNA nanoparticles were able to produce functional hFIX protein. Unfortunately there was no significant difference in the hFIX protein levels of cells treated with Ch/PS/DNA versus Ch/DNA. This is a similar trend to what was seen in the Caco-2 transfected cells, as such, we expected that the Caco-2 cells were the primary cell line being transfected. qPCR analysis of mRNA extracted from Caco-2 and HEK293 cells in the Transwell experiments validated that nearly all of the transfection occurred in the Caco-2 cells. This indicated that the nanoparticles were not being transported through the monolayer, but instead were uptaken by the Caco-2 monolayer cells, transfecting the cells, and releasing the hFIX protein on both the basolateral and apical sides of the monolayer. This demonstrated a promising outcome for *in vivo* experiments, that cells transfected in the intestinal wall monolayer could potentially release protein into the non-digestive space to reach blood circulation where the hFIX is required to have a therapeutic effect.

The first round of *in vivo* testing was done with a pLuc plasmid because the luminescence readout is simple and shows where the transfection is occurring. A single dose of 200 µg of plasmid DNA in the form of Ch/PS/DNA nanoparticles was given because that was the highest dose of nanoparticles we could give in the allotted volume without creating an overly viscous solution in which the nanoparticles would not

completely resuspend. We saw pLuc transfection in 1 out of the 4 mice given the Ch/PS/DNA nanoparticles; this was considered successful because this was a low overall dose at only one administration time. The luminescence showed that there was some transfection in the stomach; however, the highest amounts of transfection were seen in the intestine. The intestine is ideal for transfection because it is where nutrient uptake occurs, providing facile access to circulation. This was enough validation of efficacy to move forward into larger studies with the plasmid of interest, phFIX.

With normal hFIX physiological concentrations ranging from 3-5 $\mu\text{g}/\text{mL}$ ⁹⁷, our Ch/PS/phFIX nanoparticles are able to reach 0.1 – 4.4 % of physiological hFIX levels therefore showing the potential to correct a severe (<1%) or moderate (2-5%) form of hemophilia B⁶, assuming that the hFIX produced is active. Other studies testing high molecular chitosan of 250 kDa and 150-400 kDa chitosan, in an oral delivery platform with a FVIII plasmid were able to achieve a comparable range of 1-4% of normal functional FVIII protein in the blood over a 30 day period^{52,98}. Although the activity of the hFIX protein following *in vivo* administration was not tested in this study, we were able to detect comparable amounts of hFIX protein as those in studies using a recombinant adeno associated virus delivery system^{99,100}. The increased transfection efficiency of the ternary Ch/PS/phFIX oral delivery system is attributed to the increased

DNA condensation and therefore stabilization of the nanoparticles using protamine sulfate, a concept which has been validated in previous studies^{78,101,102}.

3.5 Conclusion

Non-viral gene carriers have a challenging task of protecting DNA extracellularly while allowing for DNA release once uptaken into cells. This is a balance that can be achieved by designing multifaceted copolymers or combining multiple components into one nanoparticle. The copolymers we designed showed promise in their gene delivery capabilities; however, the success of the gene carrier is not limited to merely transfection efficiency, but also therapeutic capacity. These copolymers were highly unstable when stored at -20°C and the batch to batch variation made it nearly impossible to replicate results. Although a more structured approach to copolymer synthesis can be done, it does not eliminate the instability of the copolymer. As such, we concluded that these copolymers were not ideal for therapeutic and systemic gene delivery or miRNA delivery.

The oral delivery studies using variations of chitosan nanoparticles indicate that the addition of the ternary component, protamine sulfate, to chitosan nanoparticles increased the efficacy of oral gene delivery using chitosan nanoparticles. The *in vivo* results show that the Ch/PS/phFIX nanoparticles effectively produce hFIX protein in the blood of ~42% of the mice following oral delivery, both BALB/c and hemophilic mice

inclusive. Although these mice do have detectable levels of protein, it should be noted that the amount of protein varies from as little as 3.3 ng/mL to as much as 34.3 ng/mL in the BALB/c mice and 8 ng/mL to 132 ng/mL in the hemophilic mice. Together, these results validate our hypothesis that the chitosan nanoparticle oral delivery platform can be improved with protamine sulfate, however, the results remain extremely variable *in vivo* and further optimization is needed for a viable oral gene therapeutic.

4. SPECIFIC AIM 2: Development and *in vitro* testing of nucleic acid scavenging nanofibers.

In this aim we develop a Nucleic Acid Scavenging Fiber (NASF) by electrospinning poly(styrene-*alt*-maleic)anhydride and covalently attaching polycationic polymers. These NASFs are used to remove nucleic acids from solution and dampen the corresponding inflammatory response.

4.1 Introduction and significance

Endogenous extracellular nucleic acids (eNA) can elicit pro-inflammatory responses by activating the innate immune system through the same pathways as pathogenic nucleic acids, such as viral RNAs and bacterial DNAs. Nucleic acids released by necrotic cells activate Pattern Recognition Receptors (PRRs), such as the Toll-like Receptors (TLRs) ⁵⁶⁻⁵⁸ leading to autoimmune reactions. TLR activation by endogenous eNA can be exacerbated by the formation of immune complexes where antibodies to the eNA or NA-protein complexes aid in cellular uptake, leading to increased cytokine production and prolonged immune activation. Various pro-inflammatory autoimmune diseases are thought to proceed in this way, including rheumatoid arthritis (RA), and multiple sclerosis (MS), and systemic lupus erythematosus (SLE). Studies in lupus-prone MRL/lpr mice confirm that activation of the nucleic acid receptors TLR7 and TLR9 can mediate the pathogenesis of SLE ⁶¹⁻⁶³.

Current therapies, such as monoclonal antibodies, can reduce the symptoms of SLE, but fail in many patients due to serious side effects originating from widespread immunosuppression¹⁰³. Because of these side effects, researchers have shifted their focus to blocking the antibody and DNA interactions using oligonucleotides, peptides, and small molecules to block the antibody binding site on DNA. However, these approaches are limited due to the expression of DNA antibodies that interact with diverse sites on the DNA molecule therefore limiting the efficacy of single antibody blocking. Previous work from our laboratory has demonstrated the effectiveness of certain nucleic acid-binding polymers (e.g., PAMAM-G3, CDP, HDMBR, protamine, polyethylenimine) for inhibiting nucleic acid-mediated activation of nucleic acid-sensing PRRs, irrespective of whether they recognize ssRNA, dsRNA or hypomethylated DNA¹⁰⁴. While the use of freely circulating cationic molecules (Figure 20A) has demonstrated promise in inhibiting nucleic acid-mediated activation of PRRs, they may present issues with regards to cytotoxicity and non-specific cellular uptake^{105,106}.

To build upon the success of nucleic acid scavenging using polycationic polymer treatment, we suggest the use of a localized cationic therapy for nucleic acid removal. In this work, we show that a highly cationic NASF can be used to scavenge extracellular nucleic acids in a controlled and localized manner (Figure 20B). Further, NASFs do not compromise TLR responses to other non-nucleic acid, pathogen-derived stimulators.

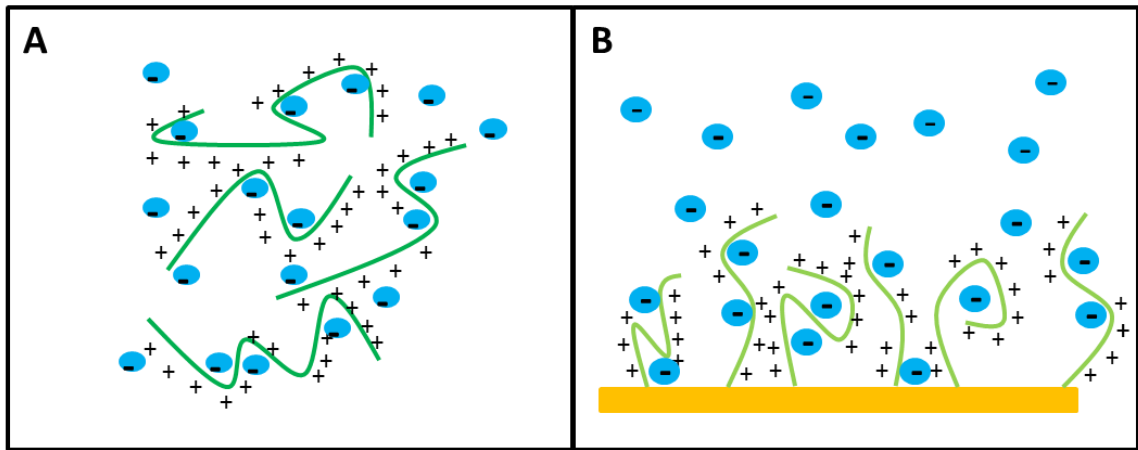


Figure 20: Schematic of nucleic acid scavenging by (A) free polycationic polymers versus (B) nanofiber bound polycationic polymers.

NASFs were fabricated by electrospinning a solution of poly(styrene-alt-maleic anhydride) (PSMA). Electrospinning is a method of forming continuous fibers using a polymer solution with an applied voltage that develops an elongated polymer jet that is collected onto a mandrel as the solvent evaporates, forming a fibrous sheet^{107,108}. This process is versatile, continuous, easily replicated, simple, stable¹⁰⁸, and inexpensive¹⁰⁷. The combination of polystyrene and maleic anhydride provides reliable mechanical properties¹⁰⁹⁻¹¹² and ease of chemical modification. PSMA has been used for electrospinning of nanofibers for applications in aptamers and gas sensing^{112,113} while larger micro-diameter fibers of PSMA have been investigated for hydrogel formation and enzyme stabilization¹¹⁴⁻¹¹⁶. In this aim, we present the covalent modification of PSMA nanofibers with the amine-containing polycation, branched polyethylenimine (bPEI), for applications where high levels of eNA debris cause prolonged inflammation.

We demonstrate the utility of NASFs for nucleic acid scavenging, a concept that has only been demonstrated once before¹¹⁷.

4.2 Materials and methods

4.2.1 Poly(styrene-alt-maleic anhydride) electrospun nanofiber formation

Preparation of neutral fibers was optimized by testing various concentrations of poly(styrene-alt-maleic anhydride) (PSMA) with solvent combinations of one or more of the following: tetrahydrofuran (THF), acetone, and dimethylformamide (DMF). Effective electrospinning occurred with PSMA (0.6g or 1g) (Sigma-Aldrich, St. Louis, MO) dissolved in a 1:1:1 (v:v:v) mixture of THF: acetone: DMF (10 mL) (Sigma-Aldrich) by constant mixing for 24 hrs at room temperature. PSMA nanofibers were electrospun using 2 mL of polymer solution in a 2cc glass syringe (Cadence Science, Staunton, VA) at a dispensing rate of 1 mL/hr, achieved by insertion of the syringe into an automated syringe pump, with an applied voltage of +15 kV. The polymer fibers were collected on a grounded cylindrical mandrel (~6.4 cm wide with a ~21.6 cm circumference) spinning at ~130 rpm at a distance of 10 cm away from the tip of the syringe needle. The neutral electrospun PSMA fibers were soaked in a solution of 1.8 kDa bPEI (0.1M) (Polysciences, Inc., Warrington, PA) for 72 hrs at room temperature with constant shaking to form NASF. To form PAMAM-NASF, the neutral fibers were soaked in PAMAM-G3 (0.004M) (Sigma-Aldrich) at 4°C for 72 hrs with constant shaking. Following conjugation

the NASF was washed for 10 min with deionized water a total of 5 times. NASF was sterilized for 30 min in ethanol, the ethanol was removed, and the NASF was allowed to air-dry in a sterile environment. PAMAM-NASF was washed 5 times for 10 min each in sterile water and allowed to air-dry in a sterile environment, skipping the ethanol sterilization step.

4.2.2 Scanning electron microscopy (SEM)

Dry fibers were placed on aluminum foil and mounted to a SEM stub. Mounted fibers were gold sputter-coated for 250 sec using the Denton Vacuum Desk IV sputter unit (Denton Vacuum, Moorestown, NJ) and imaged using a FEI XL30 SEM-FEG (FEI, Hillsboro, OR). Images were analyzed in Scandium (ResAlta Research Technologies, Golden, CO).

4.2.3 X-ray photospectroscopy (XPS)

XPS measurements were taken on a Kratos Analytical Axis Ultra XPS (Kratos, Manchester, UK) using a monochromated Aluminum K-alpha source. The source was operated at 15 kV and 10 mA (150 watts). Electron collection was made at 90 degrees to the sample surface. Survey scans were taken with pass energy of 160 eV while region scans were performed with pass energy of 20 eV.

4.2.4 Nucleic acid adsorption

Alexa Flour 488 labeled CpG (3.33×10^{-4} to 1×10^{-3} $\mu\text{g}/\text{mL}$) (IDT, Coralville, IA) was incubated with 3 mm diameter NASFs for 4 hrs at room temperature under constant shaking. The NASFs were washed 3 times with deionized water, placed on a microscope slide, and mounted with *SlowFade* Diamond reagent (Life Technologies, Carlsbad, CA). Fluorescent images of adsorbed DNA onto NASFs were captured with an Upright AxioImager A1 microscope (Zeiss, Oberkochen, Germany) powered by a Zeiss HBO100 power supply and lamp housing. To generate the DNA adsorption curve, salmon sperm DNA (25 ng-100 ng) (Life Technologies) in 1xTris-EDTA (TE) buffer was added to 3 mm diameter NASFs for 4 hrs at room temperature with constant shaking. Total salmon sperm DNA concentration remaining in the 1xTE solution was determined using a PicoGreen assay (Life Technologies).

4.2.5 Cell culture

All *in vitro* experiments were performed in complete growth media unless stated otherwise, with cells incubated at 37°C (5% CO₂). STO (ATCC, Manasses, VA), RAW (ATCC), Panc-1 (ATCC), HEK293, and KPC-4580 cells were cultured in DMEM (Gibco 11960-044) supplemented with 10% FBS and 1% Pen-Strep. Ramos-Blue cells (InvivoGen, San Diego, CA) were cultured in IMDM (Gibco 12440-053) supplemented with 10% FBS, 1% Pen-strep, and 100 $\mu\text{g}/\text{mL}$ Zeocin every 4 passages. WM266-4 (ATCC)

cells were cultured in MEM (Gibco 11095) supplemented with 10% FBS, 1mM sodium pyruvate, 1% non-essential amino acids, and 1500 mg/L sodium bicarbonate. NHDF (Lonza, Basel, Switzerland) cells were cultured in DMEM (Gibco 11960-044) with 10% FBS, 1% Pen-Strep, 1% Non-essential amino acids, 1% Sodium pyruvate, 1% Glutamax, 0.1% β -mercaptoethanol.

4.2.6 Cell viability

For viability experiments, STO cells (40,000 cells/well) were plated 18-24 hrs before experiments to ensure cellular adhesion. Ramos-Blue cell viability experiments were performed by plating cells (200,000 cells/well) immediately prior to adding the NASF into the medium. Both cell types were incubated with the NASF for 4 hrs and cell viability was measured using Cell Titer-Glo assay (Promega, Madison, WI).

Proliferation studies were performed by putting a piece of NASF, cut to fit into the well, onto the bottom of a non-tissue culture treated 48 well plate (Greiner Bio-One, Kremsmunster, Austria) using 10 μ L PBS to aid in NASF adhesion to the well. After the PBS dried, NHDF in DMEM (100,000 cells/well) were added to the top of the NASF.

Proliferation was determined using LIVE/DEAD Viability/Cytotoxicity kit (Life Technologies) at 24 hrs and 48 hrs.

4.2.7 Inhibition of Nucleic-acid driven TLR activation using cationic NASFs

For scavenging studies, NASFs or neutral PSMA fibers were incubated in media for 10 min with one of the following TLR agonists at 2.5 µg/mL: CpG 1668 (TLR 9), Poly(I:C) (TLR 3), R848 (TLR 7/8), or Pam3CSK4 (TLR 1/2) (InvivoGen). After 10 mins, the fiber sample was removed, and the fiber treated media (62.5µL) was added to Ramos-Blue cells (200,000 cells in 137.5µL of complete media) for 18-24 hrs at 37°C. For comparison, TLR agonists (10 µg/mL) were also applied directly to Ramos-Blue cells. For direct contact studies, NASFs were added directly to Ramos-Blue cells (200,000 cells/well), followed by incubation with agonists (10 µg/mL) for 18-24 hrs at 37°C. After incubation, the supernatant (40 µL) from the treated Ramos-Blue cells was added to the serum alkaline phosphatase colorimetric indicator Quanti-Blue (160 µL) (InvivoGen), incubated for 5 hrs at 37°C, and absorbance was measured at 650 nm.

4.2.8 Doxorubicin cell debris, DAMPs, inhibition of TLR activation by NASFs

Doxorubicin (3, 3.6, 6, or 9 µg/mL) (DOX) (Sigma-Aldrich) was incubated for 48 hrs with RAW cells (40,000cells/well); the supernatant from the DOX-treated cells (100 µL) was added to a 4 mm piece of NASF. The NASF and supernatant were incubated for 30 min and the entire volume was added to Ramos-Blue cells (200,000 cells in 100µL IMDM). After incubation for 18-24 hrs, Ramos-Blue supernatant (40 µL) was added to

Quanti-blue (160 μ L) (InvivoGen) and the absorbance was read at 650 nm at 3 hrs and 5 hrs.

4.3 Results

Neutral nanofibers electrospun using PSMA solutions (60% and 100% w/v) resulted in randomly aligned nanofibers with average diameters of 297 ± 13 nm and 737 ± 26 nm, respectively (Figure 21A). The 60% and 100% PSMA nanofibers demonstrated different physical characteristics after conjugation with 1.8 kDa bPEI. The 100% NASFs (NASFs made with 100% PSMA nanofibers) were brittle and difficult to handle whereas the 60% NASFs demonstrated a tissue paper-like texture, making them more malleable and easier to use. The conjugation of bPEI onto PSMA fibers was validated using XPS (Figure 21C) where a nitrogen peak present in the bPEI conjugated fibers, NASF, indicates the successful conjugation of bPEI.

After initial proof-of-concept *in vitro* experiments with both 60% and 100% NASFs, 60% PSMA fibers were chosen for preparation of the NASF sheets as they were more durable, easier to cut into various sizes, and did not show reduced efficacy as compared to 100% NASFs (Figure 25). Upon conjugation of 1.8 kDa bPEI to the 60% PSMA nanofibers, the resulting polycationic nanofibers (NASFs) had an increased fiber diameter of 486 ± 9 nm (Figure 21B) as compared to the original at 297 ± 13 nm (Figure 20A). Successful conjugation of bPEI onto the nanofibers was confirmed by contact

angle measurements, XPS, and functionality tests. The contact angle of neutral PSMA nanofibers was 122° indicating high hydrophobicity. Following bPEI conjugation, the NASFs demonstrated so much hydrophilicity that the contact angle could not be determined, validating the conversion from hydrophobic neutral nanofibers to hydrophilic cationic nanofibers. While the unmodified PSMA fibers are highly hydrophobic, the porous nature of the PSMA fibers allowed them to become wet for *in vitro* studies given time and high volumes of liquid. Additionally, XPS data confirmed the abundance of nitrogen on the surface of the NASFs at an atomic percent of 10.57%, indicating successful conjugation of amino groups onto the nanofiber surface. The unmodified PSMA fibers showed a surface nitrogen abundance of atomic percent < 0.01 % (Figure 21C).

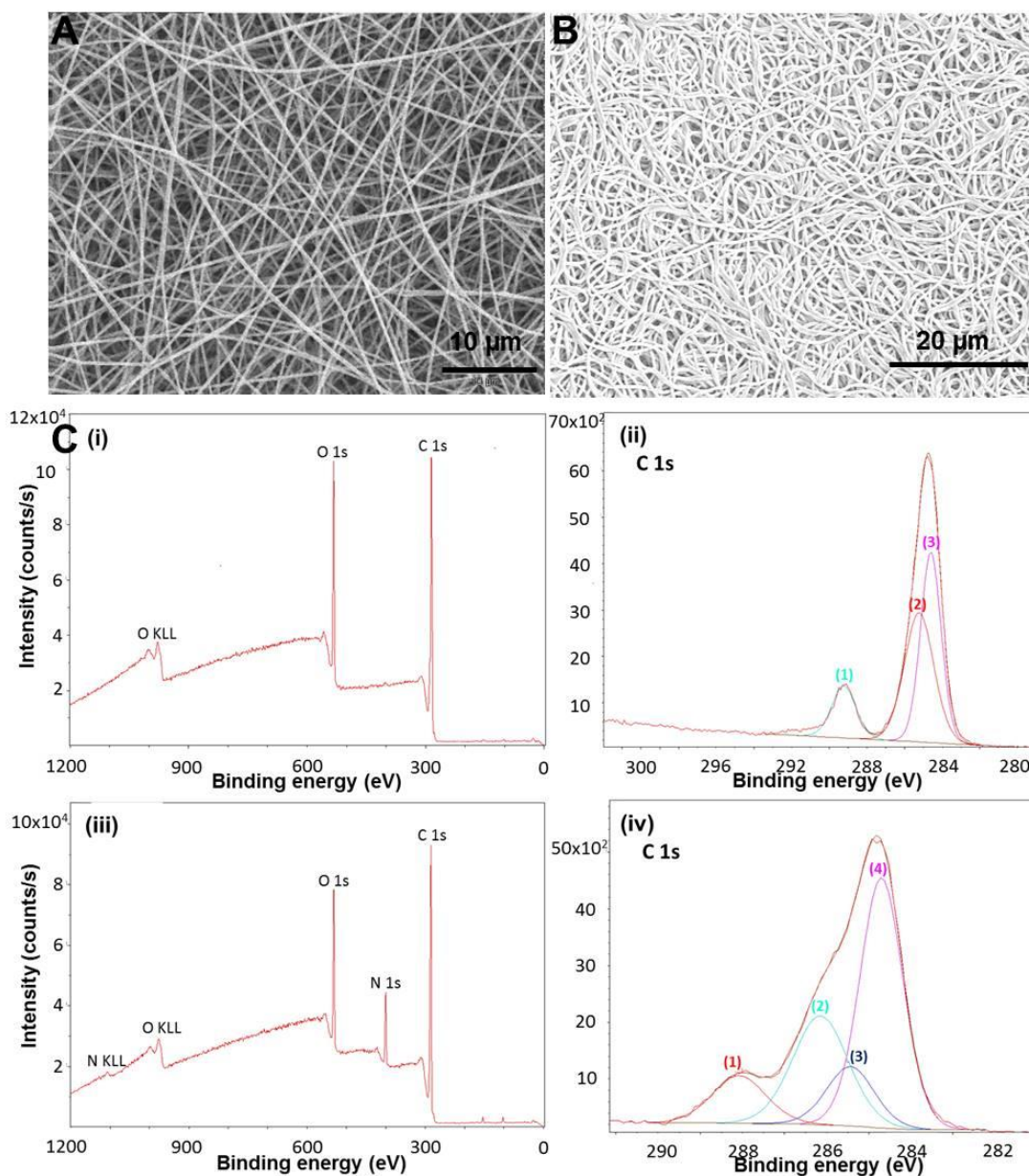


Figure 21: (A) SEM image of neutral PSMA nanofibers; (B) SEM image of 1.8 kDa modified PSMA nanofibers; (C) (i) Survey scan of neutral PSMA fibers, (ii) High-resolution XPS scan for C 1s of neutral PSMA fibers, (1) is C=O, (2) is C-O, (3) is C-C, (iii) Survey scan of bPEI conjugated NASF, (iv) High-resolution XPS scan for C 1s of bPEI conjugated NASF showing the presence of (1) C=O, (2) C-O, (3) C-N, (4) C-C.

Functionality of cationic NASFs, ie their ability to scavenge nucleic acids, was validated through electrostatic interactions with negatively charged nucleic acids including CpG DNA and salmon sperm DNA. Alexa-Fluor 488 labeled CpG 1668 was used to demonstrate binding of nucleic acids by the NASFs (Figure 22). Increasing amounts of labeled CpG resulted in increased fluorescence as compared to background nanofiber fluorescence. The increased fluorescence of the NASFs following soaking with labeled DNA confirmed the function of scavenging nucleic acids. Through adsorption analysis using salmon sperm DNA (Figure 23), the maximum adsorption capacity of the NASFs was determined to be $\sim 30 \mu\text{g DNA}/3 \text{ mm diameter fiber disc}$. SEM images show that the initial modification of neutral PSMA nanofibers with bPEI resulted in swelling of the fibers and some “melting” of the fibers (Figure 20B); however, interaction with salmon sperm DNA did not further change the morphology therefore maintaining the NASF mechanical structure after DNA scavenging (data not shown). This data confirms that the neutral PSMA nanofibers are being modified with the bPEI to produce NASFs that successfully scavenge DNA from solution. This technique of polycationic nanofiber formation is consistent and modular, allowing formation of nanofibers with differing morphologies including varying thicknesses and surface area, which affects the degree of cationic moiety conjugation, possibly resulting in tunable nucleic acid scavenging capabilities.

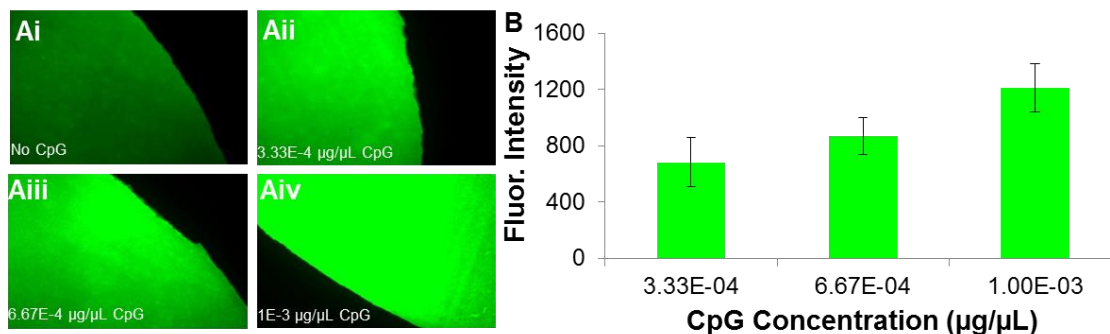


Figure 22: (Ai-Aiv) Fluorescent microscope images of polycationic nanofibers after 4hrs interaction with AlexaFluor488-CpG (Left); (B) quantification of average fluorescence after interaction with AlexaFluor488-CpG normalized to polycationic nanofiber alone and compared to the initial amount of CpG added.

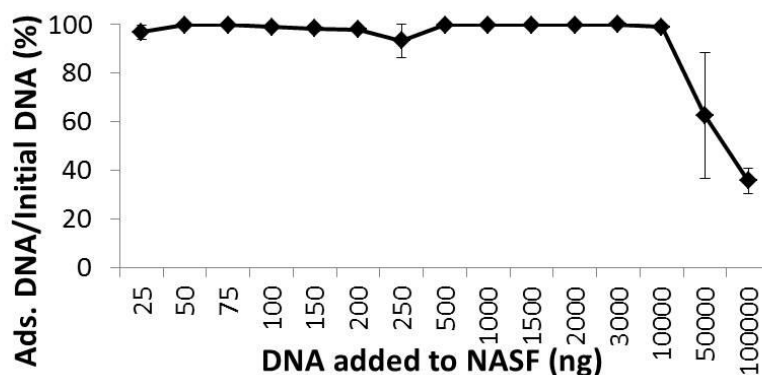


Figure 23: Salmon sperm DNA maximum adsorption curve for a 3 mm diameter disc of NASF (n=3).

Previous studies indicate that the presence of highly charged moieties, such as soluble cationic polymers, leads to cytotoxicity in some cell lines^{105,118,119}. A primary benefit of this insoluble NASF strategy is that it functions entirely in the extracellular

space, bypassing cellular uptake, and systemic circulation of the polycations which reduces the overall toxicity. When cell viability was tested with STO and Ramos-Blue cells in the presence of NASF, the cell viability remained over 70% (Figure 24A). To determine the effect of direct cellular contact with the NASF on cellular viability and proliferation, a LIVE/DEAD stain was performed after 24 hrs and 48 hrs of plating NHDF cells directly onto NASFs (Figure 24B). The LIVE/DEAD assay in NHDF shows that viability remains above 80% at all times when cells are grown directly on top of NHDF. Taken together, this indicates that the NASFs display only minor toxicity and do not prevent cell proliferation, suggesting biocompatibility.

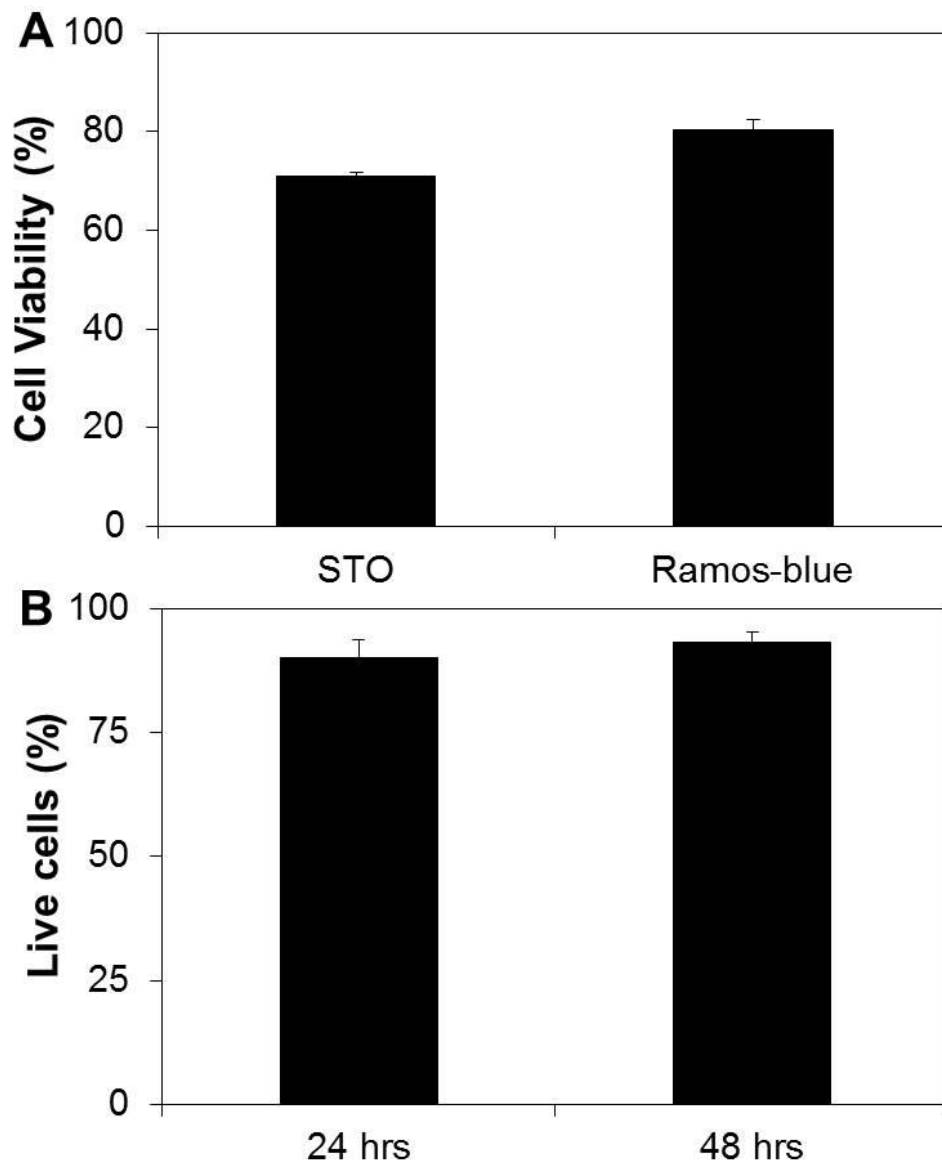


Figure 24: (A) Cell viability of STO and Ramos-Blue cells after 4 hrs of interaction with polycationic nanofibers; (B) Live/Dead assay performed on NHDF cells where Live cell % was determined at 24 and 48 hrs.

Initial tests in Ramos-Blue TLR reporter cells, demonstrated the NASFs ability to scavenge CpG 1668, prevent TLR 9 activation, and concomitantly reduce NF- κ B/AP-1-inducible secreted alkaline phosphatase (SEAP) levels down to baseline. To show that this inhibition was due to electrostatics-driven scavenging and not by non-specific adsorption, comparative experiments were done with neutral fibers (Figure 25). Neutrally charged, unmodified fibers, PSMA Fiber, had no effect on CpG 1668 TLR stimulation where the SEAP levels were no different from CpG administered directly to the cells.

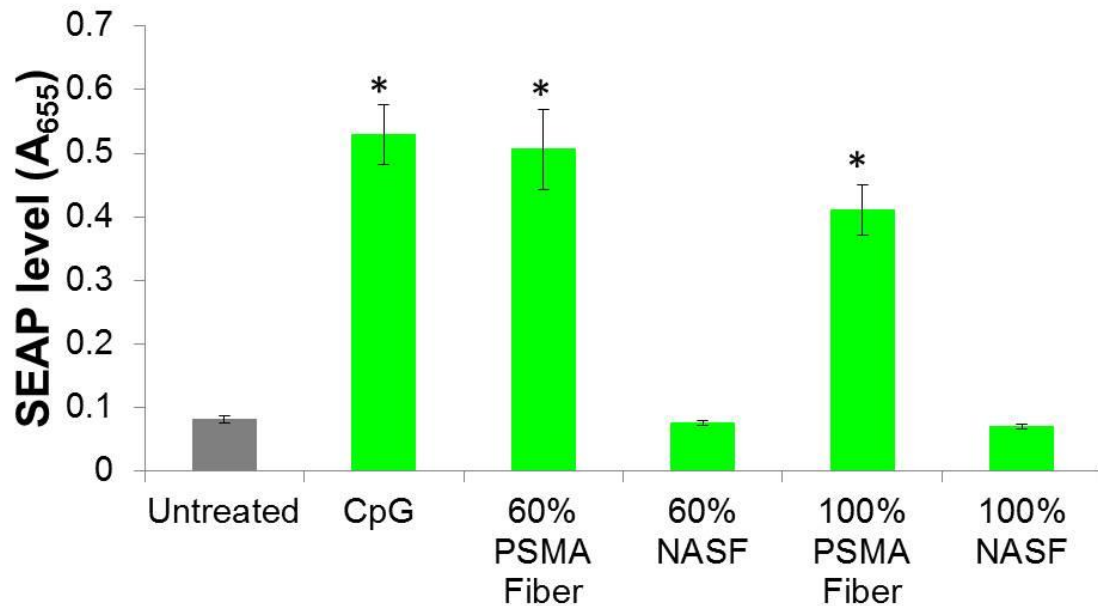


Figure 25: Secreted alkaline phosphate levels from Ramos-Blue cells. SEAP levels after pre-incubation of neutral fibers (60/100% PSMA Fiber) or NASFs with CpG as compared to CpG alone and baseline levels of SEAP (Untreated); * denotes $p \leq 0.001$, (n=3).

Specificity for negatively charged TLR agonists was demonstrated in Figure 26 by comparing the ability of the NASFs to return SEAP levels to baseline after pre-incubation with CpG 1668, Poly(I:C), resiquimod (R848), and Pam3CSK4. NASFs blocked TLR 3 and TLR 9 activation by Poly(I:C) and CpG, respectively, both negatively charged nucleic acid agonists. NASFs also significantly reduced the SEAP levels in R848 (TLR7/8) treated cells, however, the levels were not pushed back to baseline as was demonstrated in the negatively charged nucleic acid blocking of CpG and Poly(I:C). Additionally, the NASF were not able to block activation by non-nucleic acid agonist, Pam3CSK4 (TLR 2/1). To demonstrate that the NASFs effectively scavenge in the presence of cells, Ramos-Blue cells were co-incubated with the fibers, followed by administration of the TLR agonists (Figure 27).

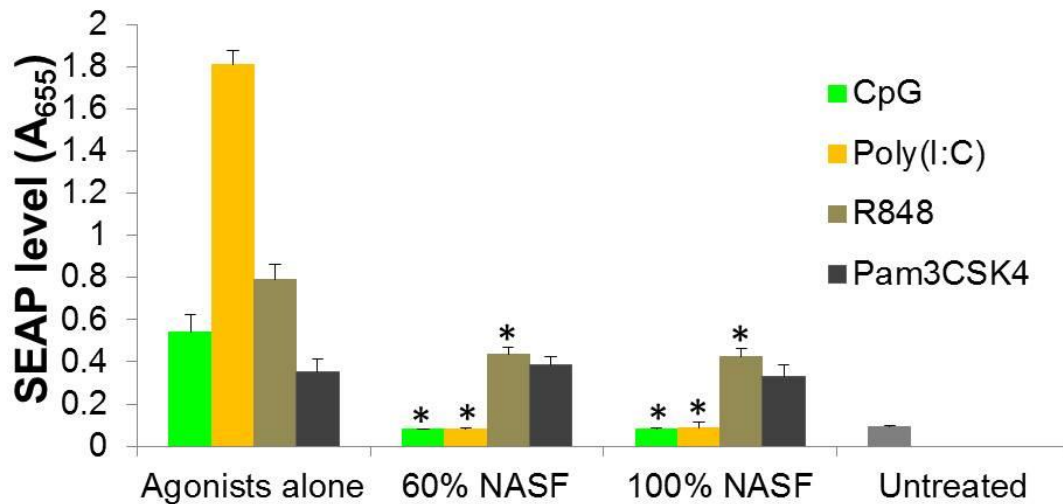


Figure 26: SEAP levels after pre-incubation of NASFs with agonists as compared to agonists alone and untreated SEAP levels of Ramos-Blue cells); (n=3) * denotes $p \leq 0.001$ as compared to agonists alone.

Co-incubation experiments mimicked the results seen in the pre-incubation studies with NASFs; both CpG and Poly(I:C) stimulation effects were brought down to baseline SEAP levels while R848 had a minimally significant effect and Pam3CSK4 retained maximal SEAP levels after treatment with NASF. To demonstrate the versatility of the PSMA fiber and this scavenging strategy, a different polycationic polymer was covalently attached to the PSMA fiber and tested for its scavenging capacity. A polyamido(amine) cationic dendrimer (PAMAM-G3) was grafted onto the neutral fibers to make PAMAM-NASF and tested for efficacy in the co-incubation studies with Ramos-Blue TLR reporter cells (Figure 27). The NASF-PAMAMs mirrored

the results seen with bPEI-grafted NASFs. SEAP expression caused by the non-nucleic acid agonist Pam3CSK4 was not affected by the NASF-PAMAM co-incubation; however, significant reduction in SEAP expression was found following co-incubation of NASF-PAMAM with nucleic acid TLR agonists CpG, Poly(I:C), and R848. Together, these results demonstrate that NASFs prevent TLR activation by CpG and Poly(I:C), and presents relevant evidence that this blocking by NASF can be extended to other stimulatory nucleic acids. Additionally, the nucleic acid scavenging effectiveness of NASFs is not limited to using bPEI as the grafted polycation. The neutral PSMA fibers can also be modified with different polycations (e.g. PAMAM-G3) while maintaining scavenging capabilities.

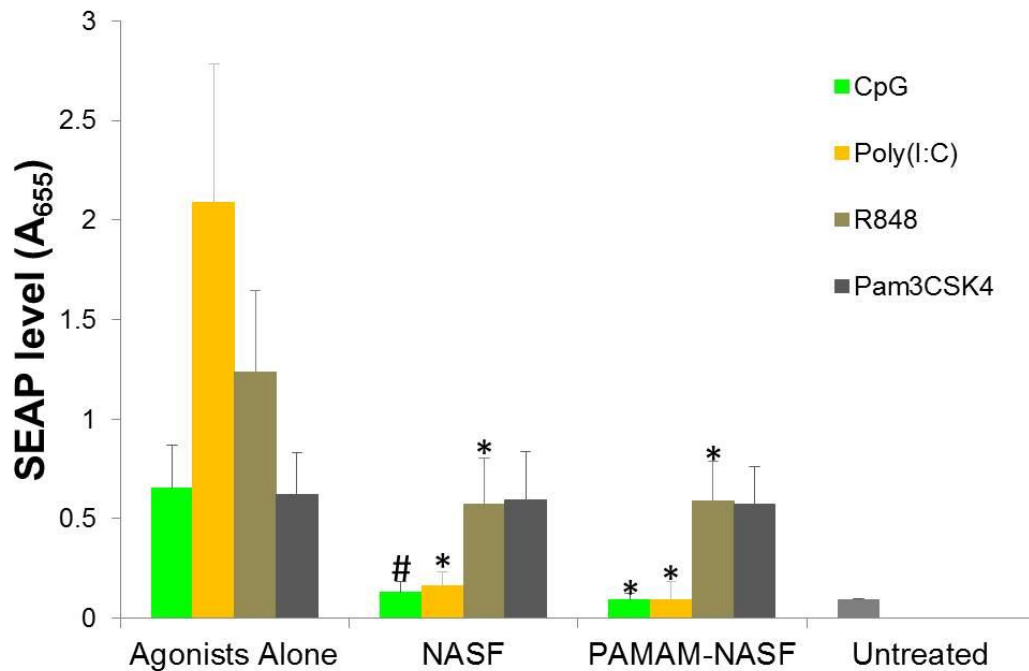


Figure 27: Co-incubation of NASFs with Ramos-Blue cells and agonists. 60% NASF and PAMAM-NASF significantly block TLR activation by CpG and Poly(I:C) and maintain SEAP levels comparable to baseline, Untreated; (n=3), * denotes $p < 0.0001$, # denotes $p < 0.05$ as compared to agonists alone.

To apply the NASFs to a more biologically relevant scenario, a doxorubicin (DOX) induced cell death model was used. DOX is a commonly used chemotherapeutic, and it has been shown that DOX-induced cell death leads to transient NF- κ B expression¹²⁰. NF- κ B expression is associated with nucleic acid fragments that are released from dead and dying cells. Increased amounts of circulating nucleic acids resulting from excessive cell death caused by chemotherapy or radiation therapy initiates inflammatory responses. High doses of DOX cause apoptotic cell death resulting in abnormal DNA fragmentation^{121,122}, these endogenous DNA and RNA fragments can subsequently be

uptaken into healthy cells leading to TLR activation ¹²³. To model increased nucleic acid amounts as released from dying cells, nanofiber scavenging was tested using DOX-killed cell debris as the pro-inflammatory TLR stimulant. Administration of DOX to RAW 264.7 cells induced cell death, releasing various TLR and/or NOD1 agonists into the media. Media containing apoptotic cellular debris was then used to stimulate NF- κ B/AP-1 and subsequent SEAP secretion from Ramos-Blue B lymphocyte cells. RAW 264.7 cells were chosen for this application because DOX treatment for 48 hrs resulted in cell-death debris that promoted high TLR/NOD1 activation. When the cell-death debris was scavenged by the NASFs, a decrease in NF- κ B/AP-1 secretion was illustrated by significant decrease in post-treatment SEAP levels compared to initial SEAP levels (Figure 28). A maximum blockade of 41.4% of TLR/NOD1 activation by NASFs was achieved after interaction with the DOX-treated cell debris administered from the lowest DOX dose (3 μ g/mL). The percent blocking by NASFs decreased to 26.9 \pm 6.1% and 28.3 \pm 9.9% after treatment with DOX-treated cell debris with initial DOX doses of 6 μ g/mL and 9 μ g/mL, respectively.

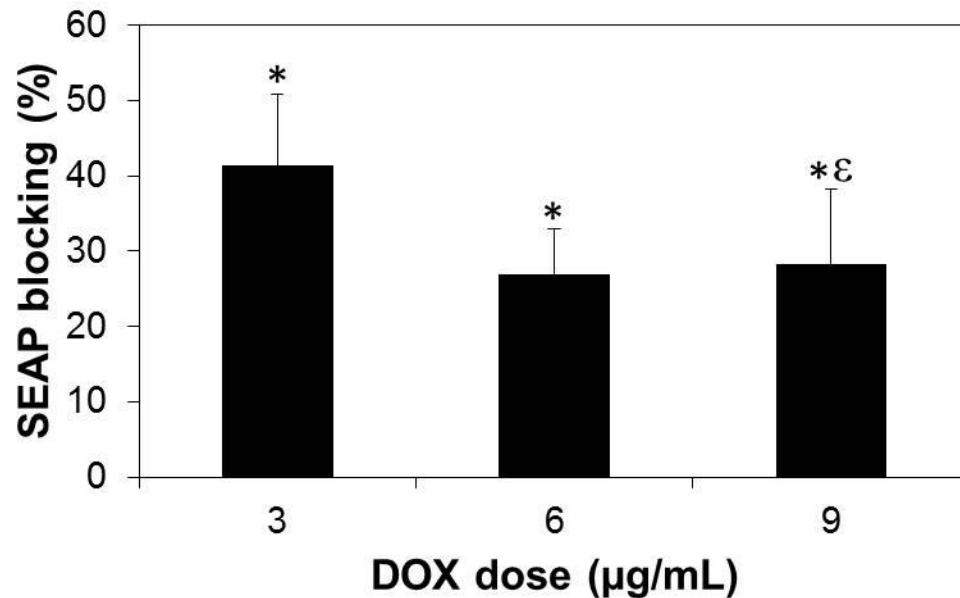


Figure 28: Blocked SEAP production from Ramos-blue cells by NASF. Initial DOX dose to Raw cells describes the amount of DOX used to treat Raw cells 48 hrs prior to using the Raw cell debris for activation of Ramos-blue cells. Polycationic nanofiber blocking demonstrates the polycationic nanofiber's ability to prevent NF- κ B production by scavenging immune-stimulating cell debris from the media; * denotes $p < 0.0001$ as compared to cells without DOX cell debris and without NASF, ϵ denotes $p < 0.03$ as compared to DOX dose at 9 $\mu\text{g/mL}$ with no NASF.

Further versatility of the electrospun PSMA nanofibers was explored by changing the mechanical structure of the fiber with the incorporation of polystyrene to the initial PSMA polymer solution for electrospinning. The conditions for electrospinning with the incorporation of polystyrene are shown in Table 2. The resulting fibers were imaged using SEM (Figure 29). The average fiber diameters were found to be $1.82 \pm 0.06 \mu\text{m}$, $1.20 \pm 0.06 \mu\text{m}$, $1.98 \pm 0.08 \mu\text{m}$, and $2.51 \pm 0.06 \mu\text{m}$, making the fibers microfibers instead of nanofibers. In the second step, 1.8 kDa bPEI was

covalently conjugated onto the R4, R6, R7, and R8 fibers to make them polycationic fibers.

Table 2: Conditions for electrospinning of fibers incorporating PS with PSMA in 3 mL of solvent, 1:1:1 THF:DMF:Acetone.

Fiber ID	Polystyrene (g)	PSMA (g)	Distance from mandrel (cm)	kV applied to polymer solution	Flowrate of polymer solution (mL/hr)
R4	.2	.4	16.5	15	1
R6	.2	.2	15.5	15	1
R7	.3	.3	13	18	1
R8	.3	.4	17.3	18	2

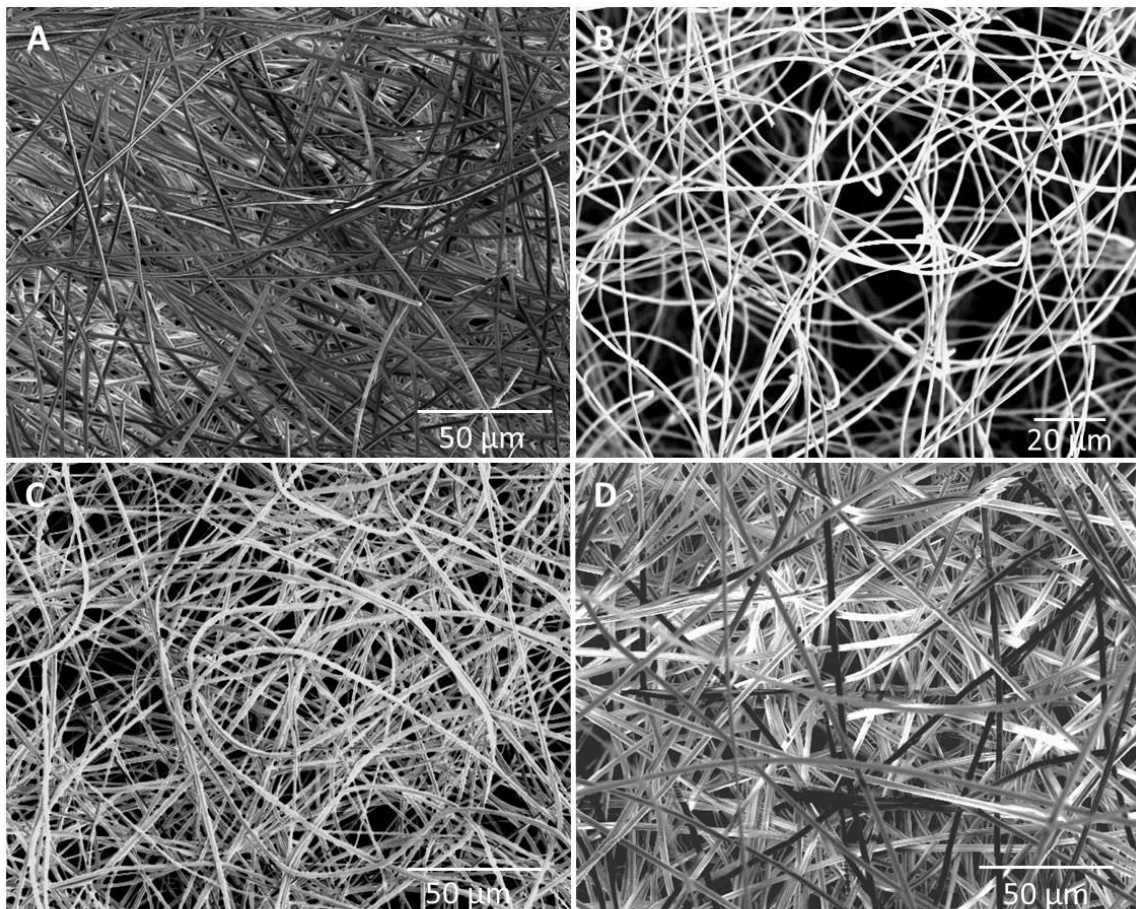


Figure 29: SEM images of the fibers spun according to the conditions listed in Table 2. (A) R4 with an average fiber diameter of $1.82 \pm 0.06 \mu\text{m}$, (B) R6 with an average fiber diameter of $1.20 \pm 0.06 \mu\text{m}$, (C) R7 with an average fiber diameter of $1.98 \pm 0.08 \mu\text{m}$, (D) R8 with an average diameter of $2.51 \pm 0.06 \mu\text{m}$.

In collaboration with Jae Woo Lee, the R8 + bPEI fiber was tested for its effects on cell viability (Figure 30) and its nucleic acid scavenging ability (Figure 31). Experiments done to test the R8 + bPEI fiber used specially-made HEK-TLR cell lines which express high amounts of TLR connected to a NF- κ B linked SEAP chromogenic output system.

Each agonist was administered to the HEK-TLR cell line that expressed the TLR it activates. As such, all experiments with LPS and heparan sulfate were done in HEK-TLR4 cells, all experiments with Poly(I:C) were done in HEK-TLR3 cells, and all experiments with CpG were done in HEK-TLR9 cells. The results show that the R8 fiber conjugated with bPEI is non-toxic in HEK-293, Panc-1, WM266-4, and KPC-4580 cell lines (Figure 30). Additionally, R8 + bPEI is able to significantly reduce the activation caused by heparan sulfate, Poly(I:C), and CpG as compared to the free bPEI and PAMAM-G3 polymers, which have no significant effect on heparan sulfate and minimal effects on Poly(I:C) and CpG (Figure 31).

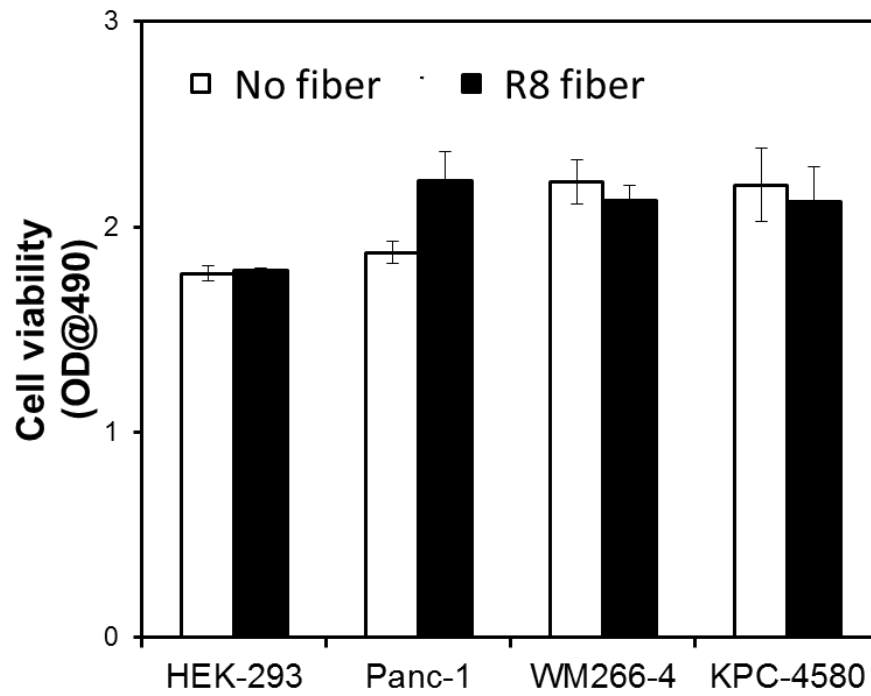


Figure 30: Cell viability after treatment with two 3x3 cm pieces of R8 + bPEI in 400 μ L of media.

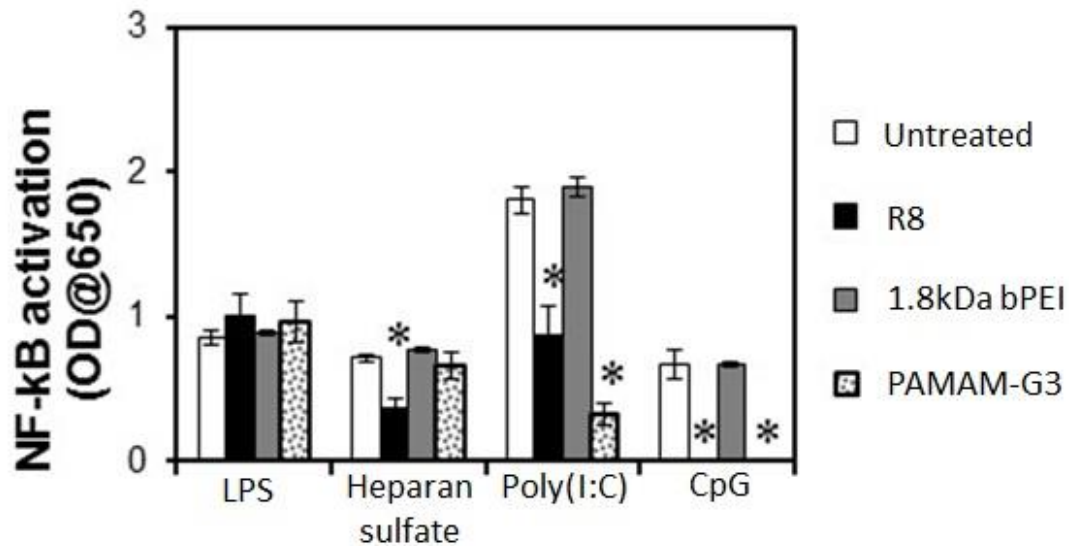


Figure 31: NF- κ B activation in HEK-TLR cells following administration of the agonist alone (white bars), agonist + [R8 + bPEI fiber] (black bars), agonist + free bPEI (grey bars), agonist + PAMAM-G3 (dotted bars); (n=3) * indicates $p < 0.05$ as compared to agonist alone.

4.4 Discussion

Extracellular nucleic acids are known to activate TLRs, which leads to downstream chronic inflammation that is associated with various auto-immune diseases such as RA, MS, and SLE⁶⁰. Reducing chronic downstream inflammation by scavenging nucleic acids has been validated using cationic polymers^{104,117,124} and in this aim, we demonstrate the development of an easy to synthesize, versatile, and modular polycationic nanofiber system to scavenge nucleic acids. We have electrospun micro- or nanofibers using PSMA with or without the addition of polystyrene. Although electrospun PSMA fibers and polystyrene-PSMA fiber sheets can be found in literature

^{112,114,125}, the novelty of our fiber comes from the conjugation of the polycations, bPEI and PAMAM to the electrospun fibers as well as the modular ease of fiber formulation unlike other studies that require copolymer synthesis, solvent, and electrospinning condition re-optimization for each change in polycation ¹¹⁷. NASF provide flexibility in that essentially any amine containing molecule can be conjugated to the PSMA fiber. Our process involves modular steps where the polymer is electrospun at constant conditions followed by covalent modification with the polycationic polymer. A similar modular approach forming PSMA microfibers with grafted anti-microbials has been demonstrated ¹²⁵, however, these fibers were on the micro- scale as opposed to the nano-scale of NASF.

NASF were modified with various polycations and studied for impact on cellular viability and inflammation. The nanoscale diameter of our original NASFs provided a higher surface area for surface modification, therefore providing the capacity for higher cationic charge than a microfiber. The porous nature of an electrospun mesh presents some concern that the nanofibers may absorb fluid, resulting in a random effect on TLR activation, demonstrated by the SEAP production. Neutral PSMA fibers did not have the same nucleic acid scavenging capacity that the NASFs had suggesting that the material alone does not have any nucleic acid scavenging effect on its own without the polycation. The NASFs also scavenge significantly higher amounts of negatively

charged nucleic acids, suggesting specificity of use. Together, these studies show that our NASF can dampen NF- κ B expression by preventing TLR activation through nucleic acid scavenging and that this effect is based on electrostatic interactions of conjugated polycation with nucleic acid. As this first study using CpG demonstrated that the neutral PSMA fibers did not scavenge any CpG, the neutral PSMA fibers were deemed ineffective at NA scavenging as compared to NASF and therefore were not tested in subsequent experiments.

The specificity experiments, where different agonists including poly(I:C), R848, and PAM3CSK4 were tested with the NASF were done to show that the NASF were specifically removing negatively charged agonists and not effecting other charged or uncharged molecules. However, we did see some off target effects on the small molecule R848, an imidazoquinoline compound that activates TLR7/8. Although R848 is protonated at neutral pH, going against our hypothesis that the positively charged NASF will only interact with negatively charged molecules, it does activate the same TLR that is activated by viral RNAs, TLR8¹²⁶. This highlights that the NASF may be able to remove molecules of a certain size threshold independent of charge. The NASF scavenged R848 in a manner unrelated to charge and this molecule is ~314 g/mol whereas the larger molecule Pam3CSK4 (~1510 g/mol) was not scavenged nonspecifically. Because these molecules are not attracted to the NASF by charge, they

must be physically stuck to the fibers if they are scavenged, which infers that this nonspecific scavenging is directly related to pore size. Presumably the pore size could be manipulated in order to reduce the nonspecific scavenging. A smaller pore size may result in less non-electrostatic related absorption of molecules, further reducing the size threshold of nonspecific absorption.

To demonstrate the utility of NASFs in a biological setting, we endeavored to show that the NASFs effectively scavenge nucleic acids in the presence of large amounts of cell debris. Studies have shown that high doses of doxorubicin lead to cytotoxic effects¹²², NF- κ B activation, and are associated with high levels of damaged DNA¹²⁰. We showed that the NASF can reduce the inflammatory effects of doxorubicin, presumably by reducing TLR activation by nucleic acids and leading to reduced secreted alkaline phosphatase/ NF- κ B levels. We were not able to show complete blocking of SEAP levels as we demonstrated in the pure agonists, Poly(I:C) and CpG. The lack of complete inhibition is probably partially due to the fact that it is improbable that all of the TLR response in the Ramos-Blue cells is due to nucleic acid agonists when exposed to the complex doxorubicin-killed cell debris. The modest blockade of TLR activation could also be due to nanofiber saturation or due to apoptosis-associated protein complexes which stimulate NOD1, inducing NF- κ B/AP-1 secretion which cannot be sequestered using NASF¹²⁷. Further investigation into the mechanism of TLR/NOD1

activation following administration of DOX-treated cell debris is underway, but these preliminary results indicate that the NASFs are functional in a clinically relevant application. We are currently investigating different cationic polymer grafts onto the nanofibers and the scavenging of circulating pro-inflammatory nucleic acids and complexes associated with necrosis, chemo- and radiation therapy induced cell death. We are also performing optimization studies to analyze if the NASF can further reduce SEAP levels by increasing the NASF dose.

One potential application for the NASFs in a clinically relevant setting is to use them in a blood cleaning circuit, similar to dialysis, to remove negatively charged, immune stimulating molecules. The nature of the original NASF makes it difficult to consider an extracorporeal circuit application because of the physical properties of the fiber which makes it a flexible gel-like substance when exposed to fluid and therefore it cannot foreseeably withstand fluid flow. In order to address this problem, a more durable polymer, polystyrene, was incorporated into the PSMA solution for electrospinning. By doping in various amounts of polystyrene, the resulting fibers became sturdier and more resistant to flow; however, they lost their nanofiber diameter and became microfibers. R6 had the smallest fiber diameter and contained the smallest mass of polystyrene and PSMA combined. Further optimization of R4, R6, R7, and R8 using the same mass ratios of polystyrene to PSMA with an overall less concentrated

polymer solution for electrospinning may lead to smaller diameter fibers. To date, this has not been tested.

All of the resulting fibers (R4, R6, R7, and R8) remained completely in-tact when exposed to fluids and were considered a viable material to use in a flowing system. Because the PSMA is required for the desired reaction between the fiber and the polycation, we wanted to move forward with a fiber that had the highest amounts of PSMA, either R4 or R8. R8 was chosen at random to be tested in the TLR activation experiments. Looking back, it might have been better to use R4 because it had a smaller average fiber diameter, 1.82 μm as opposed to 2.51 μm (the average fiber diameter of R8), leading to higher surface area for conjugation of the polycation. Nonetheless, R8 effectively scavenged heparan sulfate, Poly(I:C), and CpG from solution, demonstrating that the addition of polystyrene did not eliminate the scavenging abilities of the fibers. Ongoing studies of scavenging in sepsis patient serum, populated with DAMPs, and freeze-thaw induced death bacterial cell debris, populated with pathogen-associated molecular patterns (PAMPs), validate R8's ability to effectively scavenge TLR agonists.

4.5 Conclusion

The development of polycationic fibers has built upon the Sullenger lab's previous findings that scavenging of extracellular nucleic acids ameliorates inflammation. Both polycationic modified PSMA fibers (NASF) and PSMA +

polystyrene fibers (R8) were found to be minimally toxic and were able to scavenge polyanionic pro-inflammatory species, CpG and Poly(I:C). Scavenging allowed these NASF meshes to block improper activation of nucleic-acid sensing TLRs without compromising the ability to respond to certain non-nucleic acid agonists, such as Pam3CSK4. The results of the DOX induced cell death scavenging study suggest that this nanofiber scavenging strategy may be useful in reducing pro-inflammatory side effects associated with chemotherapy induced cell-death which releases large amounts of pro-inflammatory nucleic acids and complexes into circulation. This application, along with any application involving blood flow, requires a form of blood filtration using a dialysis-like device or an extracorporeal circuit for blood filtration. Although the NASF showed therapeutic promise, the physical aspects of the NASF made it impossible to withstand flow in a filtration device. In order to develop the polycationic nanofiber platform for blood filtration, we developed a stronger fiber that incorporated polystyrene. The resulting fibers- R4, R6, R7, and R8- absorbed less fluid than the original NASF and were found to be less disrupted by agitation with fluid, suggesting that they might be more compatible to flow. The scavenging capabilities of R8 remained intact, making this fiber a potential candidate for use in a blood filtration device.

The utility of soluble polycations as a therapeutic strategy has been limited due to the toxicity associated with cellular uptake of highly positively charged molecules.

Our extracellular scavenging strategy using insoluble, functional polycationic fibers bypasses cell internalization and cytotoxic side-effects making them potential candidates for developing materials to be used as *ex vivo* hemofiltration devices or in other applications where chronic inflammation due to extracellular nucleic acids occurs.

5. SPECIFIC AIM 3: Treatment of biofilms using nucleic acid scavenging nanofibers.

In this aim, we apply the idea of nucleic acid scavenging using nanofibers to aid in the healing of chronic wounds infected with biofilms. This is different from the focused anti-inflammatory application previously mentioned, in that the goal is to disrupt the influence of nucleic acids on the extracellular polymeric substance (EPS), which forms the basis of biofilms. Furthermore, nucleic acids contributions to the inflammatory state are also a huge factor in maintaining wound chronicity, therefore resulting in a potentially two pronged effect of the nucleic acid scavenging nanofibers (NASF). Here we look at the effect that the NASFs have on *Pseudomonas aeruginosa*, *Staphylococcus aureus*, and *Staphylococcus epidermidis* biofilm formation both *in vitro* and *in vivo*.

5.1 Introduction and significance

Chronic wounds affect approximately 5.7 million patients a year and cost an estimated 20 billion dollars annually ¹²⁸, representing a major clinical problem leading to high morbidity and expense. Complications from chronic wounds are primarily attributed to biofilm formation. Biofilms are antibiotic resistant clusters of microorganisms that contribute to wound chronicity by extending the open wound period through extracellular matrix formation and adherence to the wound bed,

disrupting normal healing and preventing wound closure ¹²⁹. The biofilm extracellular matrix is composed of a mixture of macromolecules including exopolysaccharides, proteins, and nucleic acids (NAs). Studies show that the presence of extracellular DNA (eDNA) is required for biofilm formation, that removal of extracellular DNA prevents the formation of biofilms *in vitro*, and that removal of DNA from pre-formed biofilms results in dissolution of newly formed biofilms ⁶⁸.

There are two types of biofilm-forming bacteria that have been extensively studied-the gram-negative *Pseudomonas aeruginosa* (*P. aeruginosa*) and the gram-positive *Staphylococcus aureus* (*S. aureus*). The importance of eDNA as a structural component in biofilms was first shown in *P. aeruginosa* ¹³⁰. Studies have gone on to show that eDNA in *P. aeruginosa* sets off a cascade of cell lysis and gene activation that leads to antimicrobial resistance ¹³¹. This implies that removing eDNA from biofilms has the potential to reduce antibiotic resistance. Experiments applying DNase I to forming *P. aeruginosa* biofilms have shown degradation of eDNA, which subsequently prevents biofilm formation and dissolves already present biofilms ^{67,68}. The role of eDNA in biofilms extends beyond the pseudomonas strain and effects various other bacterial strains including the staphylococcal strains *S. aureus* and *Staphylococcal epidermidis* (*S. epidermidis*).

Both *S. aureus* and *S. epidermidis* are known to form biofilms and have a significant role in wound and catheter infections. Recently, eDNA has been shown to be a component of the EPS of both *S. aureus* and *S. epidermidis*. In fact, the bacteria has a gene that is specifically responsible for promoting cell lysis and the release of DNA during biofilm development ¹³⁰, emphasizing the importance of eDNA in biofilm formation. Izano et. al. showed that biofilms of both strains were inhibited by eDNA degradation induced by DNase I ¹³² and other studies have shown that biofilm adherence is reduced in the presence of DNase I ¹³⁰. Further studies into the significance of eDNA in biofilms have shown that bacterial beta toxins cross-linked with other bacterial beta toxins in the presence of eDNA, resulting in an insoluble nucleoprotein matrix that acts as the basis upon which staphylococcal biofilms form ¹³³. These studies indicate that eDNA is an integral part of biofilm formation and maintenance and that by removing the DNA from the potential infection area, the onset of biofilms can be prevented or reduced.

In addition to eDNA, *S. aureus* planktonic bacteria proliferation also relies on the presence of an RNA molecule called RNAIII. RNAIII acts as a hemolysin, destroying red blood cells by disrupting the membrane, and also acts as a regulatory RNA molecule that upregulates the production of various secreted toxins ¹³⁴. Neutralization of RNAIII by RNAIII inhibiting peptide (RIP) has been shown to reduce the virulence of *S. aureus*

in a planktonic growth phase ¹³⁴ and has also been shown to prevent biofilm formation in *S. epidermidis* ¹³⁵. Having an RNA component that is also relevant for biofilm formation adds an additional moiety that can be targeted for scavenging by the nucleic acid scavenging platform.

In order to prevent biofilm development in chronic wounds, NASF can be applied for nucleic acid scavenging. The NASF is a nanofibrous sheet that is covalently modified with polycationic polymers. This NASF platform effectively removes eDNA and eRNA from solutions by binding with the negatively charged backbone the nucleic acids. This method of nucleic acid removal has been validated by preventing TLR response in cells that are exposed to media containing extracellular nucleic acids that have been treated with NASF. Based on the efficacy studies, we believe that NASF could be a valid treatment for chronic wounds infected with biofilm by removing eDNA from the wound bed and subsequently preventing and/or reducing biofilm formation, shortening the duration of the inflammatory stage, and allowing for wound closure.

5.2 Materials and methods

5.2.1 Preparation of nucleic acid scavenging nanofibers (NASFs)

Preparation of neutral fibers was optimized by testing various concentrations of Poly (styrene-alt-maleic anhydride) (PSMA) with solvent combinations of one or more of the following: tetrahydrofuran, acetone, and dimethylformamide. Effective

electrospinning occurred with PSMA (0.6 g or 1 g) (Sigma-Aldrich, St. Louis, MO) dissolved in a 1:1:1 (v:v:v) mixture of tetrahydrofuran: acetone: dimethylformamide (10 mL) (Sigma-Aldrich) by constant mixing for 24 hrs at room temperature. PSMA nanofibers were electrospun using 2 mL of polymer solution in a 2cc glass syringe (Cadence Science, Staunton, VA) at a dispensing rate of 1 mL/hr, achieved by insertion of the syringe into an automated syringe pump, with an applied voltage of +15 kV. The polymer fibers were collected on a grounded cylindrical mandrel (~6.4 cm wide with a ~21.6 cm circumference) spinning at ~130 rpm at a distance of 10 cm away from the tip of the syringe needle. The neutral electrospun PSMA fibers were soaked in a solution of 1.8 kDa branched polyethylenimine (bPEI) (0.1M) (Polysciences, Inc., Warrington, PA) for 72 hrs at room temperature with constant shaking to form NASF. To form PAMAM-NASF, the neutral fibers were soaked in PAMAM-G3 (0.004M) (Sigma-Aldrich) at 4°C for 72 hrs with constant shaking. Following conjugation the NASF was washed for 10 min with deionized water a total of 5 times. NASF was sterilized for 30 min in ethanol, the ethanol was removed, and the NASF was allowed to air-dry in a sterile environment. PAMAM-NASF was washed 5 times for 10 min each in sterile water and allowed to air-dry in a sterile environment, skipping the ethanol sterilization step.

5.2.2 *In vitro* biofilm studies

The bacteria used for all of the biofilm studies were *Pseudomonas aeruginosa*, *Staphylococcus aureus*, and *Staphylococcus epidermidis*. *P. aeruginosa* (PA01, ATCC 15692) was grown in Luria Broth (LB) and both Staphylococcal strains (gifts from the Soman Abraham lab) were grown in Tryptic Soy Broth (TSB); TSB was supplemented with 0.25% glucose for biofilm formation and was left without glucose for CFU quantification. Cells were grown in liquid culture overnight with constant shaking at 37°C. For *P. aeruginosa* biofilm formation, 100 µL of bacterial cell suspension diluted to 5x10⁵ CFUs in sterile PBS was plated in a 96 well plate. For Staphylococcal biofilm formation, 50 µL of bacterial cell suspension diluted to 5x10⁵ CFUs in sterile PBS was plated in a 96 well plate. NASF (4 mm discs) was added directly to the bacterial suspension and they were incubated without shaking for 24-48 hrs. After incubation, the NASF and the remaining liquid were carefully removed from the well so as not to disturb the biofilm. 200 or 100 µL of 0.1% crystal violet solution was added to the washed biofilm and left at room temperature for 15 min. The crystal violet solution was then removed and the well was washed three times with sterile PBS to remove free bacteria that was not associated with the biofilm. The plates were air dried for 15 min, and then 100 µL of 95% ethanol was added to each well and left for 15 min at room temperature in order to solubilize the dye. The contents of each well were mixed by pipetting and the optical density (O.D.)

was measured at 600 nm using a plate reader. CFUs were measured at a wavelength of 550 nm when no visible biofilm was formed. For CFU measurements, the NASF was removed, 100 μ L of 1x PBS was added to the well, the mixture was pipetted up and down, and then measured at 550 nm.

5.2.3 Formation of staphylococcal biofilms for *in vivo* experiments

S. aureus and *S. epidermidis* were a gift from the Soman Abraham lab; the *S. aureus* was a clinical isolate, and the *S. epidermidis* was the strain UAMS-1. To form preformed biofilms to place on the open wounds of mice, *S. aureus* or *S. epidermidis* were grown in overnight cultures by inoculating 5 mL of Tryptic Soy Broth (TSB) with a single bacterial colony. Overnight cultures were diluted in sterile 1x PBS by 1:1000, 1:100,000, or 1:1,000,000 and 2 μ l of the diluted bacterial suspension was plated on a Nucleopore Track-Etch Membrane (Whatman, Maidstone, United Kingdom) on top of tryptic soy agar. Biofilms were left to grow for 24-72 hrs at 37°C without shaking.

5.2.4 Fixation of biofilms on NASF for Scanning Electron Microscopy (SEM)

The NASF with the bacterial/biofilm components was fixed with 10% formalin in 1x PBS for 30 min at room temperature and then rinsed with 1x PBS for 5 min. The sample was subsequently dehydrated in a graded ethanol series as follows: 50% ethanol in water for 5 min, 70% ethanol in water for 5 min, 80% ethanol in water for 10 min, 95% ethanol in water for 10 min, and 100% ethanol 2X for 10 min. The sample was then put

through a hexamethyldisilazane (HMDS) chemical drying series as follows: 3:1 ethanol:HMDS for 15 min; 1:1 ethanol:HMDS for 15 min; 1:3 ethanol:HMDS for 15 min; and 100% HMDS and left to air dry. Dry fibers were placed on aluminum foil and mounted on an SEM stub. The fibers were gold sputter-coated for 250 sec using the Denton Vacuum Desk IV sputter unit and imaged using a FEI XL30 SEM-FEG. Images were analyzed in Scandium.

5.2.5 *In vivo* biofilm infected wound models

Three strains of bacteria were used in this study: *P. aeruginosa* (PA01, ATCC 15692), *S. aureus*, and *S. epidermidis*. Diabetic (BKS.CgDock7^m+/+Lepr^{db}/J) female mice aged 8-12 weeks old and C57BL/6J (C57) female mice aged 28–40 weeks old were obtained from the Jackson Laboratory. All mice were given an 8 mm diameter excisional wound between the shoulder blades that was covered with Tegaderm Film (3M, Maplewood, MN). Additionally, the wounds of the C57 mice were stented with a silicone ring (Grace BioLabs, Bend, OR) sutured in four locations. Diabetic mice in the biofilm groups were administered 50 μ L of *P. aeruginosa* at 10⁴ CFUs directly into the open wound 72 hrs after initial wounding. C57 mice were administered pre-formed staphylococcal biofilms directly onto the wound at either the time of initial wounding or 24 hrs following initial wounding. NASF treatment was started 72 hrs following wounding in diabetic mice and 24 hrs following wounding in C57 mice with groups

including uninfected and no NASF, uninfected with NASF, biofilm infected and no NASF, and biofilm infected with NASF. All mice received three sheets of 8 mm diameter NASF placed directly inside the open wound, which was then covered by Tegaderm Film. Diabetic mice received NASF treatment daily until experiment termination or for 7 consecutive days with the NASF sheet changes occurring every 24 hrs. C57 mice received a single NASF treatment for either 0.5 hrs or 3.5 hrs. Following treatment, the NASF was removed from the mouse wound, placed in PBS, and vortexed in pulses at the highest level for 30 sec to remove any mechanically adhered components. The NASF was then placed in 10 mg/mL of heparin sodium salt (Sigma-Aldrich) for 30 min with intermittent vortexing. After 30 min, the NASF was discarded, an initial DNA gel was run on the crude components, and then a TRIzol (ThermoFisher Scientific) extraction was performed on the solution.

5.2.6 DNA gels and PCR

DNA extracted using the TRIzol reagent was resuspended in 8 mM NaOH. 200 ng of DNA was run on a 1% agarose gel at 100 V for 90 min and visualized using GelStar Nucleic Acid Stain (Lonza, Basel, Switzerland). Two primer sets for mitochondrial cytochrome c oxidase were used for PCR. Primer set 1 included primers: 5'-ACC AAG GCC ACC ACA CTC CT- 3' and 5'-ACG CTC AGA ATC CTG CAA AGA A- 3' while primer set 2 included primers: 5'- TCC AAG TCC ATG ACC ATT AAC TG- 3' and 5'-

TAT TGG TGA GTA GGC CAA GGG- 3' leading to fragment sizes of ~101 bp and ~115 bp, respectively. Taq 2x Master Mix (New England BioLabs, Ipswich, MA) and 100 ng of DNA was used for all PCR reactions. Primer set 1 was annealed at a temperature of 54°C with an extension time of 10 sec while primer set 2 was annealed at a temperature of 50°C with an extension time of 10 sec. All PCR products were run on a 3% agarose gel at 70 V for 60 min and visualized using GelStar Nucleic Acid Stain.

5.2.7 RNA sequencing

RNA libraries were prepared using the Strand RNA-Seq Kit (Kapa, Wilmington, MA) with 10 ng of RNA. Following library preparation, the libraries were pooled in equimolar amounts, and sequenced with a 50 bp SR run on the Illumina HiSeq 2500 sequencer. RNA-seq data was processed using the TrimGalore toolkit¹³⁶ which employs Cutadapt¹³⁷ to trim low quality bases and Illumina sequencing adapters from the 3' end of the reads. Only reads that were 20 nt or longer were kept for further analysis. Reads were mapped to a custom genome and transcriptome that contained the mouse NCBIM38r73¹³⁸ data as well as the *Pseudomonas aeruginosa* data using the STAR RNA-seq alignment tool¹³⁹. Reads that mapped to a single genomic location were kept for subsequent analysis. Gene counts were compiled using the HTSeq tool¹⁴⁰. Only genes that had at least 10 reads in any given library were used in subsequent analysis.

Normalization and differential expression was carried out using the DESeq2¹⁴¹ Bioconductor¹⁴² package with the R statistical programming environment¹⁴³.

5.2.8 Protein gels and charged protein separation

Protein gels were run on 4-20% Mini-PROTEAN Precast Protein Gels (BioRad, Hercules, CA) using the Spectra Multicolor High Range Protein Ladder (ThermoFisher Scientific). 15 μ l of 2x Laemmli Sample Buffer was added to 500 ng of protein in a total volume of 15 μ L supplemented with 1X Tris-glycine SDS buffer (BioRad) and then loaded into the gel. Protein gels were run at 100 V for 1 hr and stained using the Pierce Silver Stain Kit (ThermoFisher Scientific). Proteins were separated by charge using a Mini Cation Exchange Spin Column (Pierce, Waltham, MA). 400 μ L of 25 mM sodium acetate buffer at a pH of 5.5 was added to the column and centrifuged at 2,000 X g for 5 min. Then the entire protein sample was added to the column and centrifuged at 2,000 X g for 5 min; this eluate sample was collected as positively-charged proteins. Next, 400 μ L of 25 mM sodium acetate buffer, pH 5.5, was added onto the membrane and the column centrifuged at 2,000 X g for 5 min, this step was repeated once. Finally, negatively charged proteins were eluted by adding 50 μ L of 25 mM sodium acetate buffer, pH 5.5 containing 1M NaCl.

5.2.9 Mass spectrometry

To clean up the samples, 10 ug of material was loaded into an SDS-PAGE gel and run for only 4 minutes. After colloidal coomassie blue staining, the entire stained region was excised from each lanes, and in-gel digestion was performed as detailed previously¹⁴⁴. After digestion, extraction, and dry-down, approximately 2.5% of each sample was submitted for LC-MS/MS using a nanoAcquity UPLC system (Waters Corp, Milford, MA) coupled to a Thermo Q Exactive Plus Hybrid Quadropole-Orbitrap Mass Spectrometer (ThermoFisher Scientific) via a nanoelectrospray ionization source. First, the sample was trapped on a Symmetry C18 20 mm × 180 μm trapping column for 3 min at 5 μL/min (99.9/0.1 v/v water/acetonitrile 0.1% formic acid), followed by the analytical separation on a 75 μm × 250 mm column packed with 1.8 μm Acquity HSST3 C18 stationary phase (Waters Corp). Peptides were separated using a gradient of 5 to 40% acetonitrile with 0.1% formic acid over 90 min at a flow rate of 0.4 μL/min with a column temperature of 55°C. Data collection on the QExactive Plus mass spectrometer was performed in a data-dependent acquisition (DDA) mode of acquisition with a resolution (r) of 70,000 (@ m/z 200) for full MS scan from m/z 375 – 1600 with a target AGC value of $1e6$ ions in profile mode, followed by 20 MS/MS scans at $r=17,500$ (@ m/z 200) in centroid mode, using an AGC target value of $1e5$ ions, a max fill time of 60 msec, and normalized collision energy of 30 V. A 30 sec dynamic exclusion was employed to decrease MS/MS

oversampling. The total analysis cycle time for the sample injection was approximately 125 min.

5.3 Results

The ability of NASF to reduce biofilm formation was tested *in vitro* in *P. aeruginosa* (Figure 32), *S. aureus*, and *S. epidermidis* (Figure 33). For all three bacterial strains, NASF significantly reduced biofilm mass. Because the fluid absorption capacity of the NASF could potentially contribute to the reduction in biofilm by absorbing bacterial material, in the biofilm study done with the staphylococcal strains, a Kimwipe group was added to represent an uncharged absorbable material. Figure 33 shows that the Kimwipe had no significant effect on the biofilm mass, demonstrating that the polymer's absorption capacity is not the primary means of biofilm reduction. These results suggest that the polycationic chemical composition of the NASF may play a significant role in reducing biofilm mass.

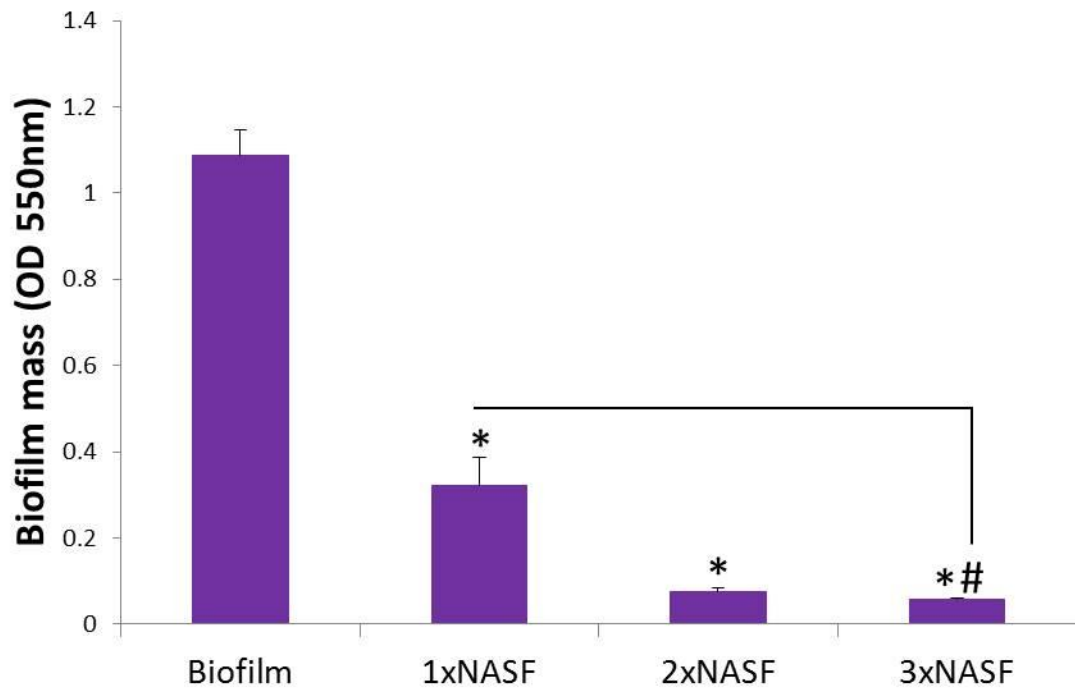


Figure 32: Reduction of *P. aeruginosa* biofilm mass by NASF. NASF is added to *P. aeruginosa* in solution in a 4 mm diameter disc; 1x indicates 1 disc, 2x indicates 2 discs, 3x indicates 3 discs, (n=3). * Indicates $p < 0.001$ as compared to biofilm group, # indicates $p < 0.05$ as compared to 1xNASF group.

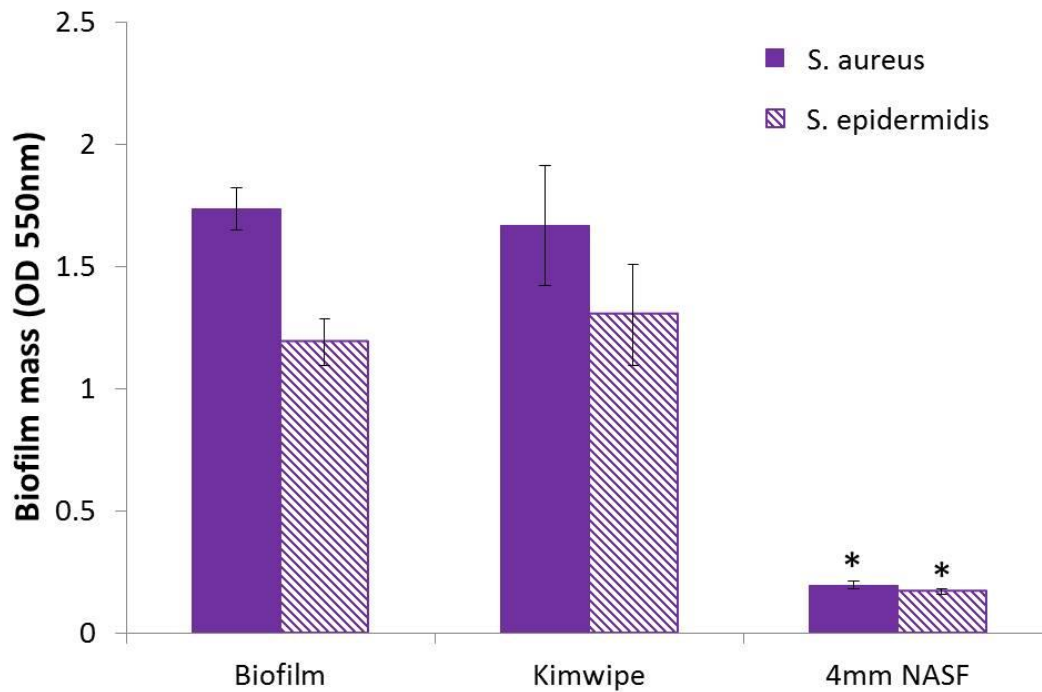


Figure 33: Reduction of *S. aureus* and *S. epidermidis* biofilm mass by NASF. NASF is added to the bacterial suspension as a 4 mm diameter disc, (n=3). The Kimwipe group represents an uncharged, absorbable material control; * indicates $p < 0.001$ compared to Biofilm.

To determine whether the NASF reduction of bacterial growth is limited to biofilms or whether NASFs also alter the growth of bacteria in planktonic culture, the staphylococcal strains were grown without forming biofilms. Figure 34 demonstrates that the NASF was able to inhibit the growth of both planktonic *S. aureus* and *S. epidermidis*. SEM of the NASFs after 24 hrs and 48 hrs of *P. aeruginosa* biofilm growth show infiltration of the biofilm onto the NASF whereas 48 hrs of *S. aureus* or *S. epidermidis* incubation show little to no bacteria and no biofilm growth on the NASF,

Figure 35. These images confirm that the NASF attracts the *P. aeruginosa* biofilm therefore reducing the amount of biofilm present on the adjacent surface. The NASF act on the Staphylococcal strains by reducing planktonic bacterial growth and subsequently preventing formation of biofilm, leading to the reduction of biofilm on the adjacent surface without any biofilm formation on the NASF itself.

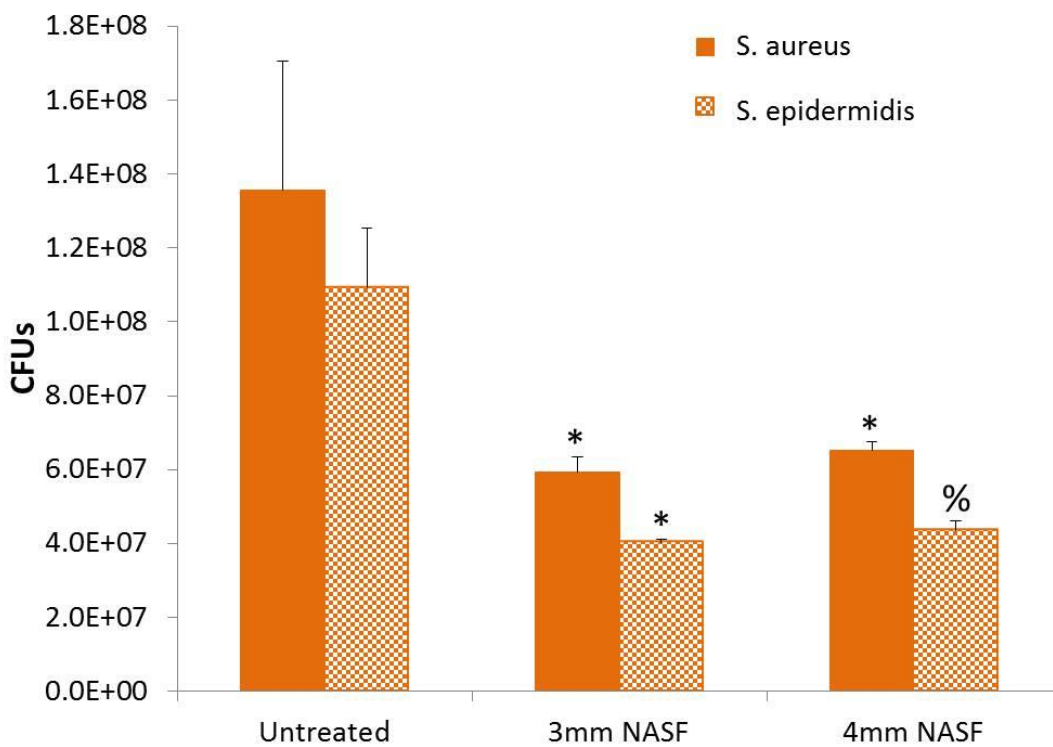


Figure 34: The reduction of planktonic bacterial growth by NASF in *S. aureus* and *S. epidermidis* over 24 hrs as indicated by colony forming unit (CFUs). 3mm and 4mm represent the diameter of the NASF discs that were added to the bacterial solution. Each well received one NASF disc (n=3); * indicates $p < 0.001$, % indicates $p \leq 0.002$ as compared to untreated.

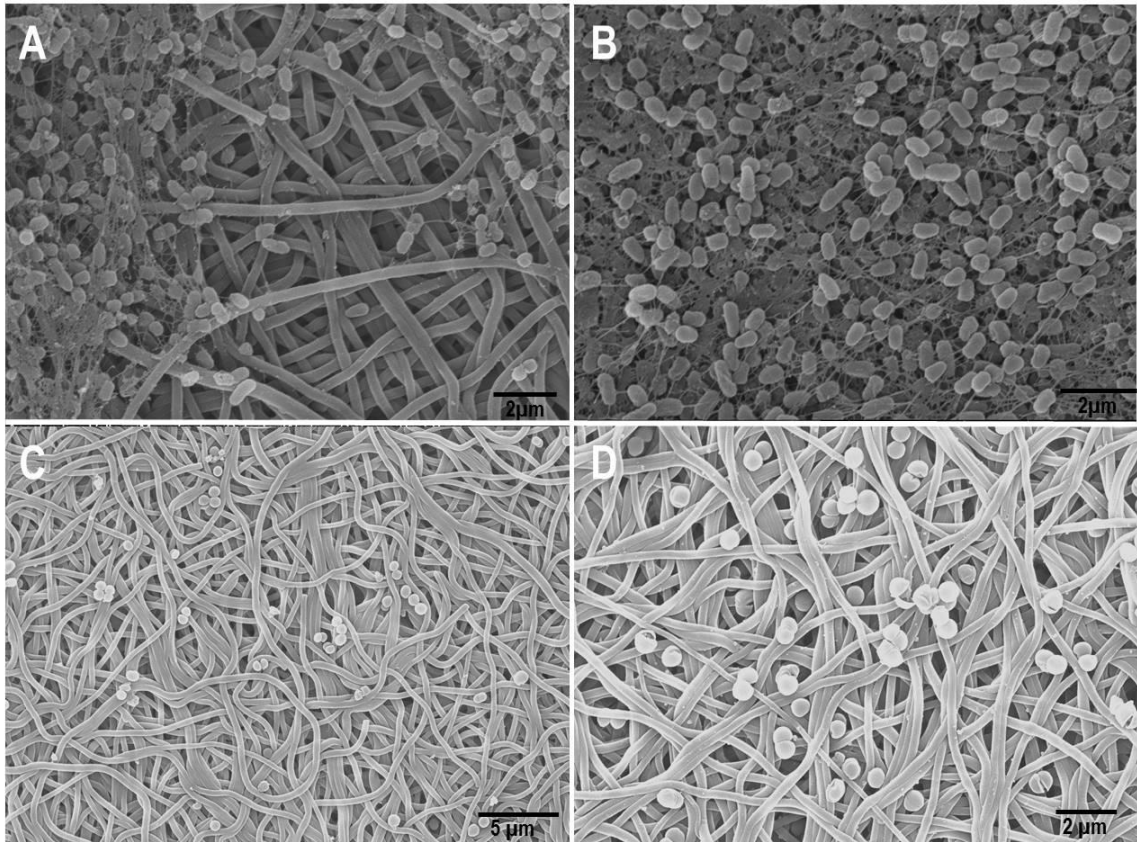


Figure 35: Scanning electron images from *in vitro* studies; (A) *P. aeruginosa* biofilm infiltrating NASFs after 24 hr incubation; (B) *P. aeruginosa* biofilm on the surface of the NASFs after 48 hr incubation; (C) *S. aureus* interaction with NASFs after 24 hr incubation; (D) *S. epidermidis* interaction with NASFs after 48 hrs.

Next, we took the NASF into mice to determine whether the polymers were able to prevent biofilm formation *in vivo*. A pilot study of diabetic mice with *P. aeruginosa* biofilm infections in an open wound showed differences in the healing times for biofilm-infected wounds versus uninfected wounds (Figure 36). While almost 50% of the

untreated mice had wound closure by day 18, mice given biofilm infections failed to achieve wound closure by the same time point. From this data, we confirmed that *P. aeruginosa* biofilms prevented wound healing in diabetic mice, therefore we hypothesized that NASF treatment should improve healing of infected wounds. The NASF should reduce the presence of biofilm in the wound, therefore allowing the wound to heal more quickly, similar to the healing seen in wounds never infected with biofilms.

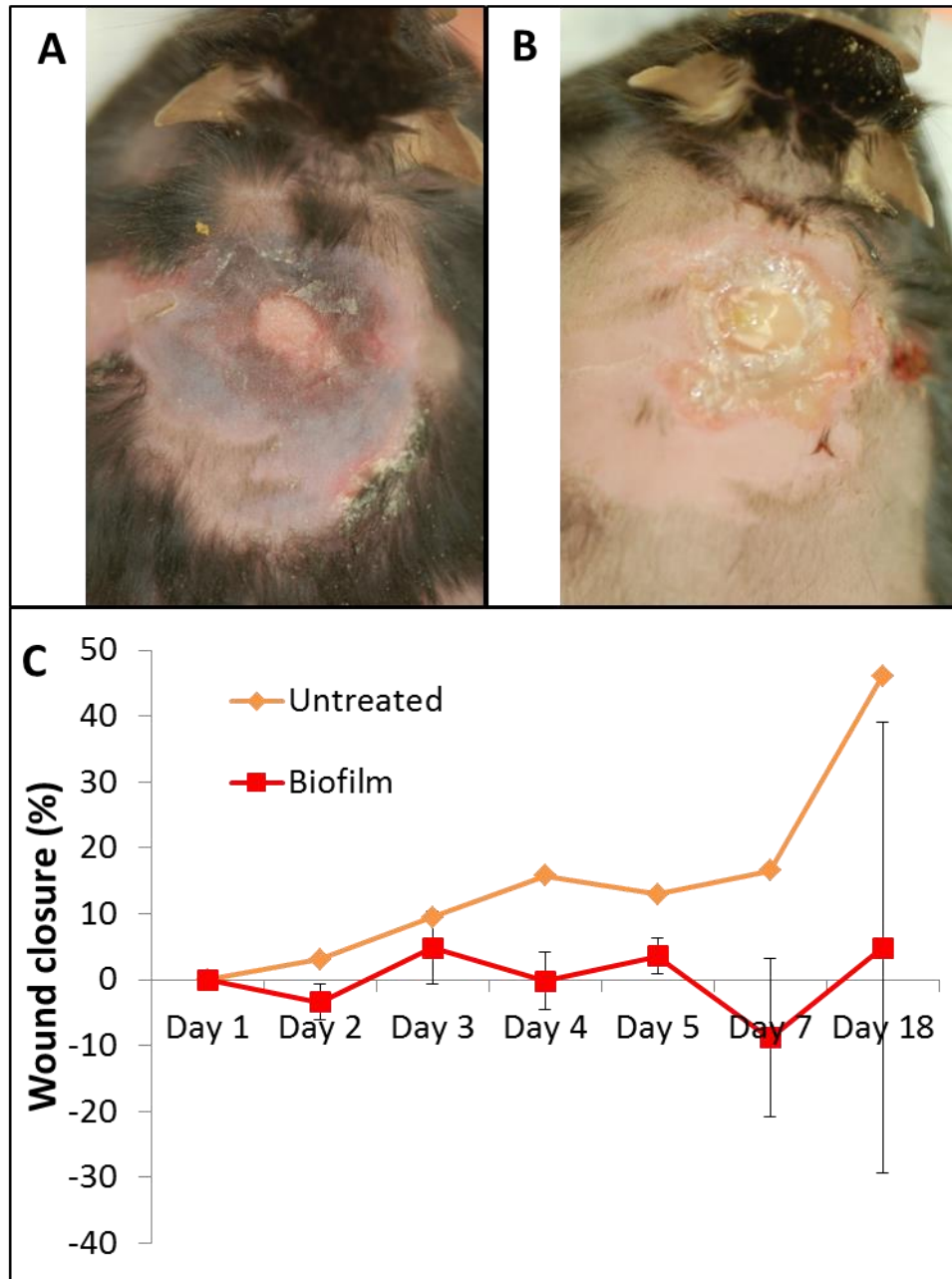


Figure 36: Results from pilot *P. aeruginosa* biofilm study in db/db mice. (A) Photo of untreated mouse wound. (B) Image of *P. aeruginosa* infected biofilm wound. (C) Wound closure of untreated versus *P. aeruginosa* biofilm infected open wounds over 18 days.

In the first *in vivo* study with NASF in diabetic mice, one 8 mm disc of NASF was added to each infected mouse wound ~24 hrs after the addition of *P. aeruginosa* bacteria, allowing the bacteria some time to establish a biofilm in the wound before the addition of the NASF. The NASF was changed daily until day 26 when the experiment was stopped. Surprisingly, by day 26, both the untreated group without biofilm and the untreated group with biofilm had completely healed (Figure 37), indicating that the NASF did not have the desired outcome with this treatment regimen.

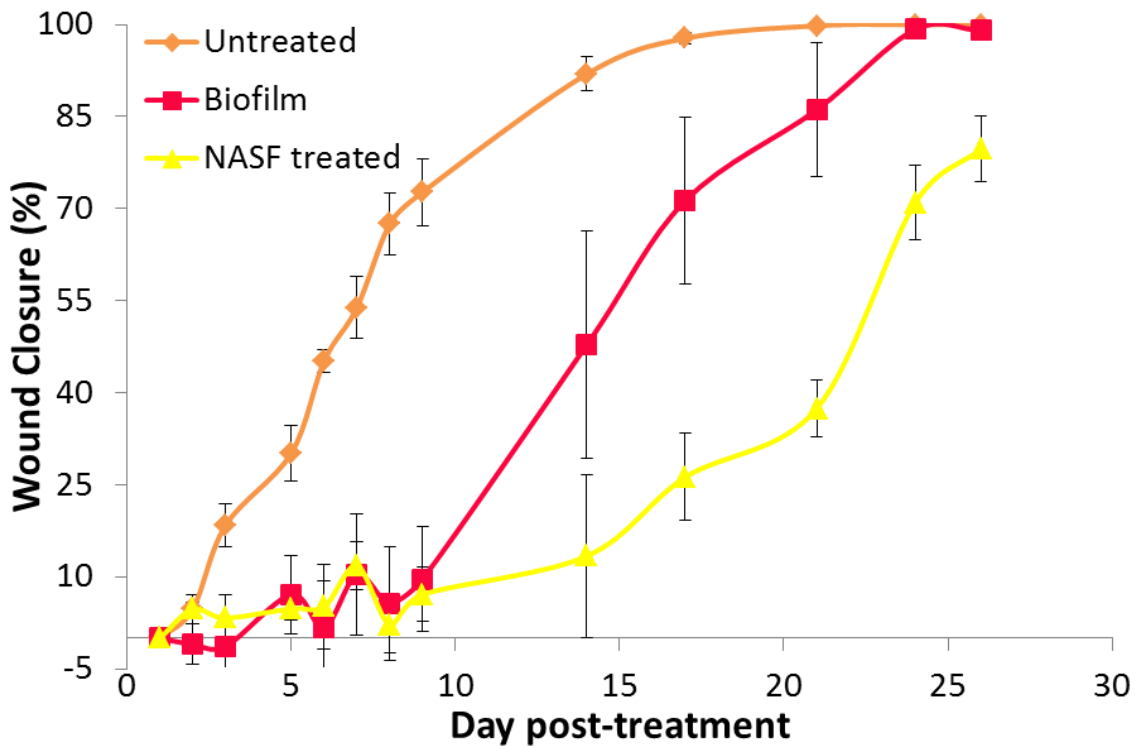


Figure 37: Wound closure of db/db mice given wounds that were left alone (Untreated) (n=5), infected with *P. aeruginosa* biofilm (Biofilm) (n=8), or infected with *P. aeruginosa* biofilm and treated with NASF (NASF treated) (n=8) – NASF were changed daily.

The results show that the NASF is detrimental to the wound healing at this dose. We hypothesized that the NASF was mechanically preventing wound healing due to its presence in the wound bed and therefore we decided to decrease the number of treatment days in an effort to reduce the negative effect on wound healing. Additionally, we increased the NASF dose to have a more powerful effect on the biofilm during the shorter treatment period. With this new treatment regimen, mice were treated with NASF for 7 days with daily changes used at a dose of three 8 mm discs of NASF per wound; this dose was used because the *in vitro* studies showed that three NASF discs were significantly better at reducing *P. aeruginosa* biofilms than one NASF disc (Figure 32). Because we hypothesized that the physical presence of the NASF may have inhibited wound healing, in this experiment an NASF treatment group to the uninfected wound was added. Wound closure results, shown in Figure 38, show a similar trend to that of the first experiment, with the NASF slowing down the wound healing process and all of the biofilm-infected wounds healing slower than the uninfected wounds. We suspected that the NASF was mechanically preventing the wound closure by being present in the wound bed. To determine if this slowed wound healing was affecting the quality of wound healing, the healed wounds were analyzed with tight junction staining and H&E staining.

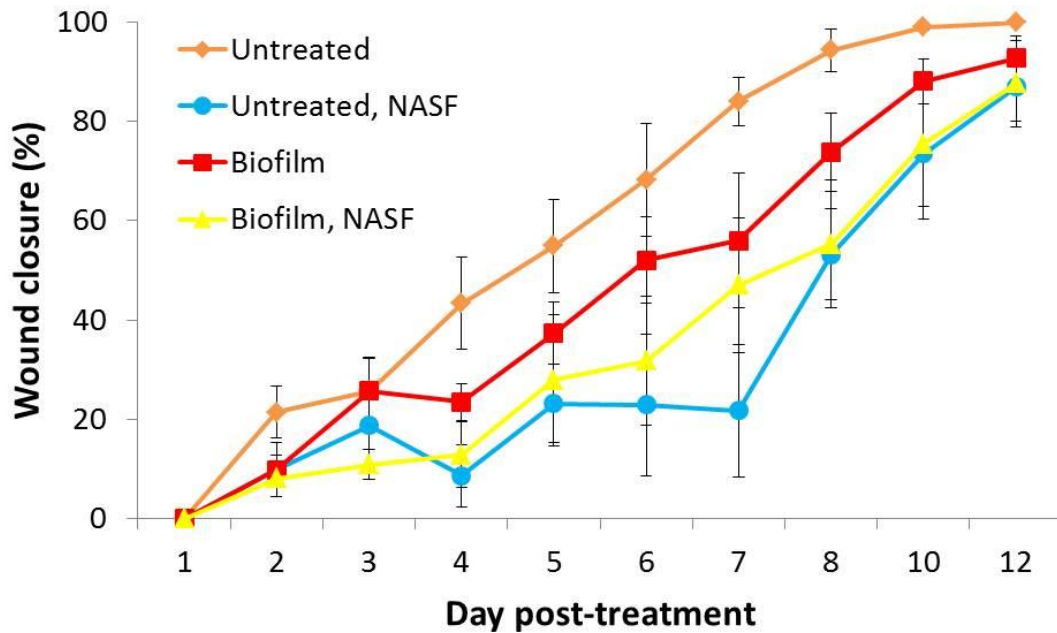


Figure 38: Wound closure of db/db mice given wounds that were left alone (Untreated) (n=5), left alone and treated with NASF (Untreated, NASF) (n=5), infected with *P. aeruginosa* biofilm (Biofilm) (n=8), or infected with *P. aeruginosa* biofilm and treated with NASF (NASF treated) (n=8) – NASF were changed daily for 7 days.

The tight junction staining of the healed wounds (Figures 39 and 40) looked similar for untreated versus NASF treated wounds. NASF treatment neither demonstrated superior wound healing nor detrimentally effected wound healing. With this data, it appeared that there was no structural benefit to the slower wound healing after NASF treatment in this wound model. H&E pathology of the healed wounds showed similar amounts of hyperkeratosis, acanthosis, and fibrosis in untreated wounds, biofilm infected wounds, and biofilm infected wounds treated with NASF (Figure 41). However, some biofilm samples showed an increased presence of

inflammatory cells (Figure 41C-D) whereas those infected with biofilm and treated with NASF did not show the presence of inflammatory cells, therefore indicating that the NASF had the capacity to reduce inflammation in biofilm infected mice.

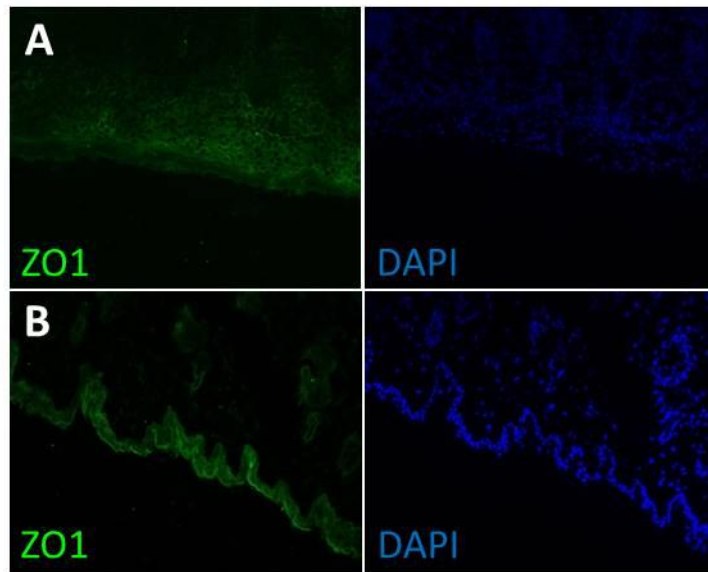


Figure 39: Representative images at 20x magnification of ZO1 tight junction fluorescent staining and DAPI staining of wounds extracted from db/db mice: (A) *P. aeruginosa* biofilm wounds and (B) untreated wounds with no biofilm.

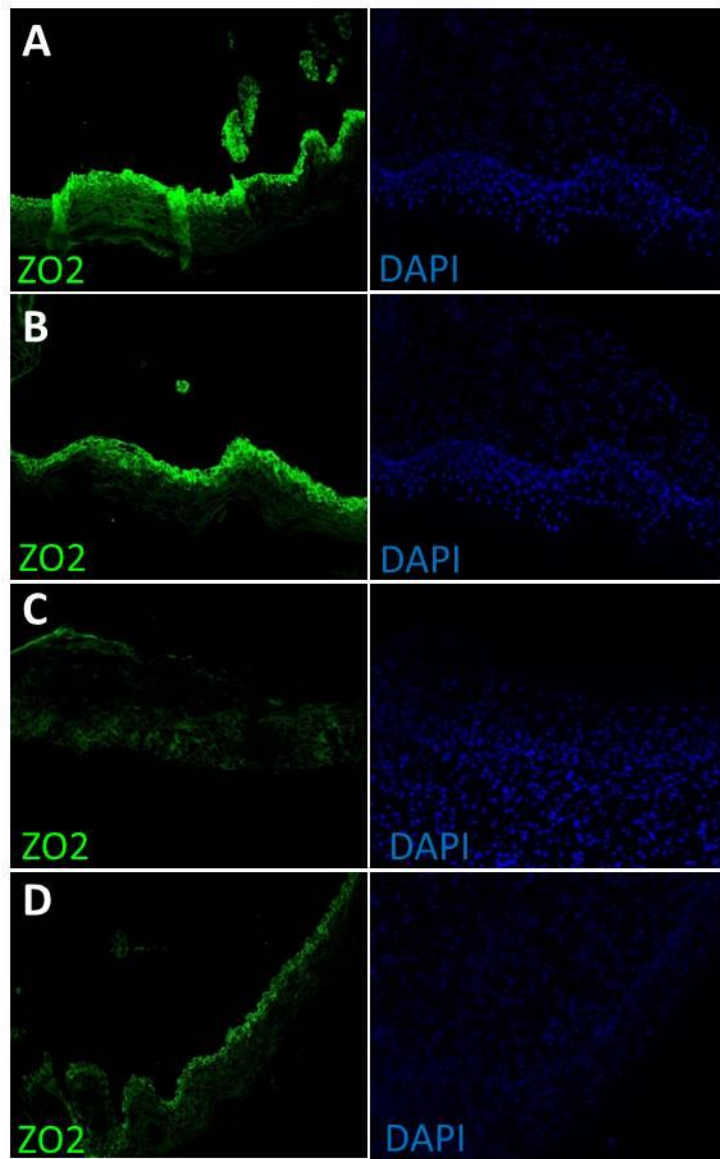


Figure 40: Representative images at 20x magnification of ZO2 tight junction fluorescent staining and DAPI staining of wounds extracted from db/db mice: (A) *P. aeruginosa* biofilm wounds, (B) *P. aeruginosa* biofilm wounds treated with NASF for 7 days, (C) untreated wounds with no biofilm, (D) wounds with no biofilm treated with NASF for 7 days.

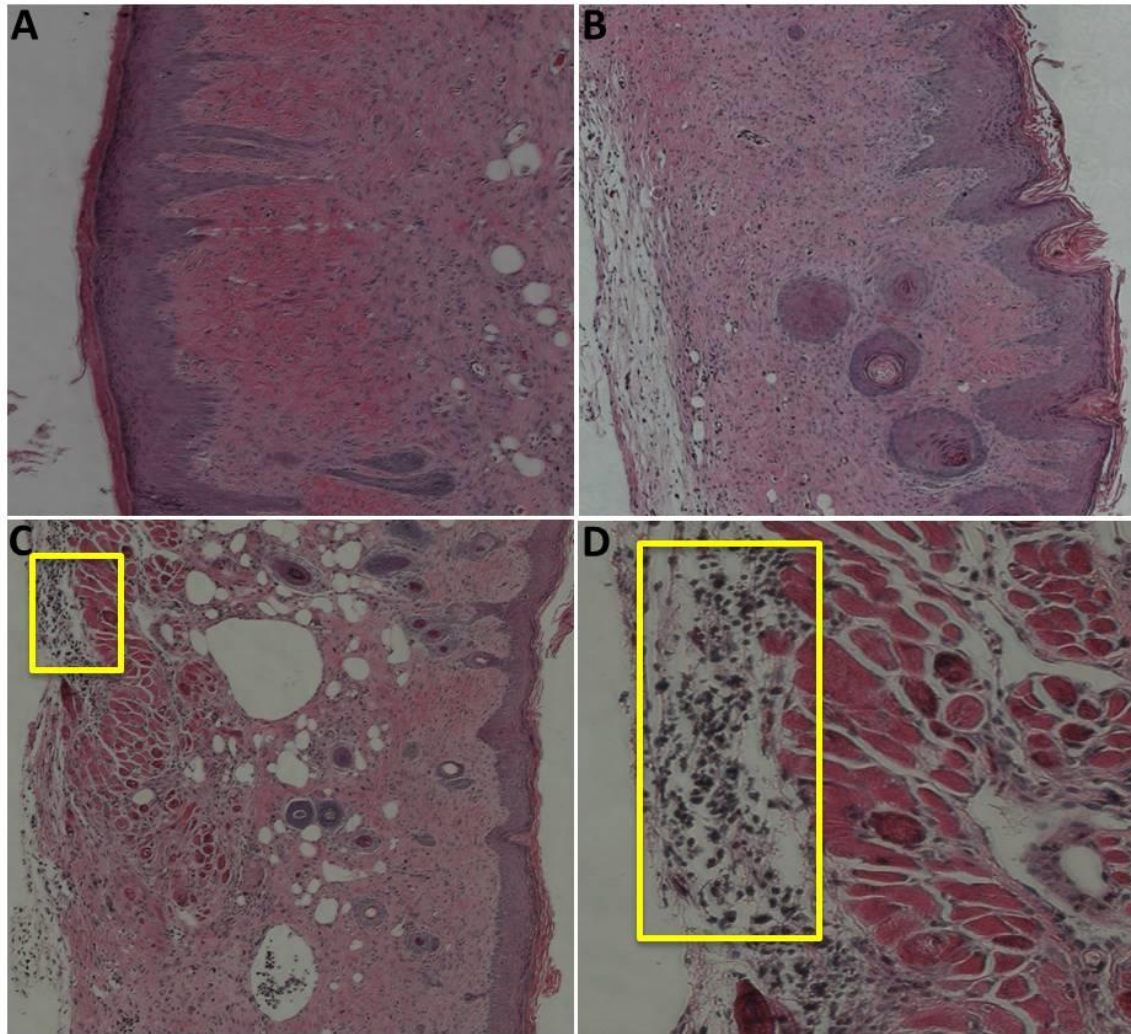


Figure 41: Representative images of H&E staining from db/db extracted wounds: (A) untreated wound with no biofilm, (B) *P. aeruginosa* biofilm wound treated with NASF for 7 days, (C) *P. aeruginosa* biofilm infected wound (yellow box highlights the inflammatory cells), (D) magnification of inflammatory cells in the *P. aeruginosa* biofilm infected wound.

Throughout the *in vivo* experiments, the NASF were collected and analyzed for the contents that they were pulling out of the wounds. The NASF were evaluated for their functionality *in vivo* by determining what combination of DNA, RNA, and protein

the NASF were pulling out of the db/db mice wounds whether infected with biofilm or not. The crude extracts from the NASF showed one prominent band when run on a GelStar stained DNA gel (Figure 42), indicating that the fibers were pulling out the same NA whether infected or not, specifying that the NA were primarily of mouse origin.

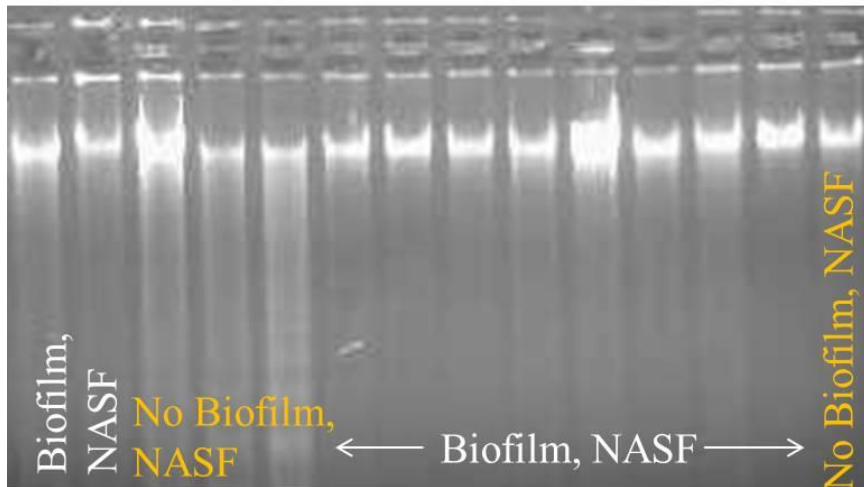


Figure 42: DNA gel from crude NASF extracts from db/db mice wounds on day 2 (lanes 1-5) or day 3 (lanes 6-14) of NASF treatment: NASF treated *P. aeruginosa* biofilm wounds (lanes 1-2, 6-13), NASF treated wounds with no biofilm (lanes 3-5, 14).

These crude extracts were separated into RNA, DNA, and protein components for further analysis. The DNA extracts revealed two prominent DNA bands that were present in almost all of the samples whether or not *P. aeruginosa* biofilm was present (Figure 43). Based on the size of the bands, one of them was determined to be the size of mitochondrial DNA (mtDNA) at ~16kb; this was validated by PCR (Figure 44). Primers to cytochrome-c oxidase were used to amplify the mtDNA. However, cytochrome-c

oxidase is also found in the bacterial genome. Therefore, to determine whether the cytochrome-c oxidase pulled down from the NASF is likely of bacterial or mouse origin, DNA extracts from NASF that were incubated *in vitro* with *P. aeruginosa* biofilms were also amplified, Figure 44B-C. Neutral PSMA fibers were also tested with *in vitro* *P. aeruginosa* biofilms as a neutral fiber control, and the resulting DNA extracts were amplified using the same primers. The *in vitro* PCR control of DNA extracts from NASF treated *P. aeruginosa* biofilms showed weak bands after PCR amplification. However, compared to the cytochrome-c oxidase DNA band amplified from the *in vivo* DNA extracts using the same primers, these *in vitro* bands were insignificant. These results indicate that the mtDNA from the *in vivo* extracts is most likely an amplification of a mtDNA segment rather than the segment of cytochrome-c on the bacterial genome; hence we trust that the NASF removed large amounts of mtDNA from wounds in db/db mice.

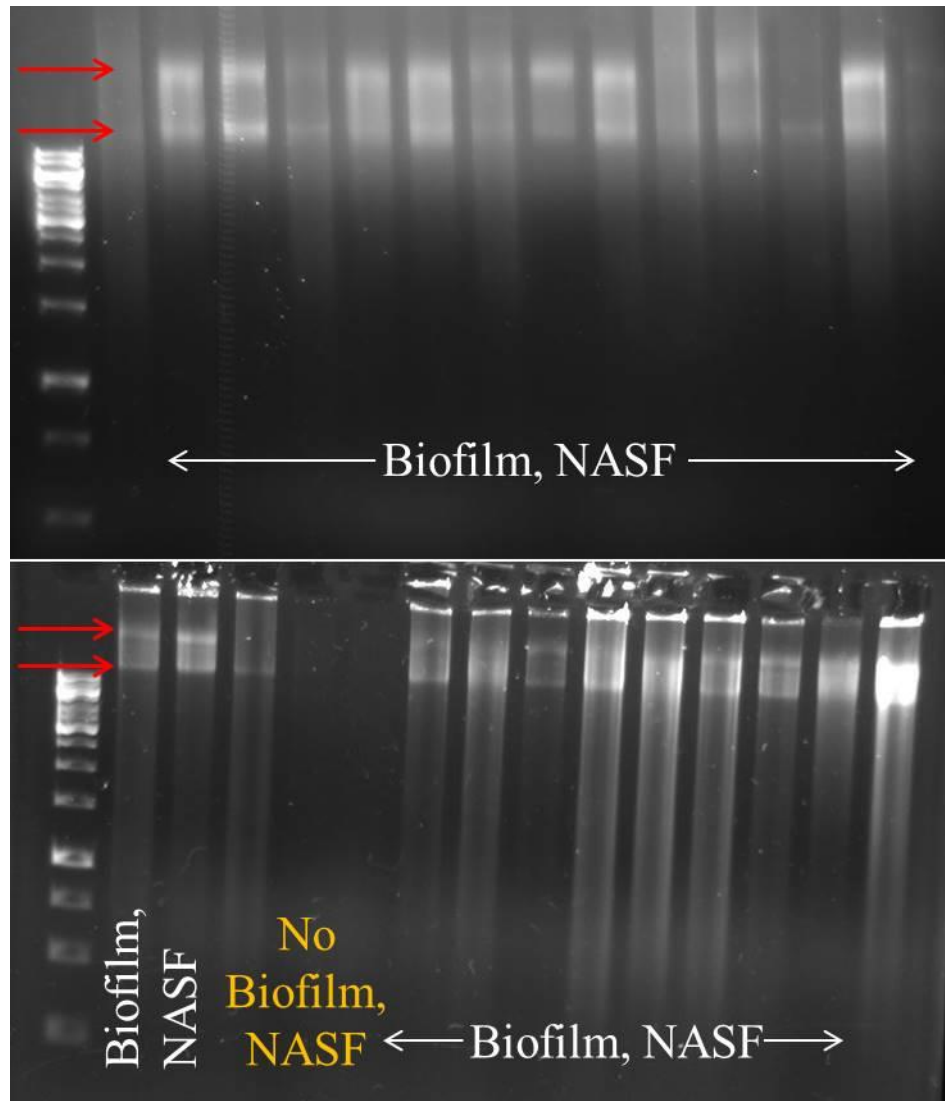


Figure 43: DNA gel from DNA separated out by TRIzol extraction of crude NASF extracts from db/db mice wounds, 1 kb DNA ladder is in lane 1 of both the top and bottom gels. Red arrows indicate prominent DNA bands found in all samples. Top gel shows NASF treated *P. aeruginosa* biofilm wounds from day 1 (lanes 2-9) and day 2 (10-15). Bottom gel shows DNA from day 2 (lanes 1-5) or day 3 (lanes 6-14) of NASF treatment: NASF treated *P. aeruginosa* biofilm wounds (lanes 1-2, 6-13), NASF treated wounds with no biofilm (lanes 3-5, 14).

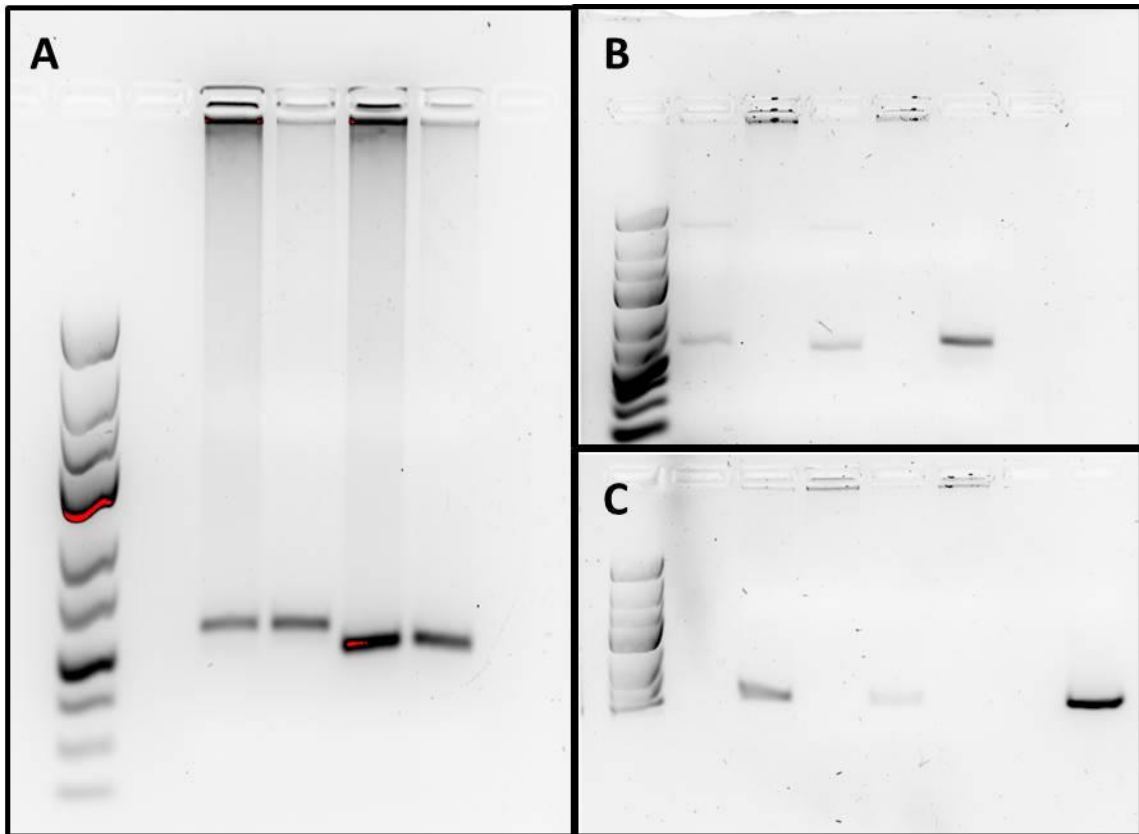


Figure 44: DNA gels of PCR products of DNA extracts from (A) db/db mice treated with NASF and infected with *P. aeruginosa*, lanes 4 and 6, or treated with NASF without biofilm present, lanes 3 and 5; (B) NASF extracts from *in vitro* *P. aeruginosa* biofilms, lanes 2 and 4, or neutral PSMA nanofibers, lanes 3 and 5, as compared to in vivo NASF extracts from *P. aeruginosa* infected db/db mouse wounds, lane 6, using primer set 2; (C) NASF extracts from *in vitro* *P. aeruginosa* biofilms, lanes 3 and 5, or neutral PSMA nanofibers, lanes 4 and 6, as compared to in vivo NASF extracts from *P. aeruginosa* infected db/db mouse wounds, lane 7, using primer set 1. Lane 1 is GeneRuler Low Range DNA Ladder.

The RNA extracts isolated from the NASF *in vivo* treatment were analyzed using RNA sequencing. The Venn diagram in Figure 45 shows the number of detected RNAs that were extracted from mouse wounds that were either infected with *P. aeruginosa* or

not infected. There was an overlap in 11983 RNAs detected. Overall the NASF that was not exposed to *P. aeruginosa* bacteria had higher numbers of RNA at 18,448 as compared to 12,693 RNAs that were detected from the NASF extract used to treat the *P. aeruginosa* biofilm; this is most likely because the biofilm prevents access to the wound where many free RNAs are present. The 656 RNAs that were unique to the biofilm infected group were primarily of bacterial origin, showing that the NASF were able to remove bacterial RNAs. The RNAseq heatmap in Figure 45 shows how the RNAs extracted from uninfected wounds and *P. aeruginosa* infected wounds differ.

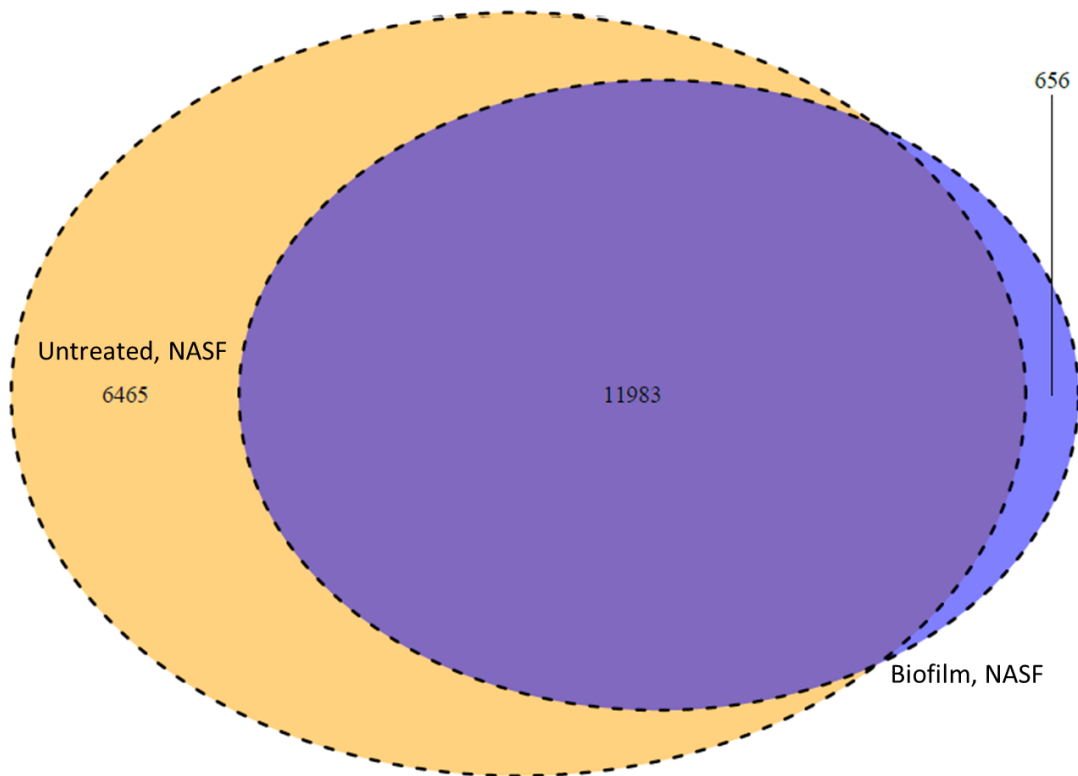


Figure 45: Venn diagram of the number of RNAs that were extracted from NASF on *P. aeruginosa* biofilm treated db/db wounds (Biofilm, NASF - purple) versus NASF on db/db wounds with no bacterial biofilm (Untreated, NASF-yellow).

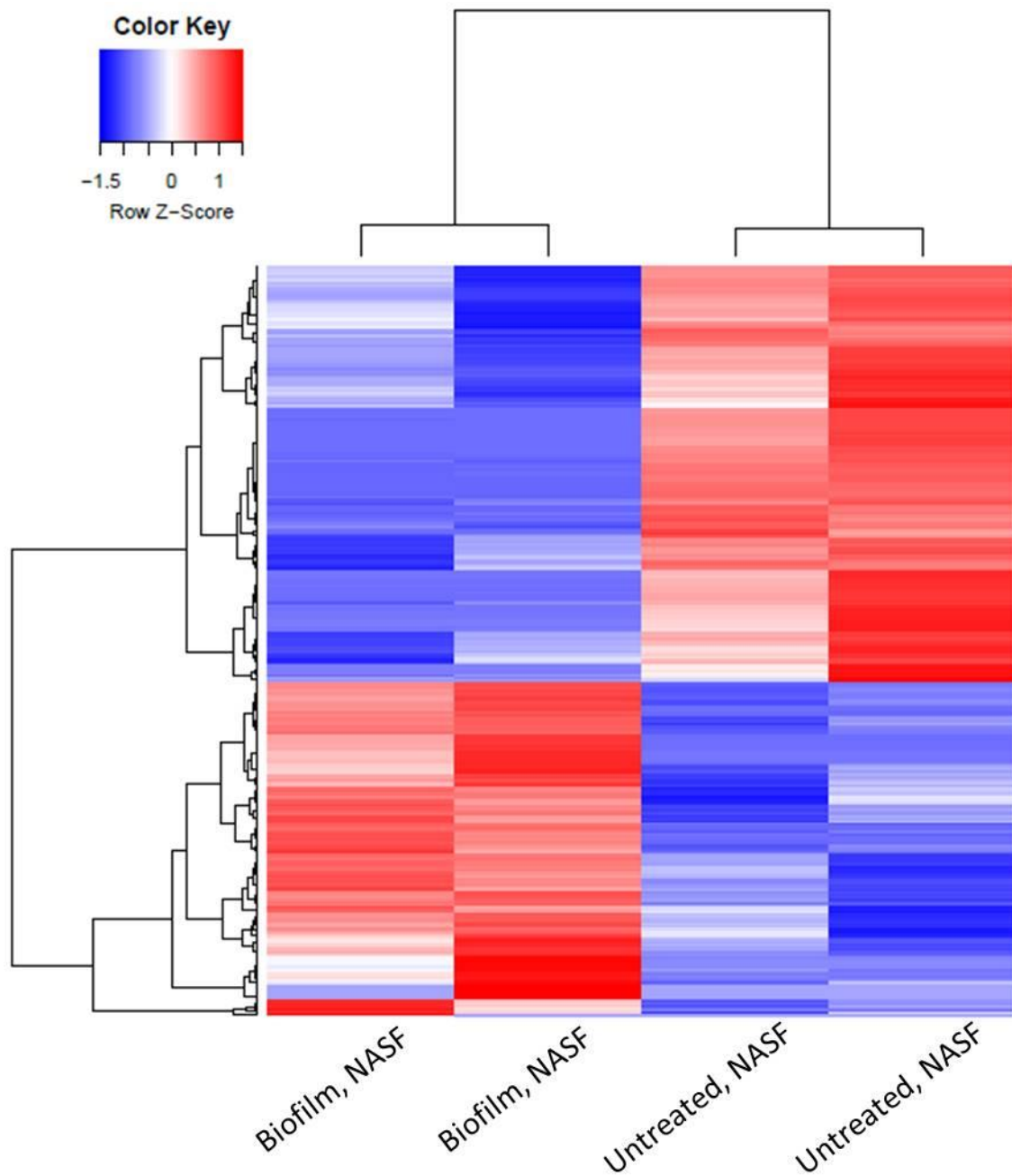


Figure 46: RNAseq heat map from RNA extracts of db/db wounds from four different mice including two that were without biofilm (Untreated, NASF) and 2 that were with *P. aeruginosa* biofilm (Biofilm, NASF).

Initial protein extracts were measured by BCA assay to determine total protein extracted (Figure 47) and then a protein gel was run to visualize the proteins (Figure 47). There was no apparent trend in the amount of total protein extracted from the wound bed whether infected or not infected. The total protein gel in Figure 48 appears to show stronger bands in the lane of the NASF extract from the uninfected wound; however this observation was not validated. In an attempt to determine the overall charge of the proteins, the protein extracts were processed through a cationic exchange column. The first flow through was deemed positively charged proteins (Figure 49A) and the proteins extracted from the column were presumed to be negatively charged proteins (Figure 49B). Based on the protein gels of the separated positively charged and negatively charged proteins, it appeared as though there were less negatively charged proteins in the total protein extracted from the NASF. This could be because more of the proteins were complexed to negatively charged nucleic acids when interacting with the fiber or that the change in pH to separate the proteins caused a charge change that was not representative of the protein's charge at neutral, body pH.

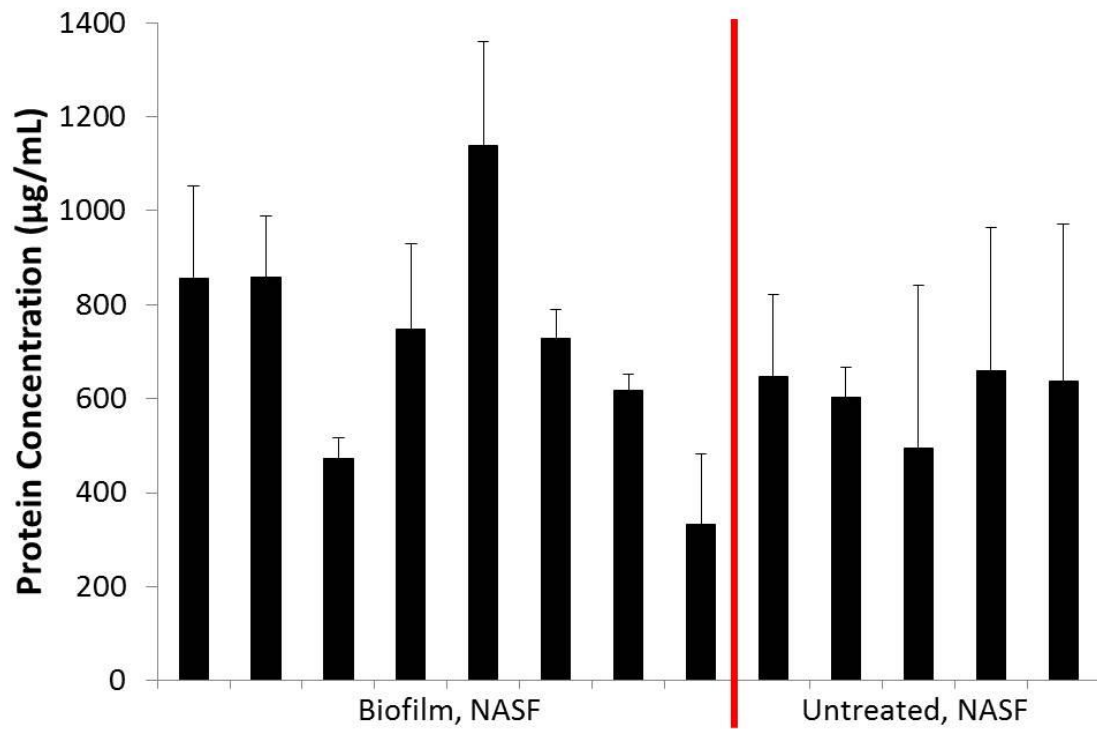


Figure 47: Average total protein extracted from NASF used on wounds in db/db mice infected with *P. aeruginosa* (Biofilm, NASF) or uninfected (Untreated, NASF). Each bar indicates an individual mouse.

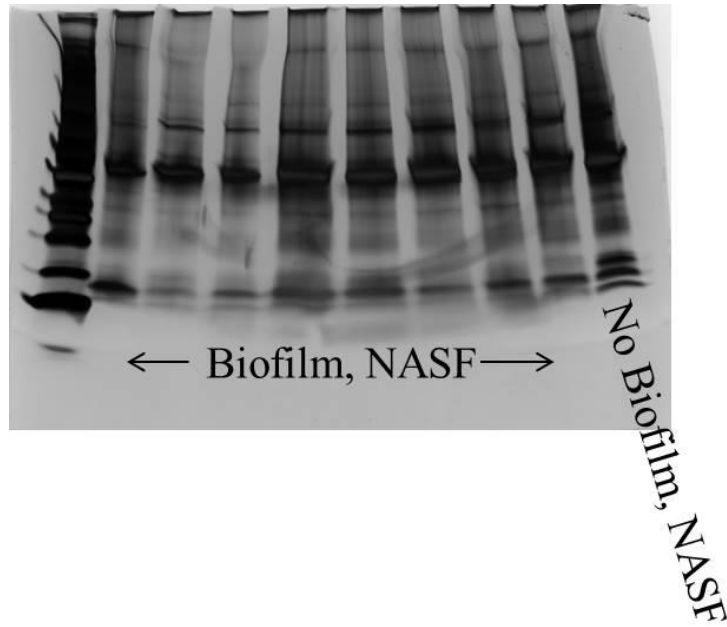


Figure 48: Total protein extracted from NASF used to treat db/db mice that were infected with *P. aeruginosa* (lanes 2-9) or not infected (lane 10). Ladder in lane 1 is Spectra HR protein ladder. Each lane indicates an extract from a different mouse.

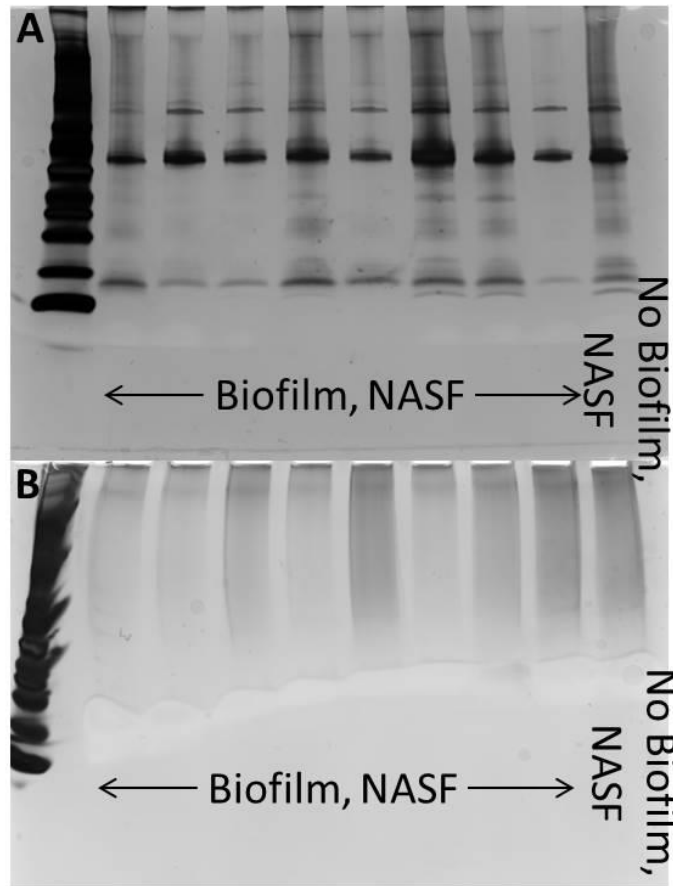


Figure 49: Protein gels after separation of positively charged and negatively charged proteins from db/db mice that were infected with *P. aeruginosa* (lanes 2-9) or not infected (lane 10) with Spectra HR protein ladder in lane 1; (A) positively charged proteins, (B) negatively charged proteins.

The protein extracts from the NASF were also analyzed using mass spectrometry. The results showed that a majority of the proteins where at least 1 peptide was found to identify the protein were an overlap between the NASF used on uninfected mice and mice that were infected with *P. aeruginosa* biofilm (Figures 50 and 51). This indicates that a majority of the proteins withdrawn from the wound were of

mouse origin. Additionally, the NASF used on uninfected mouse wounds had an overall higher number of detectable proteins at 715 as compared to NASF used to treat *P. aeruginosa* infected wounds where 686 proteins were detected. Table 3 lists the proteins that were found exclusively in extracts from *P. aeruginosa* infected wounds that had at least 4 peptide fragments indicating the protein.

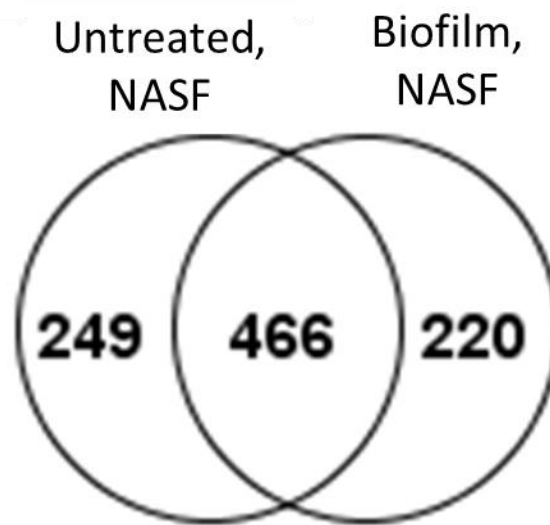


Figure 50: Venn diagram displaying the number of proteins extracted from wounds treated with NASF in db/db mice for 24 hrs that were biofilm free (Untreated, NASF) or infected with *P. aeruginosa* biofilm (Biofilm, NASF) from day 1-2 of NASF treatment.

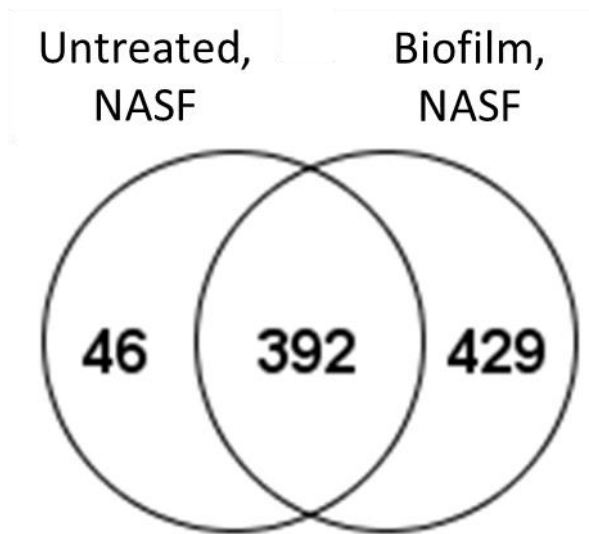


Figure 51: Venn diagram displaying the number of proteins extracted from wounds treated with NASF in db/db mice for 24 hrs that were biofilm free (Untreated, NASF) or infected with *P. aeruginosa* biofilm (Biofilm, NASF) from day 6-7 of NASF treatment.

Table 3: Proteins found exclusively in NASF extracts from db/db mice infected with *P. aeruginosa* biofilm treated with NASF for 24 hrs from day 1-2 of treatment. Proteins were identified by at least 4 different peptides.

Mouse proteins	<i>P. aeruginosa</i> proteins
SUN domain-containing protein 2	B-type flagellin
Keratin type II cuticular Hb5	60 kDa chaperonin
Junction plakoglobin	Elongation factor Tu
Alpha-1B-glycoprotein	DNA-directed RNA pol β
Keratin type I cytoskeletal 16	Succinyl CoA-ligase
Annexin A7	50s ribosomal protein L2
Unconventional myosin-If	Arginine deiminase
Citrate synthase, mitochondrial	
Aldehyde dehydrogenase family 3 member B1	
Keratin, type I cuticular Ha1	
Dolichyl-diphosphooligosaccharide protein	

The NASF pulled out proteins that have been found to be present in developing biofilms including succinyl-CoA synthetase and chaperonins. However, they also pulled out proteins that are required for normal wound healing including fibronectin, plasminogen, vitronectin, and keratin, to name a few.

A pilot study using *S. epidermidis* biofilms *in vivo* in C57 mice was attempted to test if the NASF could have a better effect on wound healing in *S. epidermidis* infected mice since the *in vitro* studies showed reduction in growth and biofilm in this strain. Following a protocol by Schierle et. al. ¹⁴⁵ proved to be fatal in initial attempts. In an effort to extract data, NASF were added to the wounds of C57 mice infected with *S. epidermidis* at the onset of apparent illness resulting in two additional time points for DNA and protein analysis, 0.5 hrs and 3.5 hrs. These time points had wounds with or without *S. epidermidis* infection that were exposed to NASF for either 0.5 hrs or 3.5 hrs before the NASF were removed and the contents analyzed. At the 0.5 hrs and 3.5 hr time points in the C57 mice infected with *S. epidermidis*, there were two visible bands on the DNA gel of the crude extracts whereas no bands were visible at the same time points in uninfected wound extracts (Figure 52), indicating that shorter time points may have a less detrimental effect on the normal wound healing process. These were not the same high kb bands that we saw in the 24 hr NASF extracts from db/db mice shown above. This indicates that there is variation in the crude extracts that is dependent on mouse

strain, bacteria type, and/or duration of NASF treatment. When the DNA was extracted and a DNA gel was run, the bands were lost and smears appeared for all conditions except the 0.5 hrs with *S. epidermidis* preformed biofilms (data not shown). However, the crude extracts from the NASF show light, low bp DNA bands (Figure 52). The lack of DNA bands in the DNA extracts as opposed to the crude extracts was most likely do to loss of material in the DNA extraction process.

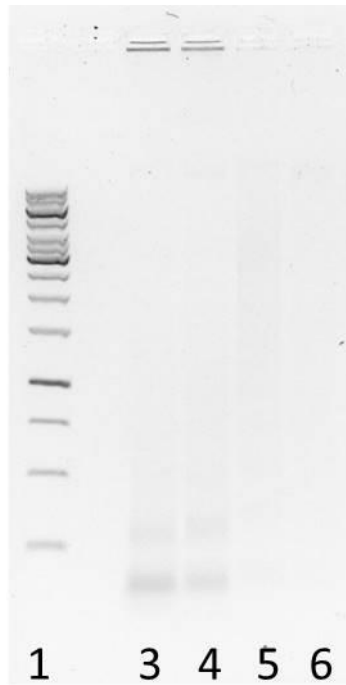


Figure 52: DNA gel of crude extracts from NASF used on C57 mice infected with *S. epidermidis* preformed biofilms (lanes 3 and 4) or uninfected (lanes 5 and 6). Lanes 3 and 5 had 0.5 hrs NASF exposure, lanes 4 and 6 had 3.5 hrs, and lane 1 is a 1 kb DNA ladder.

The total amount of protein that was extracted from the NASF used on the C57 mice is represented in Figure 53. The amount of total protein from the shorter

incubation times is lower than that of the 24 hr incubation. The total protein was visualized on a protein gel (Figure 54A), and mass spectrometry was done to compare the detectable proteins. At the shorter time periods of 0.5 and 3.5 hrs, it appears that the NASF remove more protein from the infected wounds than the uninfected wounds; however, there was still an overlap of 296-304 proteins detected in both infected and uninfected wounds. Looking at the number of proteins detected from infected wounds at 0.5 hrs, 3.5 hrs, and 24 hrs, shows an overlap of 320 proteins with trends that shorter NASF treatment periods result in lesser protein uptake; ~ 578 proteins at 0.5 hrs, ~631 proteins at 3.5 hrs, and ~821 proteins at 24 hrs. Of the 320 shared proteins, only 6 were found present in all three conditions but not in the uninfected wound extracts: these are shown in Table 4.

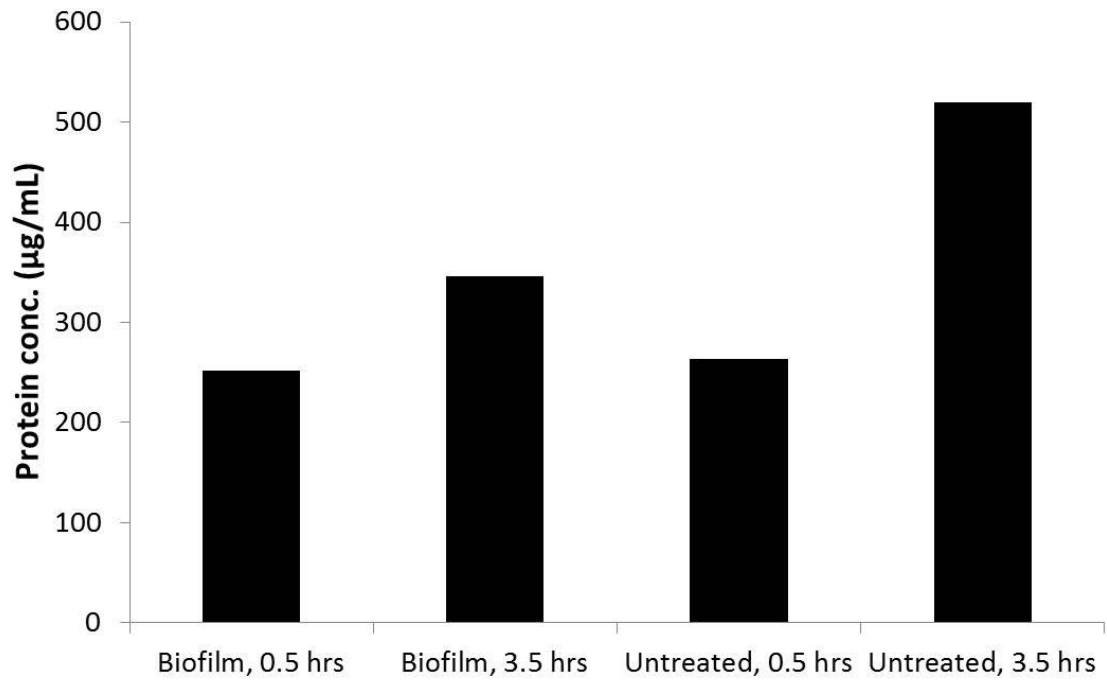


Figure 53: Average total protein extracted from NASF used on wounds in C57 mice infected with *S. epidermidis* (Biofilm) or uninfected (Untreated). 0.5 hrs and 3.5 hrs indicate how long the NASF was exposed to the wound bed.

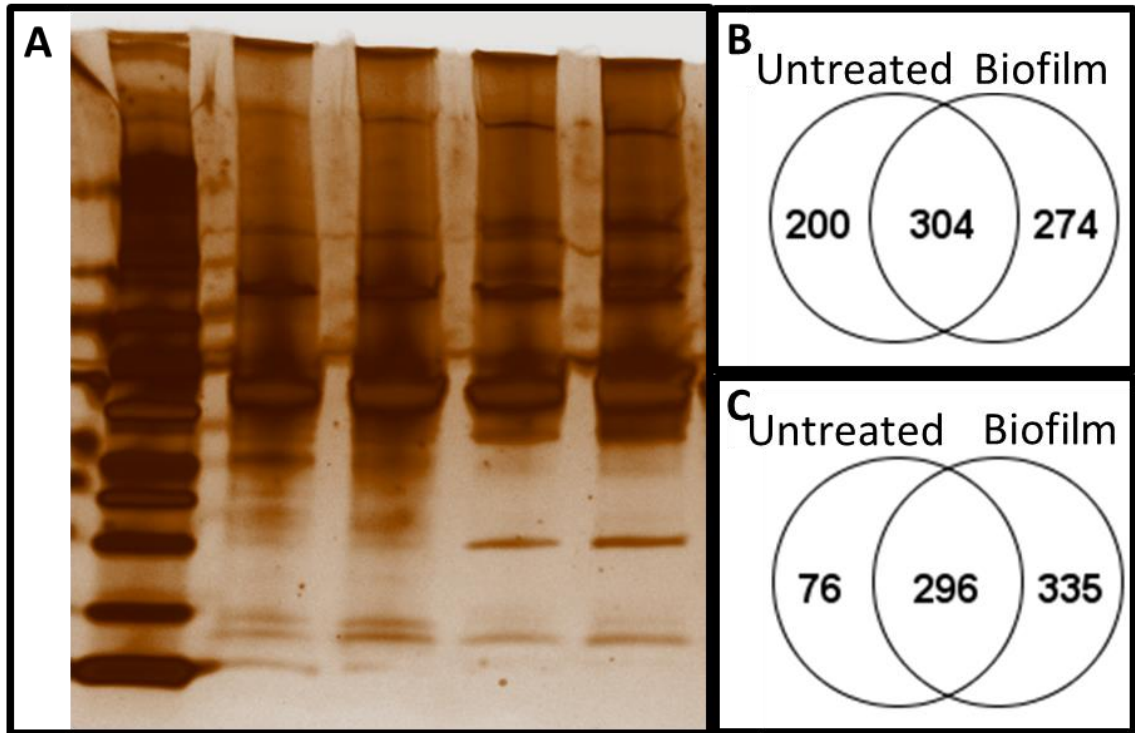


Figure 54: (A) Protein gel of NASF extracts from: lane 2- 0.5 hrs with *S. epidermidis* biofilm, lane 3-3.5 hrs with *S. epidermidis* biofilm, lane 4-0.5 hrs uninfected, and lane 5-3.5 hrs uninfected. Venn diagrams displaying the number of proteins extracted from wounds treated with NASF in C57 mice for (B) 0.5 hrs with *S. epidermidis* infection (Biofilm) or without infection (Untreated), (C) 3.5 hrs with *S. epidermidis* infection or without infection.

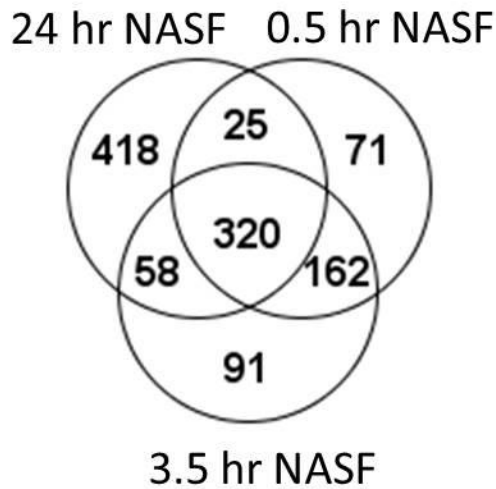


Figure 55: Venn diagram of proteins detected from NASF extracts of infected wounds treated with NASF for different time durations.

Table 4: Common proteins found in NASF extracts from mice infected with bacteria treated with NASF for 0.5 hrs, 3.5 hrs, or 24 hrs. Proteins were identified by at least 4 different peptides.

Mouse proteins	Bacterial proteins
Aspartate aminotransferase, cytoplasmic	Elongation factor
Vascular protein sorting-associated protein 35	60 kDa chaperonin
Long-chain-fatty-acid CoA ligase	Arginine deiminase

One group of mice survived beyond the 24 hr period after addition of the *S. epidermidis* preformed biofilm, and they were allowed to heal completely. The histology from these mice was compared to mice that were not infected with biofilm. Visually, it appeared that the *S. epidermidis* biofilm did not continue to grow on the mice after

application, indicating that the results from the *S. epidermidis* infected wounds are not representative of the true effect of NASF on *S. epidermidis* biofilms.

5.4 Discussion

In these studies we looked at nucleic acid scavenging as a way of preventing the onset of biofilms by reducing their initial framework of bacterial attachment and maintenance in the wound by reducing EPS formation. *In vitro* studies using *P. aeruginosa* and two Staphylococcal strains, *S. aureus* and *S. epidermidis*, showed that the NASF significantly reduced the formation of biofilms and this effect was increased by doubling and tripling the NASF “dose”. A combined effect on planktonic bacteria and biofilm formation could be seen when the NASFs were used in Staphylococcal cultures. Thus, NASFs could be beneficial in clinical practice by both reducing the number of free bacteria as well as preventing the onset of biofilms. In fact, the use of polycations as antibiotics has been extensively studied¹⁴⁶⁻¹⁴⁸, therefore validating our findings.

In vitro studies using NASF to prevent biofilm formation showed that the NASF significantly reduced biofilm formation in *P. aeruginosa*, *S. aureus*, and *S. epidermidis*. Although the NASF acted to reduce the biofilm in both Pseudomonas and Staphylococcal strains, the mechanism of the NASF for biofilm prevention appeared different for each bacterial strain based on the SEM data following *in vitro* biofilm formation. The NASF attracted the *P. aeruginosa* biofilm to its surface, therefore

preventing the biofilm growth on the adjacent surface, which represents the wound bed (Figure 56). This indicates that while the scavenging effect of NASF was not strong enough to prevent EPS formation in *P. aeruginosa* biofilms, the polymer could still be beneficial by developing an easy and effective method for biofilm removal. Instead of preventing biofilm growth, the NASF was able to remove the *P. aeruginosa* biofilm growth from the wound bed. Alternatively, NASF prevention of the Staphylococcal biofilms is most likely a combined effect from the two different mechanisms. The reduction of bacterial CFUs from planktonic Staphylococcal bacteria treated with NASF demonstrates that the polymer has an antibiotic effect against bacteria prior to biofilm formation. Additionally, the absence of bacteria bound to the NASF in the SEM images of Staphylococcal biofilms treated with NASF, indicates that unlike the way NASF acts on *P. aeruginosa* biofilm, the NASF likely inhibits biofilm growth not by physically binding and removing the biofilm but by binding and removing the extracellular nucleic acid components of the EPS. NASF removal of nucleic acid components thus prevents biofilm growth.

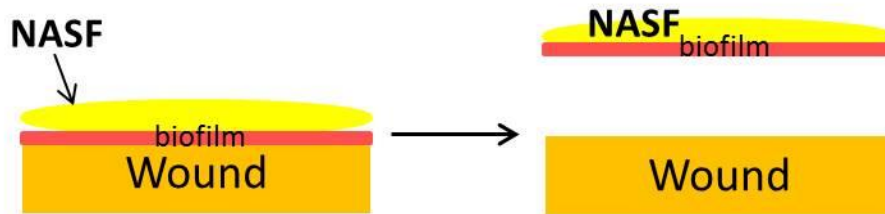


Figure 56: Schematic of how NASF acts on *P. aeruginosa* biofilms-NASF attracts the biofilm to itself thereby allowing easy removal of biofilm from the adjacent surface.

As the pilot *P. aeruginosa* animal study showed a difference in wound healing time between biofilm infected mice and uninfected mice, with wounds from biofilm infected mice failing to heal even 18 days post-infection, we decided to move forward with NASF treatment. The animal studies involved applying an 8 mm skin wound to the back of the mice, adding the bacteria to the wound 72 hrs after initial wounding, and applying one 8 mm disc of NASF 24 hrs after adding the bacteria. Initially, the plan was to change the NASF daily until the wounds heal, with the intention of prolonged biofilm disruption as the NASF bind the bacteria and result in bacterial and/or biofilm removal from the wound. However, after 9 days it appeared that the biofilm-infected wounds in the NASF treatment group were healing more slowly than those in the biofilm group that did not receive any therapeutic treatment.

At this point we hypothesized that the problem was caused by the extensive presence of the NASF that was mechanically preventing healing - and that treating for fewer days – might allow the biofilm to be eliminated early on, followed by a NASF-free

time for the wound to heal freely. Because the wound size between the untreated biofilm wounds and the NASF treated biofilm infected wounds began to separate at day 9 in the previous experiment, we decided to treat with NASF for 7 days to hopefully eliminate that slower wound healing after day 9. Additionally, another control group consisting of NASF treatment of uninfected wounds was added in order to determine the effect of NASF on normal wound healing. When looking at the wound closure results from this study, both NASF treated groups, whether infected or uninfected, healed at a slower rate than the untreated biofilm group. Although the therapeutic endpoint was not reached, it appeared that rapid healing of mouse wounds in the presence of biofilm infection was a common problem observed in wound healing studies in literature and that slower wound healing may indicate improved functional wound healing¹⁴⁹. Roy et. al. discovered that although biofilm treatment may not increase the wound healing time, it does allow for a higher quality of wound healing which can be measured using transepidermal water loss measurements or by staining for tight junctions.

However, based on H&E slides and pathology reads, there was no obvious difference in the overall quality of healing between any of the treatment groups, including the untreated biofilm groups and the uninfected and infected groups treated with NASF. The one noticeable difference was the presence of inflammatory cells in the

untreated biofilm infected group. While, these inflammatory cells were not observed to directly affect the wound healing time, they indicated a prolonged inflammatory response in the mice that were infected with biofilms. This prolonged inflammation was alleviated with NASF treatment of biofilm infected wounds, indicating that the NASF are effective at reducing the inflammatory response.

The healed wound beds were fluorescently stained for two tight junction proteins, ZO-1 and ZO-2. Differences in the tight junction staining between the biofilm group and all the other groups would indicate that the biofilms had a negative effect on tight junction formation and that the NASF could potentially resolve this issue. Unfortunately, there was no obvious difference in ZO-1 staining between the uninfected/untreated group and the untreated biofilm group, making it impossible to show any improvement of quality of wound healing, as related to tight junction formation, in the presence of NASF. In the ZO-2 staining, the uninfected/untreated group appeared to have the worst tight junction formation while the biofilm infected group and the biofilm infected and uninfected groups treated with NASF had high presence of ZO-2. Taken together, these results do not indicate reduced wound healing quality when wounds are uninfected or infected with biofilms. Therefore we could not show an improvement in wound healing, as related to tight junction formation, upon treatment with NASF. This means that although the NASF reduces the effects of the

biofilm, it has no visible positive affect on the tight junction formation and gross pathology.

Although measurements of contraction were not done on the wounds healed after treatment with NASF, it is possible that the slower wound healing and anti-inflammatory action of NASF leads to less contraction in the wound. Decreased wound contraction has been observed in a study applying PAMAM-G3 directly to open wounds; the PAMAM-G3 effectively blocked cytokine production, migration, and differentiation into myofibroblasts in an acute murine wound model of granulation and tissue contraction¹⁵⁰. While wound healing is an immensely complicated procedure, contraction, where a wound is rapidly decreased in size^{151,152}, is generally considered negative as it has effects on mobility, function, and aesthetics depending on the area covered by the wound. Because contraction is essentially a rapid closure of the wound, it can be hypothesize that by slowing down wound healing; contraction can be reduced therefore potentially leading to improved wound healing outcomes. This presumes that it is possible that the NASF may aid in reducing wound contraction, however, our experiments were not done in the appropriate wound model to confirm this result. Additionally, reduced inflammation during the healing process is correlated with less scarring¹⁵³, further indicating that the NASF, with its anti-inflammatory function, may result in positive effects on long term wound healing.

In addition to therapeutic outcome, we analyzed what the NASFs were removing from the wound bed to show how they acted *in vivo*. To do so, the DNA, RNA, and protein components after wound treatment were extracted from the fibers and analyzed. When the crude fiber extracts were run on a DNA gel, there was one obvious band, whether or not there was biofilm present. This indicated that this band was most likely made of DNA or RNA from the mouse and not the bacteria. When the DNA was separated out, two bands became apparent: one at ~16kb and one at a higher molecular weight. At this point, the 16kb band became the point of focus and was hypothesized to be mouse mitochondrial DNA (mtDNA). We validated that this band was mouse mtDNA by amplifying cytochrome-c oxidase fragments, a commonly used sequence for amplifying mtDNA, of the DNA extract using PCR. mtDNA is important because increased circulating mtDNA leads to increased TLR9 activation¹⁵⁴ resulting in a prolonged inflammatory response. Although little is known about the specific role of TLR9 activation in chronic wounds, it is known that sustained inflammatory response, specifically NF- κ B expression that is associated with TLR activation, maintains wound chronicity^{155,156}. Therefore it seems logical to assume that reduction of a TLR agonist would lead to better wound healing. While reduction in TLR9 activation may improve wound healing in chronic wounds, it has the opposite effect in acute wounds¹⁵⁵. It is possible that we did not see an increase in wound healing because we did not effectively

develop chronic wounds in our diabetic mouse wound model. However, it remains that the ability of the NASF to pull out mtDNA is important in its potential to treat chronic wounds. It's also interesting to point out that the NASF have the ability to pull out larger DNAs, something that was not validated with the CpG and salmon sperm scavenging that was shown *in vitro* in the previous chapter to validate the DNA scavenging capacity of the NASF.

The RNA extracts that were examined by RNA sequencing showed that the NASF that were used in uninfected wounds scavenged out more RNA than the NASF used to treat biofilm infected wounds. This could be because extracellular RNA is less prevalent in the biofilm and therefore the NASF have less exposure to RNA when placed on a biofilm infected wound; additionally, it could mean that the biofilm itself is blocking access to mouse RNAs in the wound bed. The RNA heatmap shows the difference in RNA expression and it appears that the biofilm infected wounds and the uninfected wounds have very different RNA profiles. This is most likely because the biofilm infected wounds are in direct contact with the bacteria, giving them more bacterial RNA results whereas in the uninfected wounds, there is more exposure to the open mouse wound and its components, giving it more of a mouse RNA profile.

There were many proteins that were found on the NASF used on both the infected and uninfected mouse wounds. It is important to note that many of the

proteins found on the NASF were very important to wound healing. Some of these proteins include fibronectin, plasminogen, vitronectin, and keratin, among others. Fibronectin is an important part of the fibrin clot that is necessary for the first stage of wound healing ^{157,158}. Wound re-epithelization is blocked and wound healing does not occur in the absence of plasminogen and keratinocytes ^{157,159}. Receptors on keratinocytes also rely on fibronectin and vitronectin in the provisional matrix of the wound bed for movement during re-epithelization ¹⁶⁰. Mass spectrometry results also showed the removal of complement in both infected and uninfected wounds. As complement plays a huge role in resistance to infection ^{161,162}, the NASF may be acting against the beneficial aspects of the immune system in the wound bed and may lead to increased infection. However, this would not be an issue in true chronic wounds where an ischemic environment prevents immune response to infection. On the other hand, fibronectin and vitronectin are also associated with contraction, meaning that certain levels of reduction of these proteins may lead to better wound healing ¹⁵⁷.

At the same time, the NASF are also pulling out proteins that are contributing to biofilm formation. One study shows that succinyl-CoA synthetase and chaperonins, both proteins that the NASF pulled out of the biofilm infected wound bed, are proteins that are upregulated in forming biofilms ¹⁶³, insinuating that reduction in these protein levels may be able to reduce or disrupt biofilm formation. Reduction of the 50s

ribosomal protein in the infected wound bed may also be preventing development of the biofilm by reducing functional protein formation in the bacteria. The presence of all of these proteins in the NASF extracts of biofilm infected wounds indicates high levels of bacterial cell death, allowing these components to be released into the wound bed.

Alternatively, after whole bacterial cells are removed by the NASF and treated with TRIzol, the components may be released and eventually detected by mass spectrometry. Most likely the TRIzol treatment is lysing the bacterial cells because we also see a large DNA band in the DNA extracts that could be curled up bacterial genome. This is further validated by the fact that we do not see the same DNA band intensity in the non-TRIzol *S. epidermidis* DNA gels. This indicates that longer NASF treatment may result in whole bacteria uptake, which could be helpful in removal of bacteria from the wound bed.

In general, most of the proteins described above have isoelectric points that would give them an overall negative charge at physiological pH. This includes vitronectin which has a pI of 4.75-5.25¹⁶⁴; type I keratins which have a pI less than 5.5¹⁶⁵; fibronectin has a pI of 5.39¹⁶⁶; and succinyl-CoA-synthetase has a pI of 5.9¹⁶⁷. Yet some of the proteins would most likely have a neutral charge such as plasminogen with a pI of 7¹⁶⁸ or even an overall positive charge such as some type II keratins that have a pI > 6¹⁶⁵. Although all of the protein's pI's were not analyzed, it appears that of the proteins that were of importance to mention in the results section, most would be negatively charged

at neutral pH and therefore be electrostatically attracted to the positive charge of the NASF, confirming the function.

We also treated a Staphylococcal biofilm animal model because it appeared that the NASF were capable of reducing the growth of the Staphylococcal bacteria in addition to preventing overall biofilm formation. Instead of attracting the biofilm, as the NASF does with *P. aeruginosa* biofilms, it is able to completely eradicate the Staphylococcal biofilms. The model attempted was one published by Schierle et. al. where they used pre-formed biofilms made from mouse isolates of *S. aureus* and *S. epidermidis* in open wounds of C57 mice ¹⁴⁵. In the first attempts to infect the open wounds with the pre-formed Staphylococcal biofilms, the mice became fatally sick after 24 hrs. NASF was applied to the sick mice to collect the 0.5 hr and 3.5 hr time points. After several attempts, we discovered that the survival of the mice was dependent on the time point of biofilm application: waiting until 24 hrs after wounding to apply the biofilm instead of applying it at the time of wounding allowed for mouse survival. Although this resulted in mouse survival, it did not appear that the biofilm effectively infected the wound.

Overall, the DNA and protein profiles from the shorter treatment times of 0.5 hrs and 3.5 hrs in the Staphylococcal C57 animal model differed from those of the 24 hr treatment time in the db/db model treated with *Pseudomonas*. The DNA detected from

the 0.5 hr and 3.5 hr treatment times were smaller than the ≥ 16 kb DNA detected at 24 hrs. This may be because at later time points, the high charge of the larger DNA molecules competes away the small DNA fragments or that the NASF have a higher affinity for smaller DNA molecules and therefore they are detected at earlier time points. At 24 hr, one of the major detectable DNAs was the mtDNA from the mouse; it's possible that at the shorter treatment times, the NASF does not have time to pull out components from deeper in the wound therefore resulting in primarily bacterial DNA components. Additionally, when looking at the protein detected, it is obvious that the shorter treatment times yield less protein extraction from the wound bed. This may be beneficial for treatment because it could result in less removal of the proteins that are required for the wound to properly heal. Many of the critical wound healing associated proteins were detected by mass spectrometry from the 0.5, 3.5, and 24 hr NASF treatment conditions, demonstrating that wound healing proteins are removed by the NASF at both earlier and later time points. However, fewer of the wound healing proteins are removed by the polymer after 0.5 hr and 3.5 hrs of treatments. These experiments demonstrated that shorter time periods of NASF should be explored to balance the positive effects of the biofilm reduction and the negative effects on the normal wound healing.

While the wound healing models used here were important for showing efficacy of NASF *in vivo*, they did not accurately represent chronic wounds. Therefore, they were not exact representations of how the NASF would work in biofilm infected chronic wounds. Chronic wounds have a specific inflammatory response and protein expression that was most likely not represented in these models and could change the effectiveness of the scavenging capabilities of NASF. Nevertheless, with this information it is evident that there is a preferred treatment time in which NASF would be effective; shorter treatment times could allow for effective biofilm reduction while not disrupting normal wound healing. Further analysis in a well-developed chronic wound model would be necessary to verify that NASF inhibit biofilm growth and improve wound healing in chronic wounds.

5.5 Conclusion

Chronic wounds are a serious medical issue that is attributed to both biofilm infections of the wound and an extended period in the inflammatory state ¹⁶⁹. Biofilms are difficult to eradicate because they do not proliferate like planktonic bacteria, instead developing an extrapolymeric substance that secures them in the wound and prevents antibiotic penetration into the wound ⁶⁵. Current treatment for biofilm infected wounds is debridement, a painful surgical procedure involving deep cleaning of the wound using high pressure fluid wash that provides a 2-3 day window where treatment

becomes more effective¹⁶⁹⁻¹⁷¹. We propose that the NASF could be a synergistic procedure with debridement, potentially having a two prong effect by reducing biofilm burden and dampening the inflammatory response, therefore eliminating two of the barriers preventing chronic wounds from healing. *In vitro* results using *P. aeruginosa*, *S. aureus*, and *S. epidermidis* biofilms show that NASF significantly reduce biofilm formation in the first 24-48 hrs. Although the NASF did not decrease wound healing time in the murine biofilm wound models tested, we were able to ascertain the scavenging capabilities of the NASF *in vivo*. It appears that a 24 hr treatment with NASF results in removal of large DNAs from the biofilm infected wound, including the removal of mtDNA. The 24 hr NASF treatment also leads to high levels of protein removal. Shorter NASF treatments of either 0.5 or 3.5 hrs result in smaller sized DNA scavenging and less overall protein removal from the wound. Additionally, the longer NASF treatment time of 24 hrs pulled out more mouse RNA while shorter NASF treatment times of 0.5 and 3.5 hrs were effective at pulling out more bacterial RNA. Although the NASF removed DNA, RNA, and biofilm supporting proteins from the biofilm infected wounds, it also scavenged out proteins that are required for wound healing. This likely explains why the wound healing time did not improve in the presence of NASF. Further studies using more accurate biofilm infected chronic wound models and various treatment time periods combined with debridement should be done

to better analyze the potential efficacy of NASF to treat biofilms in patients with chronic wounds.

6. Conclusions

The electrostatic contact between the negatively charged backbone of nucleic acids and the positively charged components of polycationic polymers is a strong interaction that can be used in various ways. In this dissertation, the electrostatic interaction is used for gene delivery as well as nucleic acid scavenging. Overall, our hypotheses for aims 1 and 2 were validated; we showed that the Ch/PS/DNA nanoparticles improve oral gene delivery and that we could develop a nucleic acid scavenging nanofiber that effectively scavenges nucleic acids. However, the hypothesis for aim 3 was disproved in the studies that we performed showing that the NASF did not decrease the wound healing time of wounds infected with biofilm.

For the application of non-viral gene delivery, a set of copolymers were developed as systemic gene carriers and a tertiary component nanoparticle of chitosan, protamine sulfate, and DNA (Ch/PS/DNA) was developed for applications in oral gene delivery. The copolymers showed higher transfection efficiency than the commercially available Lipofectamine *in vitro*, however, they were highly unstable and batch to batch variation resulted in abandonment of these polymers for further gene carrier studies. The *in vitro* studies using the Ch/PS/phFIX nanoparticles showed that they were able to transfect both HEK293 and Caco-2 cells resulting in production of functional hFIX protein. The *in vivo* results showed that the Ch/PS/phFIX nanoparticles effectively

produced hFIX protein in the blood of ~42% of the mice following oral delivery, both BALB/c and hemophilic B mice inclusive, with hFIX levels ranging from 3.3-132 ng/mL. The oral gene delivery results using Ch/PS/phFIX polyplexes demonstrate that the already developed chitosan nanoparticle platform can be improved with protamine sulfate and further studies should be done to show the efficacy of these nanoparticles in hFIX protein replacement therapy for hemophilia B.

For nucleic acid scavenging, we developed a new technology that secured polycationic polymers on an electrospun sheet made of PSMA. Both polycationic modified PSMA fibers (NASF) and PSMA + polystyrene fibers (R8) were found to be minimally toxic and were able to scavenge polyanionic pro-inflammatory species, CpG and Poly(I:C), therefore blocking improper activation of nucleic-acid sensing TLRs without compromising the ability to respond to certain non-nucleic acid agonists, such as LPS and Pam3CSK4. We showed that NASFs could reduce the effects of DAMPs by reducing NF- κ B levels to ~26-28% of normal levels. We also developed a sturdier fiber for application as a filter in flow devices; these were made by incorporating various amounts of polystyrene with PSMA and electrospinning the polymer solution into sheets, followed by covalent attachment of bPEI as done in the original NASF formulation. The resulting fibers- R4, R6, R7, and R8- absorbed less fluid than the original NASF and were found to be sturdier, water-resistant, and less swollen after

contact with fluid. The scavenging capabilities of R8 remained intact, making this fiber a potential candidate for use in a filtration device.

Another therapeutic application of NASF that was tested was for treatment of chronic wounds. Chronic wounds are a serious medical issue that is attributed to both biofilm infections of the wound and an extended period in the inflammatory state of wound healing ¹⁶⁹. Biofilms are difficult to eradicate because they don't proliferate like planktonic bacteria and they develop an extrapolymeric substance (EPS), made up of DNA and proteins, that secures them in the wound and prevents antibiotic penetration into the wound ⁶⁵. The nature of the EPS of the biofilms makes it a good target for the NASF to scavenge NA and reduce biofilm formation. *In vitro* results using *P. aeruginosa*, *S. aureus*, and *S. epidermidis* biofilms showed that NASF significantly reduced biofilm mass in the first 24-48 hrs of formation. After 24 hr treatment with NASF on diabetic mice wounds infected with *P. aureginosa*, the NASF was able to scavenge primarily two large fragments of DNA including mtDNA. After shorter periods of NASF treatment, 0.5 and 3.5 hrs, the DNA scavenged by the fibers was a smaller size, of less than 500 bp. RNA sequencing showed that the NASF were also able to scavenge RNA in this *in vivo* wound model. At all treatment times the NASF scavenged protein necessary for wound healing including plasminogen, fibronectin, and vitronectin, however, the longer NASF treatment times scavenged greater amounts of protein, indicating that a shorter

therapeutic exposure time might reduce the detrimental effects on wound healing. The NASF proved to have nucleic acid scavenging capabilities with some off target effects, demonstrating that further testing must be done to develop the NASF into effective blood filtration systems and/or chronic wound dressings.

7. Future studies

7.1 SPECIFIC AIM 1: (A) Development of polycationic gene carriers; (B) Application of polycations for non-viral oral gene delivery to treat hemophilia B.

The Ch/PS/DNA gene carrier could be improved by using a different plasmid, specifically the one described by Quade-Lyssy, et. al. ⁵⁵ that was developed specifically for the purpose of increased hFIX bioavailability following oral gene delivery. These new particles would then need to be re-characterized and efficacy shown *in vitro* in both HEK293 and Caco-2 cells. Because the plasmid may not show increased levels *in vitro*, a small pilot study in BALB/c mice should be done to look at hFIX expression levels. If this pilot study shows increased hFIX levels, then this plasmid should replace the currently used plasmid for further studies.

The non-viral oral gene delivery platform showed potential as a therapeutic agent in the small number of mice tested; however, this study could gain further significance by using a larger number of hemophilic B mice. The hemophilic B mice could be used to detect circulating hFIX protein as well as phenotypic changes in clotting time by drawing blood and performing Activated Partial Thrombin Time (aPTT) assays. Performing the aPTT assay demonstrates that the protein is functional and what percentage of normal clotting time can be regained with non-viral oral gene delivery using the Ch/PS/DNA delivery platform. In addition to aPTT studies, further

experiments looking at inhibitory antibodies should be performed, this will indicate whether or not the immune system responds to the new protein. Inhibitory antibodies can be measured using either a modified Bethesda assay or an anti-hFIX antibody detection assay. In brief, the Bethesda assay involves doping normal plasma into treatment plasma samples and measuring the differences in aPTT measured clotting time yielding results in Bethesda Units (BU), defined as the amount of an inhibitory antibody in a plasma sample that will neutralize 50% of 1 unit of FIX in normal plasma after 2 hr incubation at 37°C. The anti-hFIX antibody detection assay works like an ELISA where plates are coated with hFIX protein, plasma samples are added to the plates, then fluorescently labeled anti-mouse IgG antibodies are used to detect the amount of inhibitory antibodies present; this allows for direct measurement of the concentration of inhibitory antibodies.

Finally, in order to move forward with the Ch/PS/DNA gene carrier system it should be tested in a capsule form in larger animals, ie. rats or dogs. The capsules provide further protection from acids and enzymes in the stomach and also provide for testing of a solid capsule material to model oral delivery in humans. Rats would be the first step as they are the smallest animal that can be given capsules and would require a smaller amount of nanoparticles when the dose is scaled-up. Once encapsulated and orally delivered the rat plasma should be tested for hFIX protein levels, functionality in

aPTT assays, and inhibitory antibody levels in the plasma should be measured. The same can also be done in dogs before potentially moving into humans.

7.2 SPECIFIC AIM 2: Development and in vitro testing of nucleic acid scavenging nanofibers.

The most important future step for the NASF is to add a quality control step. This requires optimizing the wash steps following covalent attachment of the polycationic polymers. Various experimental trials have shown some rare deviations in the toxicity of certain NASF batches; this is presumed to be due to some free polymer that is causing toxicity. This problem can be resolved by optimizing the wash step. Buffers with different pHs and salt contents should be tested to find the optimum buffer to remove all of the free polymer from the NASF.

Further studies on the effect of NA size on the NASF scavenging abilities would also be beneficial. This includes looking at the rate at which different size DNA attach to the NASF by adding the DNA and measuring the DNA remaining in solution at different time points. Additionally, a competition assay, using a mixture of different size DNAs can be done to determine if there is an affinity for a certain size DNA fragment in the presence of a mixed solution. This mixture could consist of CpG (~20bp), salmon sperm DNA (~2 kb), mtDNA (~16 kb), and various plasmid DNAs that can range between ~4000-13000 bp. A mixture of these DNAs can be incubated with the NASF for any given time period and then the supernatant run on a DNA gel to look at

the amount of each size DNA left in solution. It can be assumed that the least prevalent band is the size that has that greatest affinity for the NASF. These experiments would show if the NASF has a preference for a certain size charged DNA molecule.

Additionally, the PSMA polymer solution can be adjusted and electrospinning conditions can be modified to change the porosity of the fiber. It is likely that the porosity influences the amount of non-specific uptake. The porosity of the current NASFs should be measured using a porosity flow device; furthermore several new fibers resulting in different pore sizes should be developed. The non-specific uptake can then be measured and results can be compared based on the pore size. Non-specific uptake can be measured with the agonists described in specific aim 2 including CpG, poly(I:C), R848, and Pam3CSK4. Reduced scavenging of R848 would result in more specificity than the 60% NASF described.

The results obtained from NASF scavenging of certain components in DOX-killed cell debris demonstrate that NASF has the potential to remove DAMPs associated with radiation and chemotherapy. Damage-associated molecular pattern molecules or DAMPs, such as DNA, RNA, chromatin, and high-mobility group protein 1, are highly associated with chronic inflammation in patients that have undergone radiation¹⁷². Further studies to look at the benefits of using NASF in these settings could be done starting with *in vitro* studies where cells are damaged via radiation and the NF- κ B

response to this cell debris is measured in reporter cells, HEK-TLR3/7/8/9. The same experiments can be done using patient plasma samples from radiation or chemotherapeutic treated patients. Reduction of immune response in the presence of NASF would indicate the potential of the NASF to be used as a blood filtration device for DAMP removal in patients who have undergone radiation or chemotherapeutic exposure.

The next step in this project would be the development of a device. Device development involves many steps, but first, we would want to develop the R4 or R8 NASF platform. R4 and R8 are the NASFs that were made with increased amount of polystyrene to make them more resistant to water absorption and therefore give them the ability to withstand flow. Experiments measuring the maximum flow that the R4 and R8 NASFs can withstand should be done as well as all of the tests measuring the effects on DAMPs described above. Additionally, we would need to look at the effect that the NASF has on red blood cells: the toxicity, the attachment, and the effect on clotting. All of these data would culminate to make a blood filtration device using the NASF as the filtering material.

7.3 SPECIFIC AIM 3: Treatment of biofilms using nucleic acid scavenging nanofibers.

The most important experiment to advance this aim is to use a better chronic wound model. One potential model is the ischemic wound model in rabbit ears that

involves cutting off blood flow to the rabbit ear and then inducing a wound. This model has the benefit of being able to support multiple wounds on the same animal and the ischemia prevents blood flow to the wound ¹⁷³, therefore establishing chronicity. Porcine wound models are another possibility; in these models, delayed wound healing has been established by chemical necrosis ¹⁷⁴ or radiation damage ¹⁷⁵. These porcine procedures delay wound healing but do not necessarily imitate chronic wounds. One study by Roy et. al. shows that they were able to develop chronic ischemic wounds in pigs ¹⁷⁶, similar to the aforementioned ischemic wounds in rabbit ears. For the purpose of testing the NASF, the best animal model would consist of an ischemic chronic wound that is infected with biofilm. This would allow for the wound healing protein and nucleic acid profile to better represent that of chronic wounds and would give us a better idea of how the NASF effects healing in truly chronic wounds.

To better model true biofilm infections, it would be best to test the NASF on a mixed species biofilm which could include a combination of *P. aeruginosa*, *S. aureus*, and *S. epidermidis*. Additionally, with the new animal model, it will be important to test various different treatment durations using the NASF. With the NASF, there is a very delicate balance between preventing biofilm and stunting wound healing that appears to be highly time dependent. So, different treatment durations from a gentle cleaning of the wound with NASF to up to 6 hrs of NASF exposure should be tested for the

optimum disruption of biofilm and decrease of wound healing time. Finally, it would be beneficial to test the effects of NASF in combination with debridement, as debridement is the current standard of care and combination treatment could result in a synergistic treatment effect.

References

1. Dias, R., and Lindman, B., DNA Interactions with Polymers and Surfactants. 1 ed.; Wiley, Hoboken, (2008)
2. Tang, M., and Szoka, F., *Gene therapy* (1997) **4** (8), 823
3. Borchard, G., *Adv Drug Deliv Rev* (2001) **52** (2), 145
4. Giacca, M., and Zacchigna, S., *J Control Release* (2012) **161** (2), 377
5. Broderick, J. A., and Zamore, P. D., *Gene Ther* (2011) **18** (12), 1104
6. Chavali, S., et al., *Proteins* (2008) **73** (1), 63
7. Riley, R. S., Factor IX Deficiency. VCU2005
8. George, L. A., and Fogarty, P. F., *Seminars in Hematology* **53** (1), 46
9. Osterud, B., et al., *J Biol Chem* (1978) **253** (17), 5946
10. Palta, S., et al., *Indian Journal of Anaesthesia* (2014) **58** (5), 515
11. Chang, H.-H., et al., *Journal of the Formosan Medical Association* (2007) **106** (4), 281
12. Monahan, P. E., et al., *Hum Gene Ther* (2015) **26** (2), 69
13. Wade, N., Treatment for Blood Disease Is Gene Therapy Landmark. *The New York Times* 2011

14. Mah, C., et al., *Clin Pharmacokinet* (2002) **41** (12), 901
15. Kay, M. A., et al., *Nature genetics* (2000) **24**, 257+
16. Manno, C. S., et al., *Nature medicine* (2006) **12**, 342+
17. Ramesan, R. M., and Sharma, C. P., *Expert Review of Medical Devices* (2009) **6** (6), 665+
18. Fievez, V., et al., *European Journal of Pharmaceutics and Biopharmaceutics* (2009) **73** (1), 16
19. Tahara, K., et al., *Biomaterials* (2011) **32** (3), 870
20. Garnett, M. C., and Kallinteri, P., *Occupational Medicine* (2006) **56** (5), 307
21. Trapp, S., et al., *European Biophysics Journal : EBJ* (2008) **37** (8), 1317
22. Olmedillas López, S., et al., *PeerJ* (2016) **4**, e1907
23. Roth, D. A. M. D., et al., *The New England Journal of Medicine* (2001) **344** (23), 1735
24. Jinturkar, K. A., et al., 3 - Gene Delivery Using Physical Methods. In *Challenges in Delivery of Therapeutic Genomics and Proteomics*, Ambikanandan, M., (ed.) Elsevier, London, (2011), pp 83
25. Cleland, J. L., et al., *Current Opinion in Biotechnology* (2001) **12** (2), 212
26. Cui-shuan, W., et al., *Journal of Microencapsulation* (2010) **27** (3), 205

27. Sezgin, Z., *et al.*, *International Journal of Pharmaceutics* (2007) **332** (1-2), 161
28. Lin, Y.-H., *et al.*, *Biomacromolecules* (2005) **6** (2), 1104
29. Roy, K., *et al.*, *Nature medicine* (1999) **5** (4), 387
30. Evans, D. F., *et al.*, *Gut* (1988) **29** (8), 1035
31. O'Neill, M. J., *et al.*, *Drug Discovery Today* (2011) **16** (5-6), 203
32. Yamada, T., *et al.*, *Textbook of Gastroenterology*. Blackwell Publishing Ltd.: Hoboken, NJ, 2009, pp. 1
33. Iain, C., *Anaesthesia & Intensive Care Medicine* (2009) **10** (7), 336
34. Gregory, M., *Digestive System*. Clinton Community College, Vol. 2012
35. Allen, A. a. S., D., *Gut* (1972) **13**, 666
36. Lai, S. K., *et al.*, *Advanced Drug Delivery Reviews* (2009) **61** (2), 158
37. CREAMER, B., *British Medical Bulletin* (1967) **23** (3), 226
38. Ensign, L. M., *et al.*, *Advanced Drug Delivery Reviews* (0)
39. Enslin, G. M., *et al.*, *BioDrugs* (2005) **19** (3), 165+
40. Pade, V., and Stavchansky, S., *Pharmaceutical Research* (1997) **14** (9), 1210
41. Borchard, G., *et al.*, *J Control Release* (1996) **39** (2-3), 131

42. Smith, J., *et al.*, *Pharmaceutical Research* (2004) **21** (1), 43
43. Ranaldi, G., *et al.*, *The Journal of Nutritional Biochemistry* (2002) **13** (3), 157
44. Schneeberger, E. E., and Lynch, R. D., *American Journal of Physiology - Cell Physiology* (2004) **286** (6), C1213
45. Lozier, J. N., *et al.*, *Hum Gene Ther* (1997) **8** (12), 1481
46. Rieux, A. d., *et al.*, *European Journal of Pharmaceutical Sciences* **25** (4-5), 455
47. Hase, K., *et al.*, *Nature* (2009) **462** (7270), 226
48. Kawashima, Y., *et al.*, *Pharmaceutical Development & Technology* (2000) **5** (1), 77
49. Lamprecht, A. e. a., *Nanotechnology* (2006) **17**, 3673
50. Glangchai, L. C., *et al.*, *J Control Release* (2008) **125** (3), 263
51. Dhadwar, S. S., *et al.*, *Journal of Thrombosis and Haemostasis* (2010) **8** (12), 2743
52. Bowman, K., *et al.*, *J Control Release* (2008) **132** (3), 252
53. Chen, M.-C., *et al.*, *Advanced Drug Delivery Reviews* (2013) **65** (6), 865
54. Dass, C. R., and Choong, P. F., *Journal of drug targeting* (2008) **16** (4), 257
55. Quade-Lyssy, P., *et al.*, *Journal of thrombosis and haemostasis : JTH* (2014) **12** (6), 932
56. Kawai, T., and Akira, S., *Journal of Biochemistry* (2007) **141** (2), 137

57. Lotze, M. T., *et al.*, *Immunol Rev* (2007) **220**, 60
58. Palm, N. W., and Medzhitov, R., *Immunol Rev* (2009) **227** (1), 221
59. Guiducci, C., *et al.*, *Journal of Internal Medicine* (2009) **265** (1), 43
60. Su, K. Y., and Pisetsky, D. S., *Scandinavian Journal of Immunology* (2009) **70** (3), 175
61. Berland, R., *et al.*, *Immunity* (2006) **25** (3), 429
62. Christensen, S. R., *et al.*, *Immunity* (2006) **25** (3), 417
63. Nickerson, K. M., *et al.*, *Journal of immunology (Baltimore, Md. : 1950)* (2010) **184** (4), 1840
64. Hurlow, J., *et al.*, *Advances in Wound Care* (2015) **4** (5), 295
65. Lindsay, D., and von Holy, A., *Journal of Hospital Infection* (2006) **64** (4), 313
66. Flemming, H.-C., and Wingender, J., *Nature Reviews Microbiology* (2010) **8**, 623+
67. Tetz, G. V., *et al.*, *Antimicrobial Agents and Chemotherapy* (2009) **53** (3), 1204
68. Whitchurch, C. B., *et al.*, *Science* (2002) **295** (5559), 1487
69. Das, T., *et al.*, *PLoS One* (2014) **9** (3)
70. Jayawardena, T. M., *et al.*, *Circulation research* (2012) **110** (11), 1465
71. Li, Q., *et al.*, *Journal of cell science* (2010) **123** (Pt 14), 2444

72. Arangoa, M. A., *et al.*, *Gene Ther* (2003) **10** (1), 5
73. Mayer, G., *et al.*, *J Control Release* (2005) **106** (1-2), 181
74. Yuan, H., *et al.*, *Int J Pharm* (2010) **392** (1-2), 224
75. Gao, X., and Huang, L., *Biochemistry* (1996) **35** (3), 1027
76. Du, Y.-Z., *et al.*, *International Journal of Biological Macromolecules* (2011) **48** (1), 153
77. Delgado, D., *et al.*, *International Journal of Pharmaceutics* (2012) **425** (1-2), 35
78. Sorgi, F. L., *et al.*, *Gene Ther* (1997) **4** (9), 961
79. No, H. K., and Meyers, S. P., *Journal of Agricultural and Food Chemistry* (1989) **37** (3), 580
80. Zhang, Z.-t., Chen Cong-hui, Chen Liang, *Journal of Dong Hua University (Eng. Ed.)* (2002) **19** (3), 36
81. Behrens, I., *et al.*, *Pharmaceutical Research* (2001) **18** (8), 1138
82. Bowman, K., and Leong, K. W., *International Journal of Nanomedicine* (2006) **1** (2), 117
83. Strand, S. P., *et al.*, *Biomaterials* (2010) **31** (5), 975
84. Richardson, S. C., *et al.*, *Int J Pharm* (1999) **178** (2), 231
85. Koping-Hoggard, M., *et al.*, *Gene Therapy* (2004) **11**, 1441

86. Lavertu, M., *et al.*, *Biomaterials* (2006) **27** (27), 4815
87. Waikato, T. U. o., *Timeline-Digestion Chemistry*. (2011)
88. Köping-Höggård, M., *et al.*, *Gene Therapy* (2001) **8** (14), 1108
89. Lee, M., *et al.*, *Pharmaceutical Research* (2001) **18** (4), 427
90. Arunachalam, B., *et al.*, *Proceedings of the National Academy of Sciences of the United States of America* (2000) **97** (2), 745
91. Lin, C., *et al.*, *J Control Release* (2007) **123** (1), 67
92. Oh, N., and Park, J.-H., *International Journal of Nanomedicine* (2014) **9** (Suppl 1), 51
93. Gamboa, J. M., and Leong, K. W., *Adv Drug Deliv Rev* (2013)
94. Mahler, G. J., *et al.*, *The Journal of Nutritional Biochemistry* (2009) **20** (7), 494
95. McClean, S., *et al.*, *European Journal of Pharmaceutical Sciences* (1998) **6** (2), 153
96. Narai, A., *et al.*, *Toxicology in Vitro* (1997) **11** (4), 347
97. *Applications of Cell Immobilisation Biotechnology*. Springer: Dordrecht, The Netherlands, 2005
98. Dhadwar, S. S., *et al.*, *Journal of thrombosis and haemostasis : JTH* (2010) **8** (12), 2743
99. Jin, D.-Y., *et al.*, *Blood* (2004) **104** (6), 1733

100. Herzog, R. W., and High, K. A., *Thrombosis and haemostasis* (1999) **82** (2), 540
101. Arangoa, M. A., *et al.*, *Gene Therapy* (2003) **10** (1), 5
102. Masuda, T., *et al.*, *FEBS Letters* (2005) **579** (10), 2143
103. Stearns, N. A., *et al.*, *PLoS ONE* (2012) **7** (7), e40862
104. Lee, J., *et al.*, *Proceedings of the National Academy of Sciences of the United States of America* (2011) **108** (34), 14055
105. Goodman, C. M., *et al.*, *Bioconjugate Chemistry* (2004) **15** (4), 897
106. Lv, H., *et al.*, *J Control Release* (2006) **114** (1), 100
107. Dzenis, Y., *Science* (2004) **304** (5679), 1917
108. Bhardwaj, N., and Kundu, S. C., *Biotechnology Advances* (2010) **28** (3), 325
109. Sun, T., *et al.*, *Tissue Engineering* (2005) **11** (7-8), 1023
110. Uyar, T., and Besenbacher, F., *Polymer* (2008) **49** (24), 5336
111. Kang, M., *et al.*, *Colloids and Surfaces A: Physicochemical and Engineering Aspects* (2008) **313–314** (0), 411
112. Lee, S. J., *et al.*, *Biosensors and Bioelectronics* (2012) **38** (1), 302
113. Tatavarty, R., *et al.*, *Reactive and Functional Polymers* (2011) **71** (2), 104

114. Tang, C., *et al.*, *Polymer* (2007) **48** (15), 4482
115. Stoilova, O., *et al.*, *European Polymer Journal* (2010) **46** (10), 1966
116. Ignatova, M., *et al.*, *European Polymer Journal* (2009) **45** (9), 2494
117. Kang, J., and Yoo, H. S., *Biomacromolecules* (2014) **15** (7), 2600
118. Sarkar, K., *et al.*, *Carbohydrate Polymers* (2013) **92** (2), 2048
119. Fillion, M. C., and Phillips, N. C., *Biochimica et Biophysica Acta (BBA) - Biomembranes* (1997) **1329** (2), 345
120. Eom, Y. W., *et al.*, *Oncogene* (2005) **24** (30), 4765
121. Eom, Y.-W., *et al.*, *Oncogene* (2005) **24** (30), 4765
122. Müller, I., *et al.*, *Biochemical and Biophysical Research Communications* (1997) **230** (2), 254
123. Guiducci, C., *et al.*, *The Journal of experimental medicine* (2010) **207** (13), 2931
124. Holl, E. K., *et al.*, *PLoS ONE* (2013) **8** (7), e69413
125. Ignatova, M., *et al.*, *Macromol Biosci* (2010) **10** (8), 944
126. Gibbard, R. J., *et al.*, *J Biol Chem* (2006) **281** (37), 27503
127. Iwasaki, A., and Medzhitov, R., *Nature Immunology* (2004) **5** (10), 987

128. Branski, L., Gauglitz, GG, Herndon, DN, et. al., *Burns* (2008)
129. Zhao, G., et al., *Wound Repair and Regeneration* (2010) **18** (5), 467
130. Mann, E. E., et al., *PLoS ONE* (2009) **4** (6), e5822
131. Mulcahy, H., et al., *PLoS Pathogens* (2008) **4** (11), e1000213
132. Izano, E. A., et al., *Applied and environmental microbiology* (2008) **74** (2), 470
133. Huseby, M. J., et al., *Proceedings of the National Academy of Sciences of the United States of America* (2010) **107** (32), 14407
134. Gov, Y., et al., *Peptides* (2001) **22** (10), 1609
135. Balaban, N., et al., *Journal of Infectious Diseases* (2003) **187** (4), 625
136. Institute, B., Babraham Bioinformatics.
137. Martin, M., *EMBnet.journal* (2011) **17** (1), 10
138. Kersey, P. J., et al., *Nucleic acids research* (2012) **40** (Database issue), D91
139. Dobin, A., et al., *Bioinformatics (Oxford, England)* (2013) **29** (1), 15
140. Anders, S., HTSeq: Analysing high-throughput sequencing data with Python; EMBL Heidelberg (Genome Biology Unit)2010
141. Love, M. I., et al., *Genome biology* (2014) **15** (12), 550

142. Robinson, M. D., *et al.*, *Bioinformatics (Oxford, England)* (2010) **26** (1), 139
143. Foundation, T. R., *The R Project for Statistical Computing.*
144. Directions for in-gel tryptic digestions of coomassie-stained 1D Bands and 2D Spots.
145. Schierle, C. F., *et al.*, *Wound repair and regeneration : official publication of the Wound Healing Society [and] the European Tissue Repair Society* (2009) **17** (3), 354
146. Xue, X., *et al.*, *The AAPS journal* (2013) **15** (1), 132
147. Yudovin-Farber, I., *et al.*, *Journal of Nanomaterials* (2010) **2010**
148. Castonguay, A., *et al.*, *New Journal of Chemistry* (2012) **36** (2), 199
149. Roy, S., *et al.*, *The Journal of pathology* (2014) **233** (4), 331
150. Holl, E. K., *et al.*, *Plastic and reconstructive surgery* (2014) **134** (3), 420e
151. Goel, A., and Shrivastava, P., *Indian Journal of Plastic Surgery : Official Publication of the Association of Plastic Surgeons of India* (2010) **43** (Suppl), S63
152. Shin, D., and Minn, K. W., *Plast Reconstr Surg* (2004) **113** (2), 633
153. Rosique, R. G., *et al.*, *International Journal of Inflammation* (2015) **2015**, 9
154. Oka, T., *et al.*, *Nature* (2012) **485** (7397), 251

155. Dasu, M. R., and Rivkah Isseroff, R., *The Journal of investigative dermatology* (2012) **132** (8), 1955
156. Dasu, M. R., et al., *Laboratory Investigation* (2010) **90** (11), 1628
157. Martin, P., *Science* (1997) **276** (5309), 75
158. Tsirogianni, A. K., et al., *Injury* (2006) **37** (1, Supplement), S5
159. Romer, J., et al., *Nature medicine* (1996) **2** (3), 287
160. Gailit, J., et al., *Journal of Investigative Dermatology* **103** (2), 221
161. Ziegler, J. B., et al., *Journal of Clinical Investigation* (1975) **55** (3), 668
162. Matsuyama, W., et al., *Internal medicine* (2001) **40** (12), 1254
163. Waite, R. D., et al., *BMC Genomics* (2006) **7** (1), 1
164. Preissner, K. T., and Seiffert, D., *Thrombosis Research* (1998) **89** (1), 1
165. *The Journal of Cell Biology* (1984) **98** (4), 1388
166. Pages, U. M., *Fibronectin*. (2014)
167. Enzymes, C., *Succinyl-CoA synthetase from Prokaryote, Recombinant*.
168. ProMetic Life Sciences, I., *Understanding PLGD*. (2015)
169. Attinger, C., and Wolcott, R., *Advances in Wound Care* (2012) **1** (3), 127

170. Allan, N., Olson, M., Nagel, D., Martin, R., The Impact of hydrosurgical debridement on wounds containing bacterial biofilms. *Wound Repair and Regeneration*, (2011)
171. Wolcott, R. D., *et al.*, *J Wound Care* (2010) **19** (8), 320
172. Schaeue, D., *et al.*, *Seminars in Radiation Oncology* (2015) **25** (1), 4
173. Bonomo, S. R., *et al.*, *Archives of Surgery* (2000) **135** (10), 1148
174. Mekkes, R. J., *et al.*, *Archives of Dermatological Research* **290** (3), 152
175. Bernatchez, S. F., *et al.*, *Wound Repair and Regeneration* (1998) **6** (3), 223
176. Roy, S., *et al.*, *Physiological Genomics* (2009) **37** (3), 211

Biography

Jennifer Gamboa Jackman was born Jennifer Marie Gamboa on November 9, 1988 in West Covina, CA, USA. Jennifer earned her Bachelors of Science in Chemical Engineering from Arizona State University in May of 2011. She received the National Hispanic Scholarship to support her undergraduate degree at ASU. Jennifer proceeded with her education at Duke University where she received the Dean's Fellowship, the Center for Biomolecular and Tissue Engineering grant support, and the National Science Foundation Graduation Research Fellowship to support her 5 years of study. During her studies she received a Master of Science in Biomedical Engineering in May of 2014 and published one first author paper entitled "*In vitro* and *in vivo* models for the study of oral delivery of nanoparticles" (2013). Jennifer is also a quarter contributor to a provisional patent filed in April 2014 under the title: Electrospun cationic nanofibers and methods of using the same. Following completion of her PhD at Duke in Jun 2016, Jennifer will pursue a carrier related to clinical research.